Université de Strasbourg

École doctorale des sciences de la Terre et de l'environnement (ED 413)

&

Université de technologie Sharif

Department of Civil Engineering

Présentée par:

Samirasadat SOLTANI

Soutenance prévue: le **24 June 2022**

Pour obtenir le grade de: **Docteur de l'Université de Strasbourg**

Discipline/Spécialité: Sciences de l'environnement

Assimilating remote sensing information into a distributed hydrological model for improving water budget predictions

---

THÉSE dirigée par:

Monsieur Marwan Fahs	**Maitre de conferences, Université de Strasbourg**
Monsieur Behzad Ataie-Ashtiani	**Maitre de conferences, Université de technologie Sharif**

RAPPORTEUR:

Monsieur Matteo Camporese	**Université de Padova, Italie**
Monsieur Thomas Graf	**Université de Hannover, Allemagne**

AUTRES MEMBRES DU JURY:

Monsieur Craig Simmons	**Université Flinders, Australie**
Madame Florence Le Ber	**Université de Strasbourg, France**
Monsieur Ahmad Al Bitar	**Université de Toulouse, France**

Table of Contents

List of Figures

List of Tables

Acknowledgments

First and foremost, I offer my sincerest gratitude to my supervisors, Dr. Behzad Ataie-Ashtiani (Sharif University of Technology) and Dr. Marwan Fahs (University of Strasbourg), who have guided me throughout my thesis with their patience and knowledge. You have provided me extensive personal and professional guidance and taught me a great deal about both scientific research and life in general. I would not have been able to finish this work without your support, mentorship, motivation, and unfailing faith in me.

I would like to express my deepest gratitude to Dr. Ahmad Al Bitar (the University of Toulouse) for helping me enhance my technical skills and become a better researcher. I would also like to thank the members of the defense committee, Dr. Seyed Mossa Hoseini, Dr. Sanaz Moghim, Dr. Mirmosadegh Jamali and Dr. Mahdi Zarghami for their insightful questions, valuable suggestions and comments, which have helped strengthen my work.

Finally, I must express my very profound gratitude to my family, especially to my beloved husband, Saeed, for providing me with unfailing support and continuous encouragement throughout my years of study and through the process of researching and writing this thesis. I am thankful to my parents for always supporting me and encouraging me to follow my dreams and pursue my goals. This accomplishment would not have been possible without them.

Abstract

Global climate change and anthropogenic impacts lead to alterations in the water cycle, water resource availability and the frequency and intensity of floods and droughts. As a result, developing effective techniques such as hydrological modeling is essential to monitor and predict water storage changes. However, inaccuracies and uncertainties in different aspects of modeling, due to simplification of meteorological physical processes, data limitations and inaccurate climate forcing data limit the reliability of hydrological models. Satellite remote sensing datasets, especially Terrestrial Water Storage (TWS) data which can be obtained from Gravity Recovery and Climate Experiment (GRACE), provide a new and valuable source of data which can augment our understanding of the hydrologic cycle. Soil moisture retrievals from the Soil Moisture and Ocean Salinity (SMOS) also provide us with a great opportunity to understand changes in soil moisture. Merging these new observations with hydrological models which is called Data Assimilation (DA) can effectively enhance the model performance using advanced statistical and numerical methods, which is known as data assimilation. Assimilation of new observations constrains the dynamics of the model based on uncertainties associated with model and data, which can introduce missing water storage signals e.g., anthropogenic and extreme climate change effects. Assimilation of satellite remote sensing datasets into hydrological models is a challenging task as provision should be made for handling the errors and then merging them with hydrological models using efficient assimilation techniques.

The main objective of this thesis is to provide multi-mission satellite data assimilation into the coupled surface-subsurface hydrological model for the first time to improve predictions of sub-surface water storage, and shed light on the limitations and challenges of assimilating only one source of satellite data. We present a comprehensive data assimilation strategy including (i) GRACE-only (GRACE DA), (ii) SMOS-only (SM DA), and (iii) joint assimilation of GRACE and SMOS (multivariate DA) and how to work with GRACE TWS data errors e.g., the correlated noise of high-frequency mass variations and spatial leakage errors to use the potential of GRACE TWS data as much as possible. We provide benefits and limitations of different data assimilation strategies with emphasis on the capability of multi-mission satellite data for hydrological applications. In this thesis, multi-mission satellite data is assimilated into an integrated two-way coupled subsurface-surface hydrological model which is called ParFlow-CLM using the Ensemble

Kalman Filter (EnKF). Interaction between subsurface and surface water is a numerically challenging task and ParFlow-CLM can simulate the physical processes occurring at the interface between the deeper subsurface and the surface. Therefore, investigation of effect of the multivariate data assimilation on ParFlow-CLM model can challenge the capability of this model.

To implement this objective, in the first step, an in-depth overview of recent studies on assimilating GRACE TWS data into hydrological models is provided and sheds light on their limitations, challenges and progress. In the second step, the capability of GRACE data in estimation of water budget is investigated and for doing this the central basin of Iran is selected. In the third step, an approach to improve soil moisture and groundwater-level predictions from ParFlow-CLM model using an objective scaling of Manning's coefficient and saturated hydraulic conductivity is proposed and this approach has been tested over the Upper Rhine basin. A modification of model parametrization to take into account the impact of scale on hydrodynamic parameters should be done prior to multivariate assimilation approaches. And finally, multivariate data assimilation performance in the three assimilation methodologies is evaluated over a case study in Iran. Furthermore, multiple datasets including in-situ measurements of groundwater and different remotely sensed observations are used to examine the results.

1.1 Terrestrial Water Storage

Since climate change and anthropogenic activities can influence the cycle of water and energy, which is followed by hazards such as floods and droughts (Stocker et al., 2013), monitoring and predicting water resource changes have become more important. Accurate quantification of water storage changes is one reliable approach to determine the availability and sustainability of water resources. As a result, it is essential to monitor hydrological processes, as well as water states and fluxes at various temporal and spatial resolutions. The hydrological processes are multifaceted and different hydrological models are applied to simulate the water cycle on various system sizes from small basins to global scales to quantify the different components of it (Sood and Smakhtin, 2015). These models strive to represent reality as much as possible, but there is always a degree of simplification involved, while the empirical model parameters and insufficient and imperfect climate input data are also subject to uncertainty (Van Dijk et al., 2014). Climate input data obtained from imperfect in situ measurements impede reliable simulation results from a hydrological model due to limitations in the spatiotemporal availability of in-situ data (Soltani et al., 2020). Alternatively, remote sensing technology with different spatiotemporal resolutions provides a unique opportunity not only to obtain hydrological parameters e.g., precipitation (e.g., Alazzy et al., 2017; Najmaddin et al., 2017), soil moisture (e.g., Ray et al., 2017), evapotranspiration (e.g., Liou and Kar, 2014) but also to improve a hydrological model's performance. In particular, the Gravity Recovery and Climate Experiment (GRACE) and GRACE Follow-On (GRACE-FO) missions which have been active since 2002, have an important role in representing surface and sub-surface physical processes related to water redistribution in the Earth system by estimating Terrestrial Water Storage (TWS) (e.g., Kusche et al., 2012; Forootan et al., 2014a; Wouters et al., 2014; Soltani et al., 2020). Some studies reviewed the application of GRACE data in monitoring of TWS due to its recent developments and popularity in hydrology (e.g., Frappart and Ramillien, 2018; Güntner, 2008; Jiang et al, 2014). Jiang et al (2014), Those have reviewed the hydrological application of GRACE data in some distinct categories including 1) TWS change monitoring, 2) hydrological components evaluation, 3) drought analysis and 4) glacier mass balance detection. GRACE TWS data also can be used by advanced statistical and numerical methods to modify a hydrological model's output to reduce the input climate data

uncertainty influence and mitigate the negative impact of using an improper model structure or model parameters. GRACE TWS data obtained by using strong filtering strategies is assumed as a model constraint based on uncertainties associated with both model and data, which helps to enhance flux and storage simulations. With the growth of satellite remote sensing products, GRACE data assimilation into hydrological models has attracted enormous interest in hydrology (e.g., Zaitchik et al., 2008; Su et al., 2010; Forman et al., 2012; Eicker et al., 2014; Tangdamrongsub et al., 2015; Reager et al., 2015; Eicker et al., 2016; Schumacher et al., 2016b; Schumacher et al., 2016a; Tangdamrongsub et al., 2017; Khaki et al., 2018b; Khaki et al., 2018c; Tangdamrongsub et al., 2018). In fact, the interaction of models and data is a reciprocal process in which data can serve the modeling purpose by supporting model discrimination, parameter refinement, uncertainty analysis, and in which models deliver a tool for data fusion (assimilation), interpretation, interpolation (Rajabi et al., 2018). Some studies provide a technical review of large-scale hydrological models (Kauffeldt et al., 2016) and data assimilation techniques (Montzka et al., 2012; Lahoz and Schneider, 2014; Houtekamer and Zhang, 2016; Bannister, 2017).

1.1.1 Application of GRACE Satellite Remote Sensing

Investigating the interaction between TWS and other components of the water budget is very important in assessing the availability of freshwater resources (Van Dijk et al., 2014). To date, different tools have been used to investigate water storages and their interactions with other components of the water balance that can be referred to ground measurements, hydrological models, and satellite remote sensing data.

Hydrology benefits from the gravity data from GRACE satellite because a large portion of the changes in *g* is due to changes in water in the ocean, atmosphere and continental water storage (Ramillien et al., 2008). Climate and geophysical processes need an understanding of the water cycle across the continents which can be derived from the mass changes of the earth surface (Ilk et al., 2004). In order to isolate the hydrological part of the GRACE signal, Ramillien et al. (2004), Rodell and Famiglietti (1999), Seitz et al. (2010), Grippa et al. (2011), Awange et al. (2009) and Longuevergne et al. (2010) have presented various methods. They all mention that the water storage in the continents and its changes in time and space can be obtained from the gravimetry satellite observations (Schmidt et al., 2006). TWS across the globe first became available as a unified database with the application of GRACE. Many models that simulate the hydrological

cycle can be validated and improved with GRACE data (Schmidt et al., 2006). GRACE TWS has varying time resolutions of one day (Kurtenbach et al., 2009) to one month (the publicly available data) which is also dependent on the method of data analysis. The resolution in space is on the order a few hundred kilometers (Schmidt et al., 2006). GRACE TWS has found applications in geophysical applications as well as climate and hydrology studies (see Kusche et al., 2012; Famiglietti and Rodell, 2013; Wouters et al., 2014; Famiglietti et al., 2015; Chen et al., 2016; Soltani et al, 2020). The monthly GRACE products have been compared to global hydrology models in terms of the terrestrial water storage variation by Wahr et al. (2004) and Schmidt et al. (2006). Seasonal GRACE data generally agree with the hydrological model's output (Schmidt et al., 2006), although there are some errors. The problems in model description or parameters can be alleviated using GRACE. Syed et al. (2005), Yamamoto et al. (2007) and Winsemius et al. (2006) have stated that GRACE is not good for application in small basins (<150,000 km^2) because of its resolution.

GRACE cannot differentiate between TWS components such as subsurface or soil moisture. As a result, TWSA components separation of GRACE have been attempted for snow (e.g., Frappart et al., 2006; Niu et al., 2007 and Llubes et al., 2007), evapotranspiration (e.g., Rodell et al., 2004) and groundwater (e.g., Rodell et al., 2007). For this purpose, model outputs and ground measurements are used to separate known components, and the integral gravity signal of the GRACE is thus decomposed. Several methods exist for separation of the signals in recent studies. Inversion and statistical decomposition were applied by Rietbroek (2014), Schmeer et al. (2012) and Forootan (2014b) in order to separate GRACE TWS into different storage compartments.

1.1.2 Hydrological Modeling

Hydrological models are considered as an important and necessary tool for water and environment resource management. Hydrological models at the regional scale (e.g., Chiew et al., 1993; Wooldridge and Kalma, 2001; Christiansen et al., 2007; Huang et al., 2017) and global scale (e.g., Döll et al., 2003; Huntington, 2006; Coumou and Rahmstorf, 2012; Van Dijk et al., 2013) are important tools that are used for simulation of hydrological process. Hydrological models give us a better insight into the water cycle on the global and regional scale. Various hydrological models (Moradkhani and Sorooshian, 2008; Devia et al., 2015) have been applied with different levels of success to obtain water storage components e.g., water in ice, glaciers, snow caps, groundwater,

surface water and soil moisture and the rate of their changes (e.g., Chiew et al., 1993; Wooldridge and Kalma, 2001; Döll et al., 2003; Huntington, 2006; Van Dijk, 2010). Models are also used for information extraction, data assimilation, interpretation, generalization and interpolation, and identification of information-rich data (Ataie-Ashtiani et al., 2020).

Models are still being developed to better simulate all available hydrological processes and the inclusion of all interactions between water cycle components e.g., interaction between runoff, precipitation and evapotranspiration (Simmons et al., 2019). In any case, uncertainties exist and the modeling remains imperfect. Data sets are still limited in time and space, and our knowledge about empirical parameters is still limited (Vrugt et al., 2013; Van Dijk et al., 2011, 2014). Danesh-Yazdi and Ataie-Ashtiani (2019) argue that planning and management of hydrological systems "without appropriate data and model is gambling", as for a consistent understanding of the system both are required. As a result, the simulation model results are imperfect and uncertain. Some of the model parameters are not easy to interpret, and the computational burden of the more complex models is higher.

Another alternative is incorporating accurate observations into the model for handling these limitations (e.g., McLaughlin, 2002; Zaitchik et al., 2008; Van Dijk et al., 2014; El Gharamti et al., 2016). Since remotely sensed data for different quantities are becoming increasingly available in different coverages and resolutions, model reliability improvement can be achieved with these data. Satellite data assimilation specifically, GRACE into hydrological models can be used 1) to effectively separate TWS into its components and downscale the coarse resolution of it and 2) to constrain the models' simulations and also their parameters through data assimilation.

1.2 Data Assimilation Methodology

Ocean, earth science and atmospheric studies employ numerical solution of DA with the advancement of high power computing systems and in hydrology with the emergence of state-of-art satellite datasets, it has started to be applied in models for soil moisture (e.g., Brocca et al., 2010; Renzullo et al., 2014; Kumar et al., 2014, 2015), runoff (e.g., Vrugt et al., 2006; Komma et al., 2008; Neal et al., 2009; Lee et al., 2011; McMillan et al., 2013; Li et al., 2015), water storage in surface reservoirs (e.g., Neal et al., 2009; Giustarini et al., 2011), evapotranspiration (e.g., Schuurmans et al., 2003; Pipunic et al., 2008; Irmak and Kamble, 2009) and TWS changes (e.g.,

Landerer and Swenson 2012; Longuevergne et al. 2013; Awange et al. 2014; Forootan et al. 2014a).

Based on these studies, it is obvious that assimilation of satellite remote sensing data into hydrological models, separately or simultaneously, provides a great opportunity to improve and calibrate hydrological models. Better results can be achieved by multi-satellite products when properly accounting for the measurement errors (see, e.g., Montzka et al. 2012; Renzullo et al. 2014; Tian et al. 2017).

With the availability of TWS from the GRACE, assimilation of GRACE TWS into hydrological models has been done in the past few years to update hydrological model estimates of various water compartments (e.g., Zaitchik et al., 2008; Van Dijk et al., 2014; Tangdamrongsub et al., 2015; Kumar et al., 2016; Girotto et al., 2016, 2017; Khaki et al., 2017a; Schumacher et al., 2018). In addition to different datasets, different DA techniques have also been implemented and tested in hydrological studies as well as hydrologic operational systems.

Various filtering techniques have been proposed and developed in various fields for DA objectives. Among these, variational methods and sequential filtering have gained a lot of attention during the past few decades. In the variational approach, the model solution is fitted to the data given a cost function that measures the error between the state variables and observations (Talagrand and Courtier, 1987). Computer coding of the adjoint system is necessary which needs a lot of time to write the code and also significant computer power to execute the code (Hoteit et al., 2005). Also, the variational methods have limited accuracy because of the DA process and the estimation statistics in this process (Kalnay, 2003; Courtier et al., 1994).

1.2.1 Assimilation Strategy: Multivariate (joint) data assimilation

With GRACE TWS data assimilation, the components of the water balance including soil moisture and groundwater storage can be quantified since errors are considered for both observations and the model. In addition, total water storage observation from GRACE can be spatially downscaled with the model, giving better resolution of water storage for the study area (see, e.g., Schumacher and Kusche, 2016). In addition, by using soil moisture data from satellite and assimilation of this dataset, soil moisture component becomes more accurate, thereby improving its updated estimates (e.g., Tian et al., 2017). It has been shown that using total water storage from GRACE and satellite soil moisture product is successful in constraining the hydrologic model outputs to more accurate

----

values (Tangdamrongsub et al., 2020). Soltani et al. (2021) reviewed several studies that indicate GRACE TWS (e.g., Zaitchik et al., 2008; Houborg et al., 2012; Li et al., 2012; Eicker et al., 2014; Reager et al., 2015; Girotto et al., 2016; Girotto et al., 2017; Khaki et al., 2018a; Khaki et al., 2018b) and satellite soil moisture (e.g., Renzullo et al., 2014; Dumedah et al., 2015; Tian et al., 2017; Kolassa et al., 2017) for data assimilation can successfully constrain the hydrological models simulations.

Therefore, the main objective of this chapter is to use multi-mission satellite data products to improve predictions of sub-surface water storages in the hydrology model over a case study in Iran. As a result, GRACE-derived TWS and soil moisture observations from the SMOS are assimilated in the couple ParFlow-CLM hydrological model (or TerrSys-MP). TerrSys-MP coupled to the to the PDAF library (Parallel Data Assimilation Framework) (Kurtz et al., 2016; Nerger and Hiller, 2013). This is an efficient numerical tool which is capable of performing assimilation tasks in parallel, thereby making it attractive for applications at large spatial scales and high-resolution over long periods of time (Kurtz et al., 2016). This work uses the Ensemble Kalman Filter (EnKF) filter method (Whitaker and Hamill, 2002) in order to assimilate TWS from GRACE and soil moisture products from SMOS via the ensemble-based sequential technique into the Terrsys-MP.

1.3 Scientific Context and Objectives of the Thesis

Assimilating remotely-sensed data specially, GRACE data into hydrological models presents several challenges. The temporal and spatial (horizontal and vertical) resolution mismatch between simulated model states and observed remotely-sensed data requires the use of sophisticated strategies to connect them (Girotto et al., 2016). Furthermore, data assimilation requires information on uncertainties of model and observations. The model error is difficult to quantify as it depends on uncertainties in model structure, atmospheric forcings, and soil data sets. For example, GRACE TWS data are contaminated with correlated noise, which requires careful post-processing of the GRACE solutions. Currently, no standard way exists for the assimilation of GRACE data into hydrological models.

So far, only few groups have assimilated GRACE data into a hydrological model. Typically, the applied hydrological models have a spatial resolution between 0.5° (50 km) to 1° (100 km) and

run at daily time steps, whereas the resolution of climate data might be restricted (e.g., number of cloud-free days per month, precipitation averaging). One exception for assimilation experiments at higher spatial resolution is the assimilation of GRACE data into a lumped rainfall-runoff model set up for the Rhine catchment at 1km resolution, which however uses atmospheric forcing data resolved at 0.25° to 0.5° (Tangdamrongsub et al., 2015). Another example is the catchment-based land surface model running at a 1/8° grid with 15-minute time steps and daily atmospheric forcing data (Kumar et al., 2016).

This thesis aims at assimilating GRACE-derived TWS variability into a fully coupled surface-subsurface model (CLM-ParFlow) at 0.25° spatial resolution over a case study in Iran using 3-hourly atmospheric forcing data. CLM-ParFlow is a physics-based land-surface model, which has a more complex structure than conceptual models like WGHM, as several hydrological, bio geophysical, and biogeochemical processes are represented. Physical relationships between model variables cause particular challenges regarding a physically consistent update of the model states during assimilation.

CLM-ParFlow is part of the Terrestrial Systems Modeling Platform (TerrSysMP), which also includes a groundwater component and an atmospheric model (Shrestha et al., 2014). Including the assimilation of GRACE data into CLM-ParFlow using TerrSysMP will allow for extending the experiments to the groundwater component, or even to simulations of the whole terrestrial water cycle, i.e., simulations with a fully coupled model that includes atmospheric, land-surface, and groundwater components.

Previous studies investigated different strategies of assimilating GRACE data by varying governing parameters such as, the assimilation algorithm, correlated versus white observation noise (Schumacher et al., 2016), and the observation grid (Khaki et al., 2017a). This thesis goes further and provides a systematic study of the most important assimilation strategies including multivariate data assimilation of GRACE data and another remotely-sensed data like SMOS data at the same time, which results in better assimilation results. This thesis addresses two main issues:

1. What is the optimal way of assimilating multivariate GRACE- SMOS data into a land-surface model in terms of an improved description of water storage variability?

2. What is the impact of the assimilation of multivariate GRACE-SMOS data on the performance of CLM-ParFlow in terms of the realism of simulated water storage compartments?

For answering the first question, a detailed review on the findings from previous GRACE and SMOS assimilation studies is performed and, subsequently, different assimilation strategies are carried out. The second question is answered by validating water storage compartments of CLM-ParFlow against independent observation-based datasets, both before and after data assimilation. Finally, this thesis provides a reanalysis of TWS and its components at 0.25° resolution and daily time steps over a case study for the time span 2015 to 2020.

1.3 Contexte scientifique et objectifs de la these

L'assimilation de données à distance, en particulier les données GRACE, dans les modèles hydrologiques présente plusieurs défis.Le déséquilibre de résolution temporelle et spatiale (horizontale et verticale) entre les états de modèle simulés et les données télédétectées observées nécessite l'utilisation de stratégies sophistiquées pour les connecter (Girotto et al., 2016). De plus, l'assimilation de données nécessite des informations sur les incertitudes du modèle et des observations. L'erreur de modèle est difficile à quantifier car elle dépend des incertitudes dans la structure du modèle, des forçages atmosphériques et des jeux de données de sol. Par exemple, les données TWS de GRACE sont contaminées par un bruit corrélé, ce qui nécessite un post-traitement minutieux des solutions GRACE. Actuellement, il n'existe pas de méthode standard pour l'assimilation de données GRACE dans les modèles hydrologiques.

Jusqu'à présent, seuls quelques groupes ont assimilé les données GRACE dans un modèle hydrologique. Les modèles hydrologiques appliqués ont généralement une résolution spatiale entre 0,5° (50 km) et 1° (100 km) et fonctionnent par pas de temps quotidien, alors que la résolution des données climatiques peut être restreinte (par exemple, nombre de jours sans nuages par mois, moyenne des précipitations). Une exception pour les expériences d'assimilation à plus haute résolution spatiale est l'assimilation de données GRACE dans un modèle pluie-débit regroupé mis en place pour le bassin versant du Rhin à une résolution de 1 km, qui utilise cependant des données de forçage atmosphérique résolues de 0,25° à 0,5° (Tangdamrongsub et al., 2015). Un autre exemple est le modèle de surface terrestre basé sur le bassin versant fonctionnant sur une grille de

1/8° avec des pas de temps de 15 minutes et des données de forçage atmosphérique quotidiennes (Kumar et al., 2016).

Cette thèse vise à assimiler la variabilité de la TWS dérivée de GRACE dans un modèle surface-sous-surface entièrement couplé (CLM-ParFlow) à une résolution spatiale de 0,25° sur une étude de cas en Iran en utilisant des données de forçage atmosphérique toutes les 3 heures. CLM-ParFlow est un modèle de surface terrestre basé sur la physique, qui a une structure plus complexe que les modèles conceptuels comme WGHM, car plusieurs processus hydrologiques, biogéophysiques et biogéochimiques sont représentés. Les relations physiques entre les variables du modèle posent des défis particuliers en ce qui concerne une mise à jour physiquement cohérente des états du modèle pendant l'assimilation.

CLM-ParFlow fait partie de la plateforme de modélisation des systèmes terrestres (TerrSysMP), qui comprend également une composante d'eau souterraine et un modèle atmosphérique (Shrestha et al., 2014).

Inclure l'assimilation des données GRACE dans CLM-ParFlow à l'aide de TerrSysMP permettra d'étendre les expériences au composant des eaux souterraines, voire aux simulations de l'ensemble du cycle de l'eau terrestre, c'est-à-dire à des simulations avec un modèle entièrement couplé qui comprend des composantes atmosphériques, de surface terrestre et des eaux souterraines. Des études antérieures ont examiné différentes stratégies d'assimilation des données GRACE en variant les paramètres gouvernants tels que l'algorithme d'assimilation, le bruit d'observation corrélé par rapport au bruit blanc (Schumacher et al., 2016), et la grille d'observation (Khaki et al., 2017a). Cette thèse va plus loin et propose une étude systématique des stratégies d'assimilation les plus importantes, y compris l'assimilation multivariée des données GRACE et d'autres données télédétectées telles que les données SMOS en même temps, ce qui donne de meilleurs résultats d'assimilation. Cette thèse aborde deux problèmes principaux:

1. Quelle est la meilleure façon d'assimiler les données multivariées GRACE-SMOS dans un modèle de surface terrestre en termes d'amélioration de la variabilité du stockage d'eau?

2. Quel est l'impact de l'assimilation des données multivariées GRACE-SMOS sur les performances de CLM-ParFlow en termes de réalisme des compartiments de stockage d'eau simulés?

Chapter I: Introduction

Pour répondre à la première question, une revue détaillée des résultats des études antérieures sur l'assimilation de GRACE et de SMOS est effectuée, puis différentes stratégies d'assimilation sont mises en œuvre. La deuxième question est abordée en validant les compartiments de stockage d'eau de CLM-ParFlow par rapport à des ensembles de données indépendants basés sur l'observation, avant et après l'assimilation des données. Enfin, cette thèse fournit une réanalyse du TWS et de ses composantes à une résolution de 0,25° et avec des pas de temps quotidiens sur une étude de cas pour la période de 2015 à 2020.

1.4 Organization of the Thesis

The thesis starts with an introduction into the characteristics of the data assimilation (Chapter I). The structure of this thesis is organized based on the published papers in the peer-reviewed journals or international conferences, which are presented in different chapters. The primary objective of this thesis is to propose a joint data assimilation framework to integrate GRACE TWS data and satellite soil moisture products into a hydrological model. To implement this objective, several steps have been performed, which are summarized as follows (also see **Error! Reference source not found.**):

1. A very detailed and in-depth study of challenges and limitations of data assimilation into a hydrological model. Chapter II discusses studies related to the validation of hydrological models using GRACE observations and aims at a complete survey of studies that assimilate GRACE data into hydrological models (Chapter II addresses this issue and discusses the advances and limitations of data assimilation).

2. Evaluating the efficiency of GRACE TWS data in estimating the water budget in spatial basin-scaled. To implement this objective, water budget is estimated in the Central Basin of Iran (CBI) over an 8 years period 2009–2016 (this issue is discussed in Chapter III).

3. Improving soil moisture and groundwater-level predictions simulated by ParFlow-CLM model using an objective scaling of Manning's coefficient and saturated hydraulic conductivity which emphasizes the need to reduce the uncertainty of hydrological modeling and the need for methods such as data assimilation. Finally, the real-case scenario, a 3-year (2012 to 2014) high resolution simulation run (at 12.5 km spatial resolution and hourly time step), is validated against independent observations (Chapter IV addresses this issue).

4. Implementing multivariate data assimilation with the objective of maximizing the effect of different remotely-sensed data including GRACE and SMOS data on limiting model dynamics and ultimately improving model's outputs. In single-source data integration, the focus is on improving one hydrological flux or variable, and all water budget components may not improve, and it is important to propose a multivariate data assimilation framework that improves all or most of them. The different strategies for assimilating multivariate GRACE-SMOS data into CLM-ParFlow, which were realized within this thesis for the first time, are explained in this Chapter. In this Chapter, the structure and setup of CLM-ParFlow are explained and the observation-based data sets that are used for model validation are introduced. Finally, the real-case scenario, a 5-year (2015 to 2020) assimilation run (at 0.25° spatial resolution and daily time step) is validated against independent observations (Chapter V deals with this issue and the details of its implementation).

The thesis closes with a summary, followed by final conclusions and an outlook on future possible extensions of this work (Chapter VI).

1.4 Organisation de la thèse

La thèse commence par une introduction aux caractéristiques de l'assimilation de données (chapitre I). La structure de cette thèse est organisée en fonction des articles publiés dans des revues à comité de lecture ou des conférences internationales, présentés dans différents chapitres. L'objectif principal de cette thèse est de proposer un cadre d'assimilation de données conjoint pour intégrer les données TWS de GRACE et les produits de l'humidité du sol satellite dans un modèle hydrologique. Pour mettre en œuvre cet objectif, plusieurs étapes ont été réalisées, qui sont résumées comme suit (voir aussi **Error! Reference source not found.**) :

1. Une étude très détaillée et approfondie des défis et des limites de l'assimilation de données dans un modèle hydrologique. Le chapitre II traite des études relatives à la validation de modèles hydrologiques à l'aide d'observations de GRACE et vise à effectuer une enquête complète sur les études qui assimilent les données de GRACE dans les modèles hydrologiques (le chapitre II aborde cette question et discute des avancées et des limites de l'assimilation de données).

2. Évaluation de l'efficacité des données TWS de GRACE dans l'estimation du bilan hydrique à l'échelle du bassin spatial. Pour mettre en œuvre cet objectif, le bilan hydrique est estimé

dans le bassin central de l'Iran (CBI) sur une période de 8 ans de 2009 à 2016 (ce problème est discuté dans le chapitre III).

3. Amélioration des prévisions d'humidité du sol et des niveaux d'eau souterraine simulés par le modèle ParFlow-CLM en utilisant une mise à l'échelle objective du coefficient de Manning et de la conductivité hydraulique saturée, qui souligne la nécessité de réduire l'incertitude de la modélisation hydrologique et le besoin de méthodes telles que l'assimilation de données. Enfin, le scénario réel, une simulation à haute résolution de 3 ans (2012 à 2014) (à une résolution spatiale de 12,5 km et une fréquence horaire), est validé par rapport à des observations indépendantes (le chapitre IV aborde cette question).

4. Mise en œuvre d'une assimilation de données multivariée dans le but de maximiser l'effet de différentes données télédétectées, notamment les données GRACE et SMOS, sur la limitation des dynamiques du modèle et l'amélioration des sorties du modèle. Dans l'intégration de données à source unique, l'accent est mis sur l'amélioration d'un flux ou d'une variable hydrologique, et toutes les composantes du budget en eau ne peuvent pas s'améliorer. Il est donc important de proposer un cadre d'assimilation de données multivariées qui améliore toutes ou la plupart d'entre elles. Les différentes stratégies d'assimilation de données multivariées GRACE-SMOS dans CLM-ParFlow, qui ont été réalisées pour la première fois dans cette thèse, sont expliquées dans ce chapitre. Dans ce chapitre, la structure et la configuration de CLM-ParFlow sont expliquées et les ensembles de données basées sur des observations utilisées pour la validation du modèle sont présentés. Enfin, le scénario réel, une exécution d'assimilation de 5 ans (de 2015 à 2020) (à une résolution spatiale de 0,25° et une période de temps quotidienne), est validé par

rapport à des observations indépendantes (le chapitre V traite de cette question et des détails de sa mise en œuvre).

La thèse se conclut par un résumé, suivi de conclusions finales et d'une perspective sur les extensions possibles de ce travail dans le futur (Chapitre VI).

Chapter V

Step 4:
Improving water budget predictions from ParFlow-CLM model using multivariate data assimilation

Chapter IV

Step 3:
Improving soil moisture and groundwater-level predictions from ParFlow-CLM model using an objective scaling of Manning's coefficient and saturated hydraulic conductivity

Outline

Chapter II

Step 1:
Literature Review
In-depth study of the challenges and limitations of data assimilation into a hydrological model

Chapter III

Step 2:
Evaluation of the efficiency of GRACE TWS data in estimating the water budget in spatial basin-scaled

Fig. 1.1 Outline of the thesis

1.4.1 An overview of Chapter II: Review of Assimilating GRACE Terrestrial Water Storage
Data into Hydrological Models: Advances, Challenges and Opportunities

Global climate change and anthropogenic impacts lead to alterations in the water cycle, water resource availability and the frequency and intensity of floods and droughts. As a result, developing effective techniques such as hydrological modeling is essential to monitor and predict water storage changes. However, inaccuracies and uncertainties in different aspects of modeling, due to simplification of meteorological physical processes, data limitations and inaccurate climate forcing data limit the reliability of hydrological models. Satellite remote sensing datasets, especially Terrestrial Water Storage (TWS) data which can be obtained from Gravity Recovery and Climate Experiment (GRACE), provide a new and valuable source of data which can augment our understanding of the hydrologic cycle. Merging these new observations with hydrological models can effectively enhance the model performance using advanced statistical and numerical methods, which is known as data assimilation. Assimilation of new observations constrain the dynamics of the model based on uncertainties associated with both model and data, which can introduce missing water storage signals e.g., anthropogenic and extreme climate change effects. Assimilation of GRACE TWS data into hydrological models is a challenging task as provision should be made for handling the errors and then merging them with hydrological models using efficient assimilation techniques. The goal of this chapter is to provide an in-depth overview of recent studies on assimilating GRACE TWS data into hydrological models and shed light on their limitations, challenges and progress. We present a comprehensive review of some challenges with GRACE TWS data assimilation into a hydrological model including GRACE TWS errors e.g., the correlated noise of high-frequency mass variations and spatial leakage errors, and how to work with GRACE TWS data errors to use the potential of GRACE TWS data as much as possible. We provide a review of the benefits and limitations of available data assimilation techniques with emphasis on the capability of sequential methods for hydrological applications. The topic is developed in chapter II. It has been the subject of a paper published in the Earth Science Reviews Journal (Soltani et al., 2021).

1.4.1 Aperçu du chapitre II: Revue de l'assimilation des données de stockage d'eau terrestre GRACE dans les modèles hydrologiques: avancées, défis et opportunités

Le changement climatique mondial et les impacts anthropiques entraînent des altérations dans le cycle de l'eau, la disponibilité des ressources en eau et la fréquence et l'intensité des inondations et des sécheresses. Par conséquent, le développement de techniques efficaces telles que la modélisation hydrologique est essentiel pour surveiller et prédire les changements de stockage d'eau. Cependant, les imprécisions et les incertitudes dans différents aspects de la modélisation, en raison de la simplification des processus physiques météorologiques, des limites des données et des données d'entraînement climatique inexactes, limitent la fiabilité des modèles hydrologiques. Les ensembles de données de télédétection par satellite, en particulier les données de stockage d'eau terrestre (TWS) qui peuvent être obtenues à partir de l'expérience de récupération de gravité et de climat (GRACE), fournissent une nouvelle et précieuse source de données qui peuvent augmenter notre compréhension du cycle hydrologique. La fusion de ces nouvelles observations avec des modèles hydrologiques peut améliorer efficacement les performances du modèle en utilisant des méthodes statistiques et numériques avancées, ce qui est connu sous le nom d'assimilation de données. L'assimilation de nouvelles observations contraint la dynamique du modèle en fonction des incertitudes associées à la fois au modèle et aux données, ce qui peut introduire des signaux de stockage d'eau manquants, tels que les effets anthropiques et les effets extrêmes du changement climatique. L'assimilation des données GRACE TWS dans les modèles hydrologiques est une tâche difficile car des dispositions doivent être prises pour gérer les erreurs et les fusionner ensuite avec les modèles hydrologiques en utilisant des techniques d'assimilation efficaces. L'objectif de ce chapitre est de fournir un aperçu approfondi des études récentes sur l'assimilation des données GRACE TWS dans les modèles hydrologiques et de mettre en lumière leurs limites, leurs défis et leurs progrès. Nous présentons une revue complète de certains défis liés à l'assimilation des données GRACE TWS dans un modèle hydrologique, notamment les erreurs de données GRACE TWS, telles que le bruit corrélé des variations de masse à haute fréquence et les erreurs de fuite spatiale, et comment travailler avec les erreurs de données GRACE TWS pour utiliser au maximum le potentiel des données GRACE TWS. Nous présentons une revue des avantages et des limites des techniques d'assimilation de données disponibles, en mettant l'accent sur la capacité des méthodes séquentielles pour les applications hydrologiques. Le sujet est

développé dans le chapitre II. Il a fait l'objet d'un article publié dans la revue Earth Science Reviews (Soltani et al., 2021).1.4.2 An overview of Chapter III: A probabilistic framework for water budget estimation in low runoff regions: A case study of Central Basin of Iran

Utilizing ground-based measurements to obtain water budget components, especially in large scale basins, is challenging due to the limitation in the spatiotemporal availability of in-situ data. In this chapter, we propose a probabilistic framework for estimating water budgets in low runoff regions using remote sensing products. By studying water budgets in the Central Basin of Iran (CBI) over 8 years period (2009–2016), we investigate the locations and time scales at which the water budget calculated from satellite products provides most closure. To this end, we use precipitation from the Tropical Rainfall Measuring Mission (TRMM), evapotranspiration from the Water Productivity Open Access Portal (WaPOR) and terrestrial water storage change from the Gravity Recovery and Climate Experiment (GRACE). The results show better closure and consistency of water budget in the center and South East of the basin at seasonal and annual time scales. Due to the uncertainty initiated from different data sources as well as the mismatch between the spatiotemporal resolutions of various satellite products, the validity of the results is examined through an innovative application of the First Order Reliability Method (FORM). Furthermore, the reliability sensitivity analysis also reveals that the failure probability of water budge closure is chiefly dependent on the accuracy of evapotranspiration estimations than the other components involved in the water budget equation.

The topic is developed in chapter III. It has been the subject of a paper published in the Journal of Hydrology (Soltani et al., 2020).

1.4.2 Aperçu du chapitre III: Un cadre probabiliste pour l'estimation du bilan hydrique dans les régions à faible ruissellement: Étude de cas du bassin central de l'Iran

L'utilisation de mesures sur le terrain pour obtenir les composantes du bilan hydrique, en particulier dans les grands bassins, est difficile en raison de la limitation de la disponibilité spatiotemporelle des données in-situ. Dans ce chapitre, nous proposons un cadre probabiliste pour estimer les bilans hydriques dans les régions à faible ruissellement en utilisant des produits de télédétection. En étudiant les bilans hydriques du bassin central de l'Iran sur une période de 8 ans (2009-2016), nous étudions les emplacements et les échelles de temps auxquels le bilan hydrique calculé à partir de

produits satellitaires fournit la meilleure correspondance. À cette fin, nous utilisons les précipitations de la mission de mesure des pluies tropicales (TRMM), l'évapotranspiration du portail d'accès ouvert à la productivité en eau (WaPOR) et le changement de stockage d'eau terrestre de l'expérience de récupération de gravité et du climat (GRACE). Les résultats montrent une meilleure correspondance et une meilleure cohérence du bilan hydrique dans le centre et le sud-est du bassin à des échelles de temps saisonnières et annuelles. En raison de l'incertitude due aux différentes sources de données ainsi que du décalage entre les résolutions spatiotemporelles des différents produits satellitaires, la validité des résultats est examinée grâce à une application innovante de la méthode de fiabilité de premier ordre (FORM). De plus, l'analyse de sensibilité de la fiabilité révèle également que la probabilité de défaillance de la correspondance du bilan hydrique dépend principalement de l'exactitude des estimations de l'évapotranspiration plutôt que des autres composantes impliquées dans l'équation du bilan hydrique. Le sujet est développé dans le chapitre III. Il a fait l'objet d'un article publié dans la revue Journal of Hydrology (Soltani et al., 2020).

1.4.3 An overview of Chapter IV: Improvement of soil moisture and groundwater level estimations using a scale-consistent river parameterization for the coupled ParFlow-CLM hydrological model: a case study of the Upper Rhine Basin

Accurate implementation of river interactions with subsurface is critical in large-scale hydrologic models with a constant horizontal grid resolution which use the kinematic wave approximation for both hillslope and river channel flow. The size of rivers can vary greatly in the model domain, and the implemented grid resolution is too coarse to accurately account for river interactions. Consequently, flow velocity is estimated to be too small when the width of the rivers is much narrower than the selected grid size. This leads to inaccuracy and uncertainties in calculations of water quantities because flow velocities may be underestimated. In addition to, the rate of ex- and in-filtration between the river and the subsurface may be overestimated, since a larger surface area will exchange water with the subsurface than the real river. Therefore, the present study tests the approximation of subscale channel flow by a scaled roughness coefficient in the kinematic wave equation. For this purpose, a relationship between grid cell size and river width is used to correct flow velocity, which follows a simplified modification of the Manning-Strickler equation. The rate of ex- and in-filtration between subsurface and river, is also corrected across river beds by a scaled saturated hydraulic conductivity based on the grid resolution even though the grid size is relatively

large. The scaling methodology is implemented in a hydrological model coupling ParFlow (PARallel FLOW) and Community Land Model (CLM). The model is applied over the Upper Rhine Basin (between France and Germany) for a time period from 2012 to 2014 and at a spatial resolution of 0.055° (~6 km). The validity of the results is examined with satellite and in-situ data through an innovative application of the First Order Reliability Method (FORM). The scaling approach shows that soil moisture estimates have improved, particularly in the summer and autumn seasons when cross-validated with independent soil moisture observations provided by the Climate Change Initiative (CCI). Fig. 1.2 shows the outline of this chapter. The results emphasize the use of a simple scaling procedure of the Manning coefficient and saturated hydraulic conductivity to account for the real infiltration/exfiltration rate in large-scaled hydrological models with constant horizontal grid resolution. The scaling procedure also shows overall improvements in groundwater level estimation, particularly where the groundwater level is shallow (less than 5 meters from the surface). The topic is developed in chapter IV. It has been the subject of a paper published in Journal of Hydrology and presented in EGU General Assembly 2022 (Soltani et al., 2022 a and b).

1.4.3 Aperçu du chapitre IV: Amélioration des estimations de l'humidité du sol et du niveau de la nappe phréatique en utilisant une paramétrisation de la rivière cohérente à l'échelle pour le modèle hydrologique couplé ParFlow-CLM: étude de cas du bassin du Rhin supérieur

L'implémentation précise des interactions entre la rivière et le sous-sol est cruciale dans les modèles hydrologiques à grande échelle avec une résolution de grille horizontale constante qui utilisent l'approximation de la vague cinématique pour l'écoulement sur les versants et dans les canaux de la rivière. La taille des rivières peut varier considérablement dans le domaine du modèle, et la résolution de grille implémentée est trop grossière pour prendre en compte de manière précise les interactions avec la rivière. Par conséquent, la vitesse d'écoulement est estimée être trop faible lorsque la largeur des rivières est beaucoup plus étroite que la taille de grille sélectionnée. Cela conduit à des inexactitudes et à des incertitudes dans le calcul des quantités d'eau, car les vitesses d'écoulement peuvent être sous-estimées. De plus, le taux d'exfiltration et d'infiltration entre la rivière et le sous-sol peut être surestimé, car une plus grande surface échangera de l'eau avec le sous-sol que la vraie rivière. Par conséquent, la présente étude teste l'approximation de l'écoulement du canal à sous-échelle par un coefficient de rugosité à échelle réduite dans l'équation de la vague cinématique. À cette fin, une relation entre la taille de la cellule de grille et la largeur

de la rivière est utilisée pour corriger la vitesse d'écoulement, qui suit une modification simplifiée de l'équation de Manning-Strickler. Le taux d'exfiltration et d'infiltration entre le sous-sol et la rivière est également corrigé sur les lits de rivière par une conductivité hydraulique saturée à échelle réduite en fonction de la résolution de grille, même si la taille de grille est relativement grande. La méthodologie de mise à l'échelle est mise en œuvre dans un modèle hydrologique couplant ParFlow (PARallel FLOW) et Community Land Model (CLM). Le modèle est appliqué sur le bassin du Rhin supérieur (entre la France et l'Allemagne) pour une période allant de 2012 à 2014 et à une résolution spatiale de 0,055° (~6 km). La validité des résultats est examinée avec des données satellites et in situ par le biais d'une application innovante de la méthode de fiabilité du premier ordre (FORM). L'approche de mise à l'échelle montre que les estimations d'humidité du sol se sont améliorées, en particulier en été et en automne, lorsqu'elles sont validées croisées avec des observations indépendantes d'humidité du sol fournies par l'Initiative sur le changement climatique (CCI). La Fig. 1.2 montre le plan de ce chapitre. Les résultats mettent en évidence l'utilisation d'une procédure simple d'échelle du coefficient de Manning et de la conductivité hydraulique saturée pour prendre en compte le taux d'infiltration/exfiltration réel dans les modèles hydrologiques à grande échelle avec une résolution de grille horizontale constante. La procédure d'échelle montre également des améliorations globales dans l'estimation du niveau de la nappe phréatique, en particulier là où le niveau de la nappe phréatique est faible (moins de 5 mètres de la surface). Le sujet est développé dans le chapitre IV. Il a fait l'objet d'un article publié dans le Journal of Hydrology et présenté à l'Assemblée générale de l'EGU 2022 (Soltani et al., 2022 a et b).
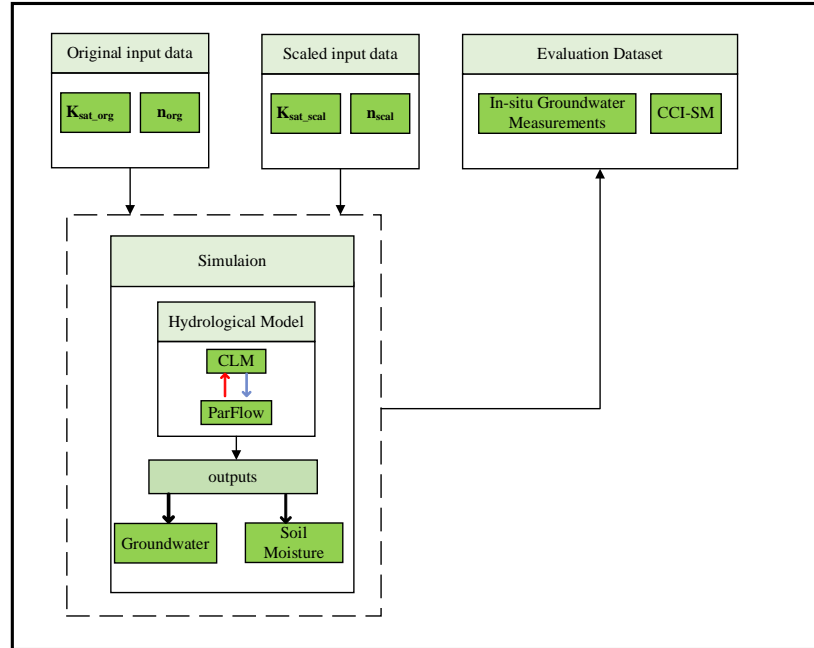
Fig. 1.2 Outline of the chapter VI

1.4.4 An overview of Chapter V: Multivariate satellite remote sensing data assimilation for improving the integrated subsurface-land surface hydrological model ParFlow-CLM: A case study of Iran

In order to make an assessment of climate change and human effects, total water storage (TWS) should be monitored constantly. Therefore, it is essential to develop effective methods such as hydrological modeling to monitor and predict TWS. However, there is great uncertainty and inaccuracy in different aspects of modeling due to the simplification of meteorological physical processes, problems arising from data limitations, and imperfect atmospheric forcing. Observation datasets from satellite remote sensing provide a new source of data that can help us better understand hydrologic processes. Data Assimilation (DA) is the process of combining these new observations with hydrological models to improve model performance.

In this study, the soil moisture from Soil Moisture and Ocean Salinity (SMOS) satellite and TWS from the Gravity Recovery and Climate Experiment (GRACE) is obtained, which assimilated into the fully coupled subsurface-surface hydrological model ParFlow-CLM using the Ensemble Kalman Filter (EnKF). Fig. 1.3 shows the outline of this chapter. The assimilation performance of different types of observations is evaluated in the three assimilation methodologies over a case study in Iran, (i) GRACE-only (GRACE DA) for the time period of 2015-2017, or (ii) SMAP (Soil

Chapter I: Introduction

Moisture Active Passive)-only (SM DA for the time period of 2015-2020, or (iii) joint assimilation of GRACE and SMOS (multivariate DA) for the time period of 2015-2017. Results indicate that the performance of DA mainly depends on the type of observations that are assimilated. GRACE DA improves only the groundwater component, while SM DA improves top soil moisture but degrades groundwater storage estimations. When both observations are incorporated (multivariate DA), the accuracy of both soil moisture and groundwater storage estimates improves. These findings show how multivariate DA can help to improve many model states simultaneously, resulting in a more resilient DA system. The topic is developed in chapter V. It has been the subject of a presentation in the international conference "Groundwater, key to the Sustainable Development Goals".

1.4.4 Vue d'ensemble du chapitre V: Assimilation de données de télédétection satellitaire multivariée pour améliorer le modèle hydrologique intégré de subsurface- surface ParFlow-CLM : une étude de cas en Iran.

Pour évaluer les effets du changement climatique et des activités humaines, le stockage total d'eau (TWS) doit être constamment surveillé. Il est donc essentiel de développer des méthodes efficaces telles que la modélisation hydrologique pour surveiller et prédire le TWS. Cependant, il existe une grande incertitude et une grande imprécision dans différents aspects de la modélisation en raison de la simplification des processus physiques météorologiques, des problèmes liés aux limitations des données et de l'imperfection de la force atmosphérique. Les ensembles de données d'observation de la télédétection satellitaire fournissent une nouvelle source de données qui peuvent nous aider à mieux comprendre les processus hydrologiques. L'assimilation de données (DA) est le processus de combinaison de ces nouvelles observations avec des modèles hydrologiques pour améliorer les performances du modèle.

Dans cette étude, l'humidité du sol provenant du satellite Soil Moisture and Ocean Salinity (SMOS) et le TWS provenant de la Gravity Recovery and Climate Experiment (GRACE) sont obtenus, qui sont assimilés dans le modèle hydrologique de subsurface-surface entièrement couplé ParFlow-CLM à l'aide du filtre de Kalman de l'ensemble (EnKF). La Fig. 1.3 montre le plan de ce chapitre. Les performances d'assimilation de différents types d'observations sont évaluées dans les trois méthodologies d'assimilation sur une étude de cas en Iran, (i) GRACE seulement (GRACE DA) pour la période de 2015-2017, ou (ii) SMAP (Soil Moisture Active Passive) seulement (SM DA)

----

pour la période de 2015-2020, ou (iii) assimilation conjointe de GRACE et SMOS (DA multivariée) pour la période de 2015-2017. Les résultats indiquent que la performance de DA dépend principalement du type d'observations qui sont assimilées. GRACE DA améliore uniquement la composante de l'eau souterraine, tandis que SM DA améliore l'humidité du sol superficiel mais dégrade les estimations du stockage d'eau souterraine. Lorsque les deux observations sont incorporées (DA multivariée), la précision des estimations d'humidité du sol et de stockage d'eau souterraine s'améliore. Ces résultats montrent comment la DA multivariée peut aider à améliorer simultanément de nombreux états de modèle, ce qui entraîne un système de DA plus résilient. Le sujet est développé dans le chapitre V. Il a fait l'objet d'une présentation lors de la conférence internationale "Groundwater, key to the Sustainable Development Goals".
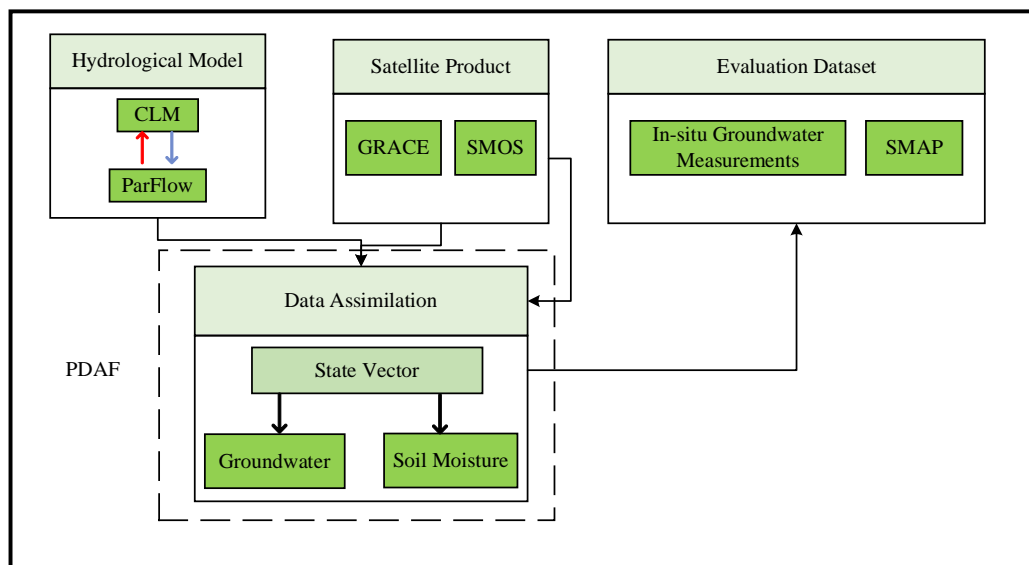
Fig. 1.3 Outline of the chapter V

Chapter II: Review of Assimilating GRACE Terrestrial Water Storage Data into Hydrological Models

---

2.1. Introduction

Since climate change and anthropogenic activities can influence the cycle of water and energy, which is followed by hazards such as floods and droughts (Stocker et al., 2013), monitoring and predicting water resource changes have become more important. Accurate quantification of water storage changes is one reliable approach to determine the availability and sustainability of water resources. As a result, it is essential to monitor hydrological processes, as well as water states and fluxes at various temporal and spatial resolutions. The hydrological processes are multifaceted and different hydrological models are applied to simulate the water cycle on various system sizes from small basins to global scales to quantify the different components of it (Sood and Smakhtin, 2015). These models strive to represent reality as much as possible, but there is always a degree of simplification involved, while the empirical model parameters and insufficient and imperfect climate input data are also subject to uncertainty (Van Dijk et al., 2014). Climate input data obtained from imperfect in situ measurements impede reliable simulation results from a hydrological model due to limitations in the spatiotemporal availability of in-situ data (Soltani et al., 2020). Alternatively, remote sensing technology with different spatiotemporal resolutions provides a unique opportunity not only to obtain hydrological parameters e.g., precipitation (e.g., Alazzy et al., 2017; Najmaddin et al., 2017), soil moisture (e.g., Ray et al., 2017), evapotranspiration (e.g., Liou and Kar, 2014) but also to improve a hydrological model's performance. In particular, the Gravity Recovery and Climate Experiment (GRACE) and GRACE Follow-On (GRACE-FO) missions which have been active since 2002, have an important role in representing surface and sub-surface physical processes related to water redistribution in the Earth system by estimating Terrestrial Water Storage (TWS) (e.g., Kusche et al., 2012; Forootan et al., 2014a; Wouters et al., 2014; Soltani et al., 2020).

Some studies reviewed the application of GRACE data in monitoring of TWS due to its recent developments and popularity in hydrology (e.g., Frappart and Ramillien, 2018; Güntner, 2008; Jiang et al, 2014). Jiang et al (2014). Those have reviewed the hydrological application of GRACE

Chapter II: Review of Assimilating GRACE Terrestrial Water Storage Data into Hydrological Models

---
data in some distinct categories including 1) TWS change monitoring, 2) hydrological components evaluation, 3) drought analysis and 4) glacier mass balance detection.

GRACE TWS data also can be used by advanced statistical and numerical methods to modify a hydrological model's output to reduce the input climate data uncertainty influence and mitigate the negative impact of using an improper model structure or model parameters. GRACE TWS data obtained by using strong filtering strategies is assumed as a model constraint based on uncertainties associated with both model and data, which helps to enhance flux and storage simulations. With the growth of satellite remote sensing products, GRACE data assimilation into hydrological models has attracted enormous interest in hydrology (e.g., Zaitchik et al., 2008; Su et al., 2010; Forman et al., 2012; Eicker et al., 2014; Tangdamrongsub et al., 2015; Reager et al., 2015; Eicker et al., 2016; Schumacher et al., 2016b; Schumacher et al., 2016a; Tangdamrongsub et al., 2017; Khaki et al., 2018b; Khaki et al., 2018c; Tangdamrongsub et al., 2018).

In fact, the interaction of models and data is a reciprocal process in which data can serve the modeling purpose by supporting model discrimination, parameter refinement, uncertainty analysis, and in which models deliver a tool for data fusion (assimilation), interpretation, interpolation (Rajabi et al., 2018). Some studies provide a technical review of large-scale hydrological models (Kauffeldt et al., 2016) and data assimilation techniques (Montzka et al., 2012; Lahoz and Schneider, 2014; Houtekamer and Zhang, 2016; Bannister, 2017).

The following reasons have motivated us to write this review on assimilation of GRACE TWS data into hydrological models:

1) to address the lack of a comprehensive review of GRACE TWS data assimilation applications in hydrology and new opportunities in this subject. Although, Banerjee and Kumar (2019) have reviewed the application of GRACE TWS data into hydrological models, challenges and advances of assimilating GRACE TWS data into hydrological models, have not adequately been discussed.

2) to investigate different aspects of capabilities of popular data assimilation filtering methods in hydrology applications that must be properly understood and addressed.

Chapter II: Review of Assimilating GRACE Terrestrial Water Storage Data into Hydrological Models

----

3) to provide readers with an in-depth review of solutions of inconsistency between hydrological water fluxes, which refers one of the well-known challenges of data assimilation implementation in water budget systems.

The key objectives of this study can be categorized as follows: 1) to discuss the physics behind the acquisition of TWS data through GRACE satellites and the available data products, 2) to investigate the limitations of GRACE TWS data including coarse spatiotemporal resolution, the effect of the correlated GRACE TWS data errors on the data assimilation results and appropriate solutions for handling these errors during data assimilation procedures, 3) to highlight available data assimilation strategies to describe their benefits and limitations in the integration GRACE TWS data into hydrological models. Understanding these challenges and limitations can assist in proposing innovative assimilation filtering methods to merge GRACE TWS data with hydrological model's outputs.

The outline of the chapter is demonstrated in Fig. 2.1. In section 2.2, we describe the details of GRACE data including mathematical representation of gravity field changes and their conversion to equivalent water heights. In this section, we also provide detailed information on GRACE TWS data application in monitoring hydrology, GRACE TWS data error with an emphasis on the problems that we are facing with assimilation of GRACE TWS data into hydrological models and their solution and an extended review of available GRACE TWS data filtering techniques. Section 2.3 introduces different hydrological models which are often chosen and their important characteristics in data assimilation processes. Section 2.4 gives a thorough review of the existing assimilation filtering techniques for hydrological applications. Also, in this section, details of advances in assimilation and supplementary issues such as details of preserving water balance of models after data assimilation are given. Finally, concluding remarks and future prospects are summarized in sections 2.5 and 2.6, respectively.

Chapter II: Review of Assimilating GRACE Terrestrial Water Storage Data into Hydrological Models

----
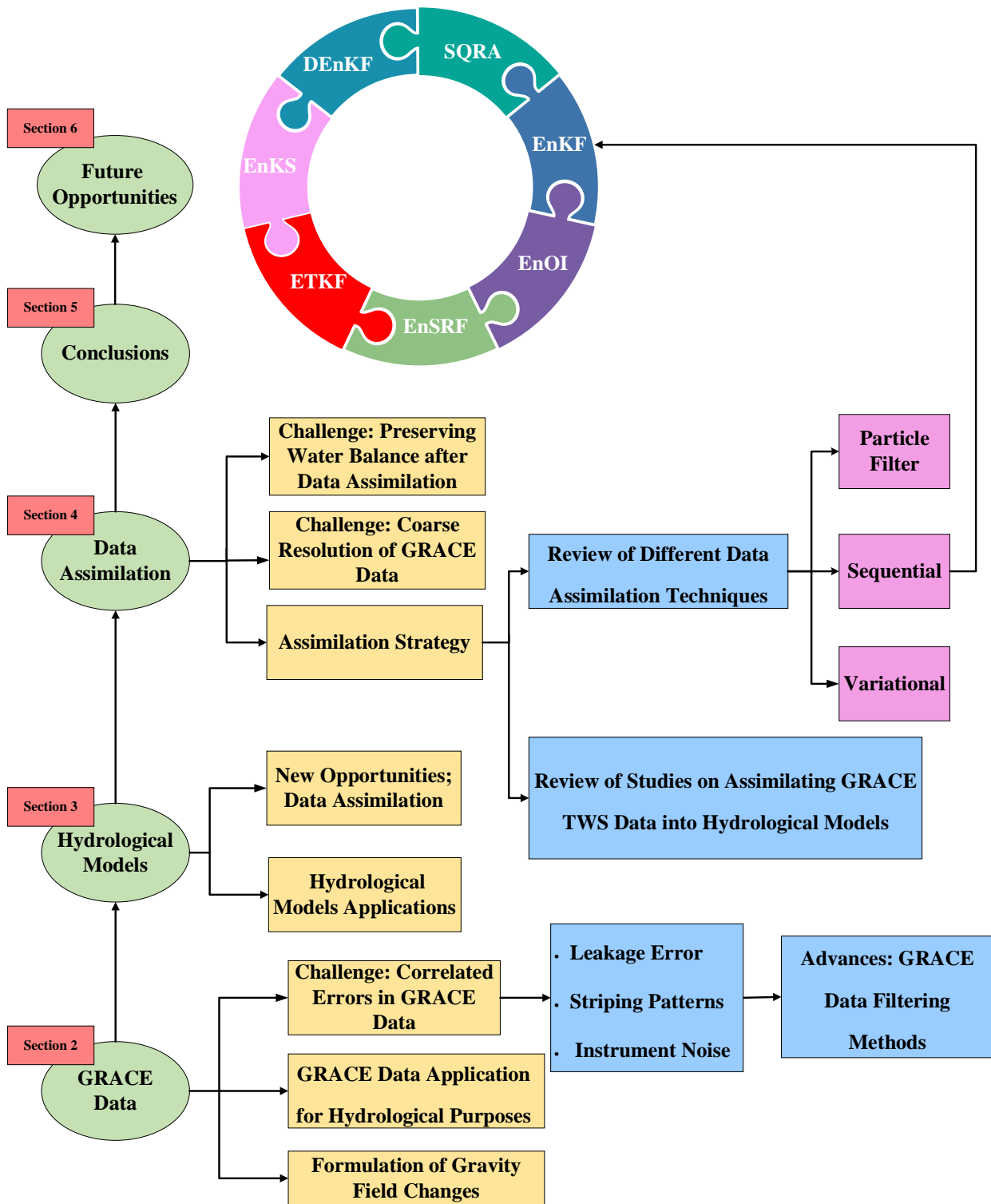
Fig. 2.1 Outline of the chapter II

Chapter II: Review of Assimilating GRACE Terrestrial Water Storage Data into Hydrological Models

----

2.2. GRACE Data and Gravity Recovery

The Gravity Recovery and Climate Experiment (GRACE) mission which has been active since 2002, has two satellites in polar orbit for monitoring the earth continuously (Tapley et al., 2004). GRACE uses geodesy to obtain global maps of the gravity field of the earth over time (Schmidt et al., 2006). National Aeronautics and Space Administration (NASA) of the USA and the Deutsches Zentrum fur Luft- und Raumfahrt (DLR) in Germany collaborate for the GRACE satellite mission (Tapley et al., 2005). The GRACE twin satellites are nearly identical and have tandem formation with a spacing of 220 km between each other in one orbital plane. Their altitude is 500 km (Mayer-Gürr, 2008). The first satellite may reach a gravity anomaly of positive sign which will increase its attraction and thereby, the distance between the satellites increases. When the second satellite reaches the anomaly, it will be attracted to it, thereby reducing the inter-satellite distance. As a result, GRACE can demonstrate the mass changes in the earth surface in an aggregate form but cannot distinguish the components. GPS receivers inside the satellites allow them to accurately determine their positions. The K-band measurements are also time-tagged. Satellite laser ranging reflectors are used to determine the orbit location. Accelerometers are installed on the satellites which measure the surface forces from sources that are not due to gravity such as air drag. This influence is removed from the GRACE data (Mayer-Gürr, 2008). Finally, the relative and absolute satellite orientations are determined via two-star cameras (see more details in Inacio et al., 2015).

The GRACE data are analyzed in three centers which are the CSR (Center for Space Research) in USA, the Geo-ForschungsZentrum (GFZ) in Germany, and the JPL (Jet Propulsion Laboratory) in USA. Other research centers that analyze the level-2 products are the University of Graz in Austria, the University of Bonn in Germany, NASA Goddard Space Flight Center in USA, Delft University of Technology in Netherlands, Space Geodesy Research Group in France, and The Ohio State University in the USA (Tapley et al., 2004; Güntner et al., 2008). GRACE data are presented in the form of Mass Concentration (mascons) potential spherical harmonic coefficients (C_{nm} and S_{nm}) which are called the level 2 GRACE product. They should be converted to TWS which is the summation of different subsurface and surface of water compartments such as surface water storage, snow, soil moisture, vegetation and groundwater.

Chapter II: Review of Assimilating GRACE Terrestrial Water Storage Data into Hydrological Models

----

2.2.1 Formulation of Gravity Field Changes

Laplace's equation in the vacuum is satisfied by V which represents gravitational potential. V can be expressed as a sum of harmonic functions $Y_n(\lambda, \theta)$ in spherical coordinates because it is harmonic. In Eq. (2.2), (λ, θ, r) shows the geocentric location vector in spherical coordinates. θ, λ and r represent the geographical co-latitude (rad), longitude (rad) and the distance (m) to the origin of an Earth-fixed coordinate system, respectively (Heiskanen and Moritz, 1967).

$$\Delta V = 0 \tag{2.1}$$

$$V(\lambda, \theta, r) = \sum_{n=0}^{\infty} \frac{1}{r^{n+1}} Y_n(\lambda, \theta) \tag{2.2}$$

$$Y_n(\lambda, \theta) = \sum_{m=0}^{n} \left[c_{nm} C_{nm}(\lambda, \theta) + s_{nm} S_{nm}(\lambda, \theta) \right] \tag{2.3}$$

c_{nm}, s_{nm} and C_{nm}, S_{nm} are spherical harmonic coefficients and surface spherical harmonics of degree n and order m, respectively (Heiskanen and Moritz, 1967). Spherical harmonic coefficients introduce a complete orthogonal system on the surface of the sphere as Eq. (2.4) and Eq. (2.5).

$$C_{nm} = \overline{P}_{nm}(\cos\theta)\cos(m\lambda) \tag{2.4}$$

$$S_{nm} = \overline{P}_{nm}(\cos\theta)\sin(m\lambda) \tag{2.5}$$

The normalized associated Legendre functions ($\overline{P}_{nm}$) are often evaluated by using a new stable recursion formula (Heiskanen and Moritz, 1967). The potential field can be represented as Eq. (2.6) by regarding the radius (R) and the mass (M) of the Earth and Newton's gravitational constant (G).

$$V(\lambda, \theta, r) = \frac{GM}{R} \sum_{n=0}^{\infty} \left(\frac{R}{r}\right)^{n+1} \sum_{m=0}^{n} \left[c_{nm} C_{nm}(\lambda, \theta) + s_{nm} S_{nm}(\lambda, \theta) \right] \tag{2.6}$$

Chapter II: Review of Assimilating GRACE Terrestrial Water Storage Data into Hydrological Models

----

With choice of $\dfrac{GM}{R}$ factor, c_{nm} and s_{nm} which are called Stokes' coefficients, are dimensionless.

Mass redistributions depend on time. Therefore, consideration of changes of the gravitational potential are represented in terms of changes of the Stokes' coefficients Δc_{nm} and Δs_{nm} as Eq. (2.7).

$$\Delta V(\lambda,\theta,r) = \frac{GM}{R} \sum_{n=1}^{\infty} (\frac{R}{r})^{n+1} \sum_{m=0}^{n} \left[\Delta c_{nm} C_{nm}(\lambda,\theta) + \Delta s_{nm} S_{nm}(\lambda,\theta) \right] \qquad (2.7)$$

The GRACE observation shows the distribution of the mass in the surface of the earth. This was studied by Wahr et al. (1998) using a thin surface layer. They used surface density change $\Delta\sigma$ ($\dfrac{kg}{m^2}$) instead of Δm (kg) or mass changes. The relationship between $\Delta\sigma$ and the gravity field of the earth is:

$$\Delta\sigma(\lambda,\theta) = \sum_{n=1}^{\infty} \sum_{m=0}^{n} \Delta c^{\wedge}_{nm} C_{nm}(\lambda,\theta) + \Delta s^{\wedge}_{nm} S_{nm}(\lambda,\theta) \qquad (2.8)$$

The formula that relates the coefficients in the above formula with Stokes' coefficients is described by:

$$\begin{bmatrix} \Delta c_{nm} \\ \Delta s_{nm} \end{bmatrix} = \frac{(1+k_n{}')}{(2n+1)} \frac{4\pi R^2}{M} \begin{bmatrix} \Delta c^{\wedge}_{nm} \\ \Delta s^{\wedge}_{nm} \end{bmatrix} \qquad (2.9)$$

The surface density changes in Eq. (2.9) cause a change in direct gravity and an indirect attraction because of the loading and deformation of the crust of the earth (Wahr et al., 1998). The gravitational load Love numbers $k_n{}'$ represents the indirect effect (Farrell, 1972).

The equivalent water height or ΔE (m) of the density changes $\Delta\sigma$ can be obtained by converting the TWSA and dividing it by the seawater mean density $\rho_w = 1025 \dfrac{kg}{m^3}$ via the following relationship:

$$\Delta E(\lambda,\theta) = \frac{M}{4\pi R^2 \rho_w} \sum_{n=1}^{\infty} \sum_{m=0}^{n} \frac{2n+1}{1+k_n{}'} [\Delta c_{nm} C_{nm}(\lambda,\theta) + \Delta s_{nm} S_{nm}(\lambda,\theta)] \qquad (2.10)$$

Chapter II: Review of Assimilating GRACE Terrestrial Water Storage Data into Hydrological Models

----

Fig. 2.2 shows a summary of GRACE data processing steps and the TWS concept. This figure shows how level 2 GRACE data is processed and converted to GRACE TWS data. The low degree spherical harmonics coefficients e.g., degree 1 coefficients from Swenson et al. (2008) to account for the movement of the Earth's centre of mass and degree 2 and order 0 (C20) coefficients from Satellite Laser Ranging solutions (e.g., Wilson and Rodell, 2006) are replaced with more accurate estimates. In order to extract hydrological mass variations from the observations, tidal and non-tidal high frequency mass variations e.g., fast mass changes in the ocean and atmosphere, are removed using different gravity recovery techniques and different background models. The effect of glacial isostatic adjustment (GIA) is treated as a post-processing step in hydrological applications, as it is usually not reduced. A detailed list of post-processing steps can be found in Mayer-Gürr et al. (2012).
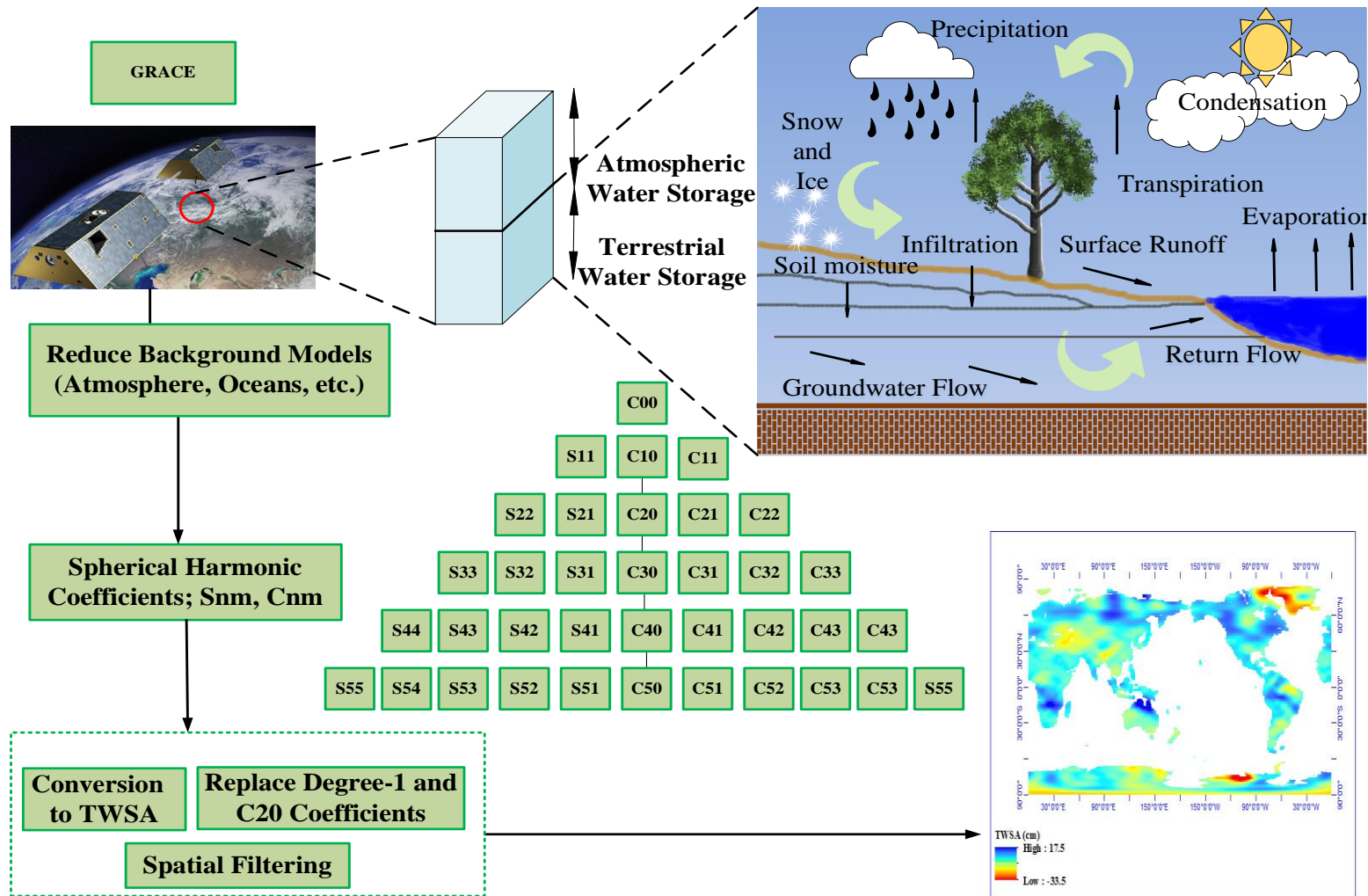
Fig. 2.2 The procedure of spherical harmonic coefficient post processing and conversion to GRACE TWS data (more details are available in section 2.2.1)

Chapter II: Review of Assimilating GRACE Terrestrial Water Storage Data into Hydrological Models

---

2.2.2 GRACE Application for Hydrological Purposes

Investigating the interaction between TWS and other components of the water budget is very important in assessing the availability of freshwater resources (Van Dijk et al., 2014). To date, different tools have been used to investigate water storages and their interactions with other components of the water balance that can be referred to ground measurements, hydrological models, and satellite remote sensing data.

Hydrology benefits from the gravity data from GRACE satellite because a large portion of the changes in *g* is due to changes in water in the ocean, atmosphere and continental water storage (Ramillien et al., 2008). Climate and geophysical processes need an understanding of the water cycle across the continents which can be derived from the mass changes of the earth surface (Ilk et al., 2004).

In order to isolate the hydrological part of the GRACE signal, Ramillien et al. (2004), Rodell and Famiglietti (1999), Seitz et al. (2010), Grippa et al. (2011), Awange et al. (2009) and Longuevergne et al. (2010) have presented various methods. They all mention that the water storage in the continents and its changes in time and space can be obtained from the gravimetry satellite observations (Schmidt et al., 2006).

TWS across the globe first became available as a unified database with the application of GRACE. Many models that simulate the hydrological cycle can be validated and improved with GRACE data (Schmidt et al., 2006). GRACE TWS has varying time resolutions of one day (Kurtenbach et al., 2009) to one month (the publicly available data) which is also dependent on the method of data analysis. The resolution in space is on the order a few hundred kilometers (Schmidt et al., 2006). GRACE TWS has found applications in geophysical applications as well as climate and hydrology studies (see Kusche et al., 2012; Famiglietti and Rodell, 2013; Wouters et al., 2014; Famiglietti et al., 2015; Chen et al., 2016; Soltani et al, 2020). The monthly GRACE products have been compared to global hydrology models in terms of the terrestrial water storage variation by Wahr et al. (2004) and Schmidt et al. (2006). Seasonal GRACE data generally agree with the hydrological model's output (Schmidt et al., 2006), although there are some errors. The problems in model description or parameters can be alleviated using GRACE. Syed et al. (2005), Yamamoto

Chapter II: Review of Assimilating GRACE Terrestrial Water Storage Data into Hydrological Models

----

et al. (2007) and Winsemius et al. (2006) have stated that GRACE is not good for application in small basins (<150,000 km^2) because of its resolution.

GRACE cannot differentiate between TWS components such as subsurface or soil moisture. As a result, TWSA components separation of GRACE have been attempted for snow (e.g., Frappart et al., 2006; Niu et al., 2007 and Llubes et al., 2007), evapotranspiration (e.g., Rodell et al., 2004) and groundwater (e.g., Rodell et al., 2007). For this purpose, model outputs and ground measurements are used to separate known components, and the integral gravity signal of the GRACE is thus decomposed. Several methods exist for separation of the signals in recent studies. Inversion and statistical decomposition were applied by Rietbroek (2014), Schmeer et al. (2012) and Forootan (2014b) in order to separate GRACE TWS into different storage compartments. Fig. 2.3-a shows the number of publications by the year which are available on Scopus website until April 17, 2020 with 'GRACE' in the title or abstract or their keywords. The number of publications has declined slightly in 2017 and the beginning of 2018, likely because of the decommissioning of GRACE and the lack of data beginning in June 2017. GRACE-FO mission has started collecting data again in late summer 2018. Therefore, the number of publications on GRACE data on all topics is expected to rise again. Taking into consideration the year 2019, which had the highest number of publications on record with 219 that year, most papers were published on assimilation of GRACE data into hydrological models or on how to calibrate and analyze the hydrological models. The next most frequent topic of published papers on GRACE in that year is on glacier mass, ice melt, and isostatic adjustment, followed by papers on groundwater storage, and then papers on earthquakes or crustal deformation. There were also a significant number of papers on ocean currents, atmosphere, weather, and surface water storage. As Fig. 2.3-b depicts, American and Chinese researchers have published more papers in this field. Fig. 2.3-c shows the top ten journals which have published the largest number of papers on GRACE.

Chapter II: Review of Assimilating GRACE Terrestrial Water Storage Data into Hydrological Models

----

a)

April 17, 2020

b)

- United States
- China
- Germany
- Australia
- France
- Netherlands
- United Kingdom
- Canada
- India
- Japan

c)

- Geophysical Research Letters
- Journal Of Geophysical Research Solid Earth
- Water Resources Research
- Geophysical Journal International
- Remote Sensing
- Journal Of Geodesy
- Journal Of Hydrology
- Journal Of Geophysical Research Oceans
- Hydrology And Earth System Sciences
- Advances In Space Research
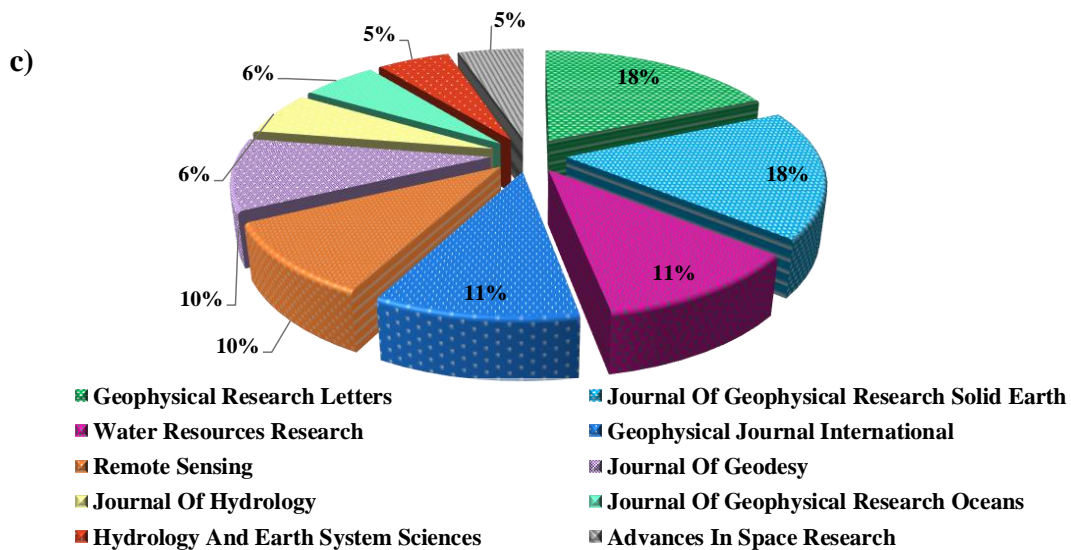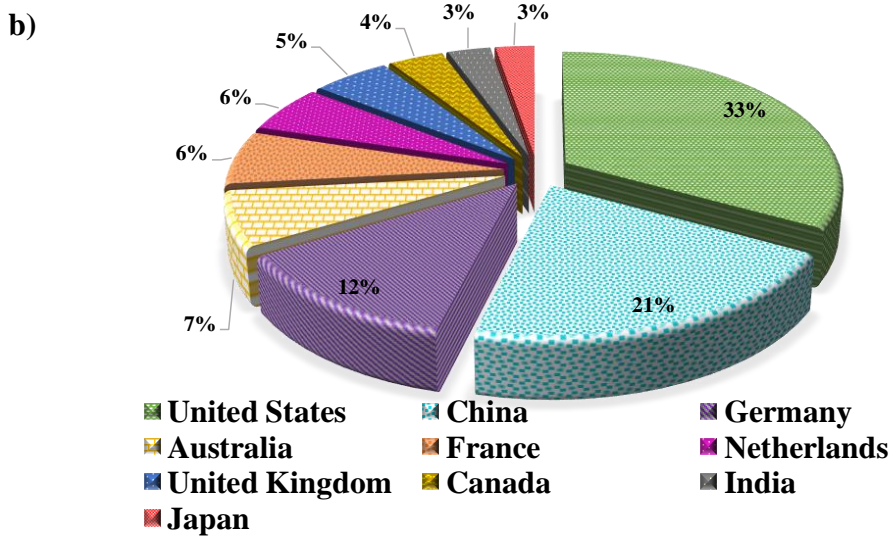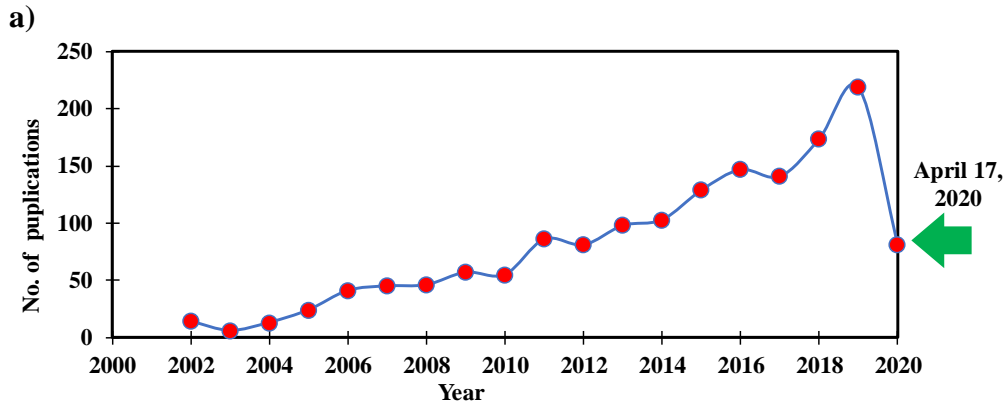
Fig. 2.3 Number of publications which are available on Scopus website until April 17, 2020 with" Recovery and Climate Experiment" or "GRACE" in the title, abstract or their keywords. a) Number of publications on GRACE per year b) Top ten countries in number of publications on GRACE c) Top ten journals in number of publications on GRACE.

2.2.3 GRACE Data Errors

Spherical harmonic coefficients of GRACE data have various error sources. Anisotropic spatial sampling of the satellite results in correlated or colored noise. The instruments such as GPS, K-band ranging system, star cameras and accelerometers have noise. In order to generate error samples of TWS in data assimilation procedures, five scenarios might be used, three of them resulting in white noise and two of them resulting in correlated errors. Fig. 2.4 depicts all five scenarios to generate GRACE data errors. In the following, we explain how these five scenarios are generated. White noise error samples can be generated by (1) using standard deviations based on literature or (2) propagating errors from standard deviations of potential coefficients c_{nm} and s_{nm} or (3) propagating errors from the full covariance matrix of potential coefficients c_{nm} and s_{nm} to standard deviations of TWSA. Correlated error samples can be generated from (4) error propagation of standard deviations of potential coefficients c_{nm} and s_{nm} or from (5) propagation of the full error covariance matrix of potential coefficients c_{nm} and s_{nm} to a full error covariance matrix of TWSA (Schumacher et al., 2016b).
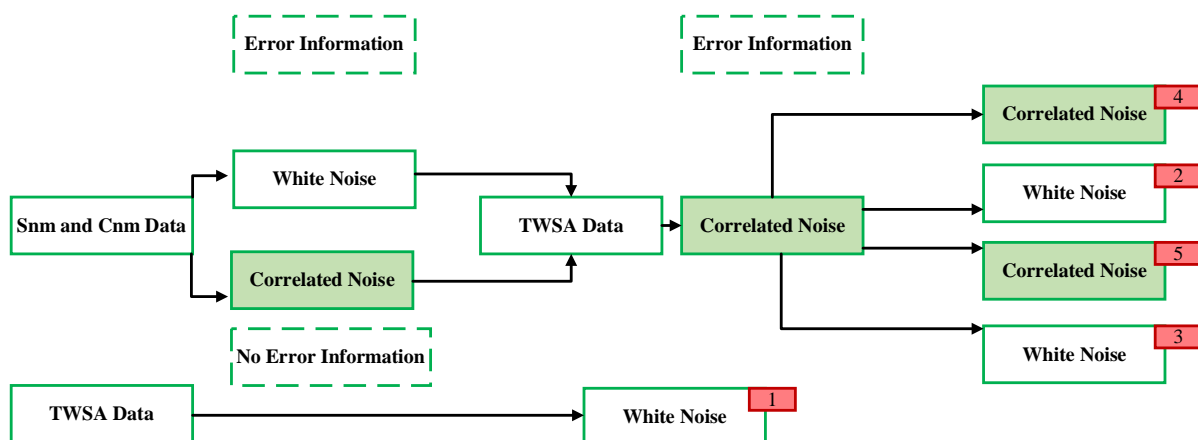
Fig. 2.4 Flowchart of GRACE data (TWSA and spherical harmonic coefficients) errors description

Chapter II: Review of Assimilating GRACE Terrestrial Water Storage Data into Hydrological Models

----

Models in post-processing do not completely reduce short-term mass changes which results in temporal aliasing (Dobslaw et al., 2016; Forootan et al., 2013, 2014b). This results in striping patterns in the north-south orientation in the spatial domain. To smooth this artefact, smoothing kernels are used including the non-Gaussian kernel (Swenson and Wahr, 2006; Klees et al., 2008; Kusche, 2007) and isotropic Gaussian kernel (Jekeli, 1981).

Spatial averaging results in interference in the values of the anomalies such as leakage which may attenuate the signal power. Because of these errors, gravity anomalies are not perfectly separated in different parts of the world and between oceans and the land surface (Baur et al., 2009). To reduce spatial leakage, various filtering methods have been implemented which are categorized into the following three groups. 1) Estimation of in and out leakage with averaging kernels have been attempted by Seo and Wilson (2005); Han et al. (2005); Baur et al. (2009); Swenson and Wahr (2002); and Longuevergne et al. (2010). 2) Some filtering techniques are based on scaling factors that are obtained from artificial data (e.g., Landerer and Swenson, 2012; Long et al., 2015). Forootan et al. (2014b); Frappart et al. (2011) and Frappart et al. (2016) have used inversion to separate the signal and reduce the leakage at the same time. Filters based on scaling factors have disadvantages such as the need for hydrological models to obtain the scale coefficient. The inversion method needs prior data for changes of mass for various components. GRACE TWSA accuracy is important in hydrological data assimilation fields at the basin scale when the basin is much smaller than the GRACE resolution (Longuevergne et al., 2010; Yeh et al., 2006). 3) To improve the consistency between various products, better post-processing techniques can be extremely helpful in studying the water cycle (Eicker et al., 2016). To achieve this, a strong filter method should be used to minimize the noise of the instruments and reduce the aliasing of high frequency changes in the mass data which is un-modelled, while simultaneously reducing the leakage. GRACE data after application of such filters is thus more suited for data assimilation. Kernel Fourier Integration (KeFIn) filter was introduced by Khaki et al. (2018a) to smooth noise in GRACE data (colored/correlated) and then decrease leakage effects. The KeFIn filtering method not only solves the existing problems such as sensitivity of other leakage filtering methods (e.g. scale factor approaches) but can also be effectively applied to a wide range of basins with differing shapes and sizes.

Chapter II: Review of Assimilating GRACE Terrestrial Water Storage Data into Hydrological Models

---

2.3. Hydrological Modeling; New Opportunities

Hydrological models are considered as an important and necessary tool for water and environment resource management. Hydrological models at the regional scale (e.g., Chiew et al., 1993; Wooldridge and Kalma, 2001; Christiansen et al., 2007; Huang et al., 2017) and global scale (e.g., Döll et al., 2003; Huntington, 2006; Coumou and Rahmstorf, 2012; Van Dijk et al., 2013) are important tools that are used for simulation of hydrological process. Hydrological models give us a better insight into the water cycle on the global and regional scale. Various hydrological models (Moradkhani and Sorooshian, 2008; Devia et al., 2015) have been applied with different levels of success to obtain water storage components e.g., water in ice, glaciers, snow caps, groundwater, surface water and soil moisture and the rate of their changes (e.g., Chiew et al., 1993; Wooldridge and Kalma, 2001; Döll et al., 2003; Huntington, 2006; Van Dijk, 2010). Models are also used for information extraction, data assimilation, interpretation, generalization and interpolation, and identification of information-rich data (Ataie-Ashtiani et al., 2020).

Models are still being developed to better simulate all available hydrological processes and the inclusion of all interactions between water cycle components e.g., interaction between runoff, precipitation and evapotranspiration (Simmons et al., 2019). In any case, uncertainties exist and the modeling remains imperfect. Data sets are still limited in time and space, and our knowledge about empirical parameters is still limited (Vrugt et al., 2013; Van Dijk et al., 2011, 2014). Danesh-Yazdi and Ataie-Ashtiani (2019) argue that planning and management of hydrological systems "without appropriate data and model is gambling", as for a consistent understanding of the system both are required. As a result, the simulation model results are imperfect and uncertain. Some of the model parameters are not easy to interpret, and the computational burden of the more complex models is higher.

Another alternative is incorporating accurate observations into the model for handling these limitations (e.g., McLaughlin, 2002; Zaitchik et al., 2008; Van Dijk et al., 2014; El Gharamti et al., 2016). Since remotely sensed data for different quantities are becoming increasingly available in different coverages and resolutions, model reliability improvement can be achieved with these data. GRACE data assimilation into hydrological models can be used 1) to effectively separate TWS into its components and downscale the coarse resolution of it and 2) to constrain the models' simulations and also their parameters through data assimilation.

Chapter II: Review of Assimilating GRACE Terrestrial Water Storage Data into Hydrological Models

----

The list of commonly applied hydrological models for simulation of water storage compartments s given Table 2.1. Some aspects of a hydrological model in the assimilation process are summarized in the following:

1. Availability of hydrological model code: Access to the code allows the user to edit and make changes. If there is a bug in the model, the open-source availability of the code will help the user to fix it faster. Many studies require a code change to implement a specific purpose. As a result, the availability of a hydrological model code is a special advantage for use in the assimilation process.

2. Data requirements: The data and parameters required to run a hydrological model should be readily available to the user at different time and spatial resolutions.

3. Flexibility of grid structure: Some hydrological models can be run on different spatial scales. However, a number of hydrological models do not have this capability and are implemented on a sub-basin scale. The flexibility of the input data grid is a very important parameter in the assimilation process. This is because it influences the choice of assimilation technique for coarse-resolution satellite data.

4. Flexibility in resolution: Models must provide the possibility of being run at different spatial resolution. If models are not run in a grid structure, flexibility in resolution of computational units should also be investigated.

Table 2.1 Various characteristics and capabilities of popular hydrological models for simulation of water storage compartments (in this table, T: Air temperature, R: Rainfall, W: Wind, PET: Potential evapotranspiration, SR: Solar radiation, Q: Humidity, T_{min}: Minimum air temperature, T_{max}: Maximum air temperature, P: Precipitation, S: Snowfall, GR: Global radiation)

Model	Availability of model code	Minimum forcing data	Flexibility to grid structure	Flexibility in resolution	Ref
CLM	Open Source	*S, R, SR, LW, SP, Q, T, W*	✓	Depends on input data	Bonan et al. (2002)

PCR-GLOBWB	Open Source	*P, T, W, PET, GR, Q*	✓	0.5°	Van Beek and Bierkens (2009)
WaterGAP	Not Available	*P, T, GR, LW*	✓	0.5°	Döll et al. (2003)
W3RA	Open Source	*R, W, T, S, P*	✓	0.5°	Van Dijk (2010)
LISFLOOD	Not Available	*P, PET, T*	✓	Depends on input dada	Burek et al. (2013)
VIC	Open Source	*P, W, T_{min}, T_{max}*	✓	Smaller than 6 km should run carefully	Liang et al. (1994)

2.4. Data Assimilation Methodology for GRACE Data

Data assimilation (DA) constrains the model dynamics and the flow of information using advanced statistical or numerical methods which relate prior and posterior information so that the model results fit better to real world results (Hoteit et al., 2012; Bertino et al., 2003). Fig.2.5 Shows the concept of DA to incorporate new observations with their corresponding uncertainties into models. DA applies corrections based on the uncertainties of simulations and observations at each assimilation step whenever a new observation is available. In other words, the accuracy of simulations and observations determine the weight of observations and correspondingly the level of corrections to be applied to the models by using the Bayesian approach (Hairer et al. 2005), which updates the probability distribution function (PDF) of each state variable which describes the model in the presence of observation and the model is run forward in time until new observations become available for the next update assimilation step. In reality, however, these computations are complex because it is not possible to analytically derive the PDF of the state anymore. When the system is either non-Gaussian or nonlinear e.g., hydrological models, DA becomes more difficult and the posterior PDF is not analytically obtainable for the state variables (Vrugt et al., 2013; Hoteit et al. 2008). Therefore, the Bayesian estimation is numerically solved with sequential or variational filter techniques (Subramanian et al., 2012).
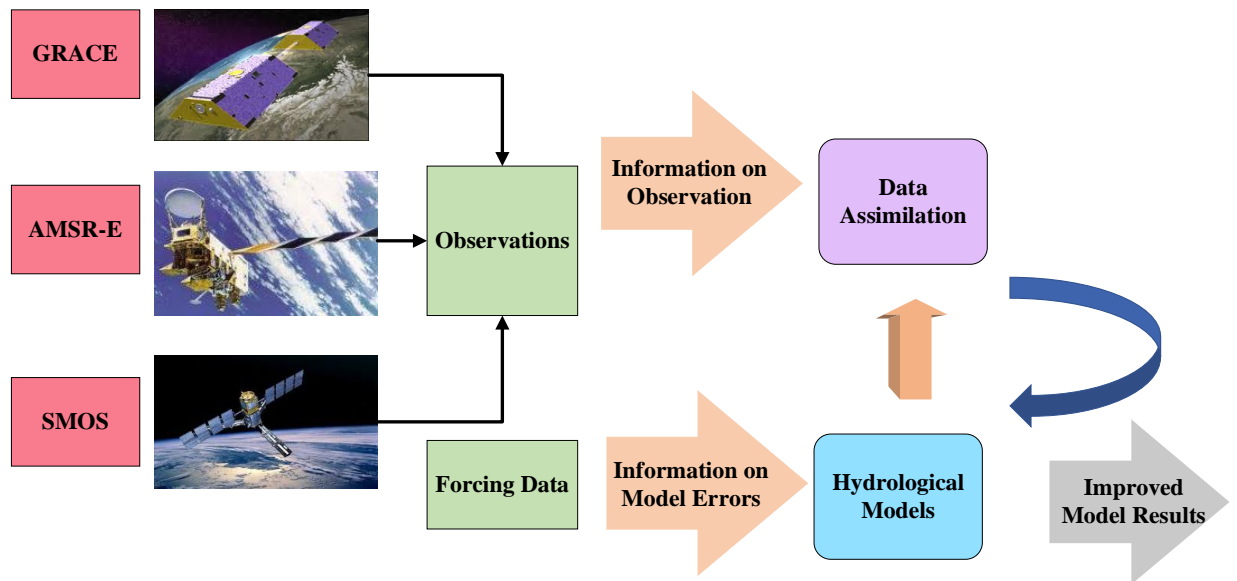
Fig. 2.5 Schematic of how the assimilation of satellite data into a hydrological model to improve a model's outputs

2.4.1 Advances in GRACE DA Techniques

Ocean, earth science and atmospheric studies employ numerical solution of DA with the advancement of high power computing systems and in hydrology with the emergence of state-of-art satellite datasets, it has started to be applied in models for soil moisture (e.g., Brocca et al., 2010; Renzullo et al., 2014; Kumar et al., 2014, 2015), runoff (e.g., Vrugt et al., 2006; Komma et al., 2008; Neal et al., 2009; Lee et al., 2011; McMillan et al., 2013; Li et al., 2015), water storage in surface reservoirs (e.g., Neal et al., 2009; Giustarini et al., 2011), evapotranspiration (e.g., Schuurmans et al., 2003; Pipunic et al., 2008; Irmak and Kamble, 2009) and TWS changes (e.g., Landerer and Swenson 2012; Longuevergne et al. 2013; Awange et al. 2014; Forootan et al. 2014a).

Based on these studies, it is obvious that assimilation of satellite remote sensing data into hydrological models, separately or simultaneously, provides a great opportunity to improve and calibrate hydrological models. Better results can be achieved by multi-satellite products when properly accounting for the measurement errors (see, e.g., Montzka et al. 2012; Renzullo et al. 2014; Tian et al. 2017).

Chapter II: Review of Assimilating GRACE Terrestrial Water Storage Data into Hydrological Models

----

With the availability of TWS from the GRACE, assimilation of GRACE TWS into hydrological models has been done in the past few years to update hydrological model estimates of various water compartments (e.g., Zaitchik et al., 2008; Van Dijk et al., 2014; Tangdamrongsub et al., 2015; Kumar et al., 2016; Girotto et al., 2016, 2017; Khaki et al., 2017a; Schumacher et al., 2018). In addition to different datasets, different DA techniques have also been implemented and tested in hydrological studies as well as hydrologic operational systems.

Various filtering techniques have been proposed and developed in various fields for DA objectives. Among these, variational methods and sequential filtering have gained a lot of attention during the past few decades. In the variational approach, the model solution is fitted to the data given a cost function that measures the error between the state variables and observations (Talagrand and Courtier, 1987). Computer coding of the adjoint system is necessary which needs a lot of time to write the code and also significant computer power to execute the code (Hoteit et al., 2005). Also, the variational methods have limited accuracy because of the DA process and the estimation statistics in this process (Kalnay, 2003; Courtier et al., 1994). Fig. 2.6 shows the efficiency of variational methods as an example. Observation data y_k (green Rhombuses) improves the initial states of the model x_0 as well as original model states x_k^- (red circles and solid line). The modified initial states x_0^+ result in the best fit of the model states x_k^+ (yellow squares and dashed line) and observations.
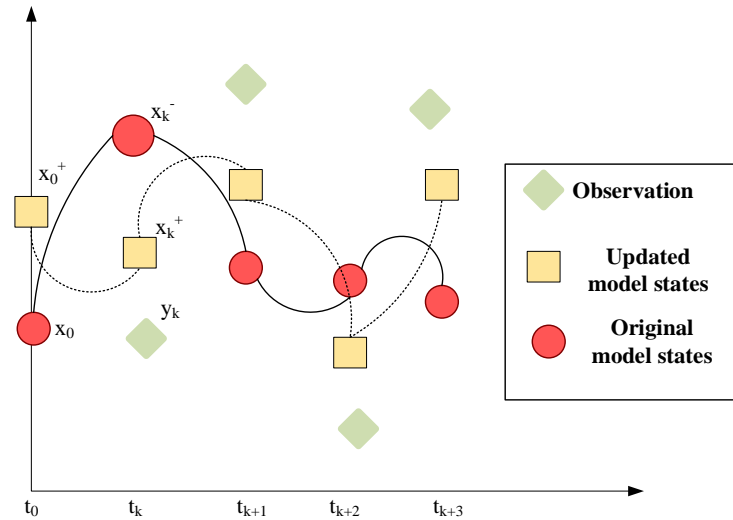
Fig. 2.6 Scheme of variational DA

In sequential methods, the state's prior PDF is used to calculate the posterior PDF with Bayes' theorem (Koch, 2007). First, a forward run is performed with the time-dependent system with Monte Carlo method. Second, an analysis step is needed to adjust assimilation PDF via point-mass weight or particle filtering (see Fig. 2.7). Fig. 2.7 shows, when y_k which is represented in yellow squares, becomes available it is used to improve the current model states x_k^- which is represented in red circles. The best fit to the observations at the current time step k is achieved through the updated model states x_k^+ which is represented in green rhombuses (Hoteit et al., 2012; Evensen, 2009).
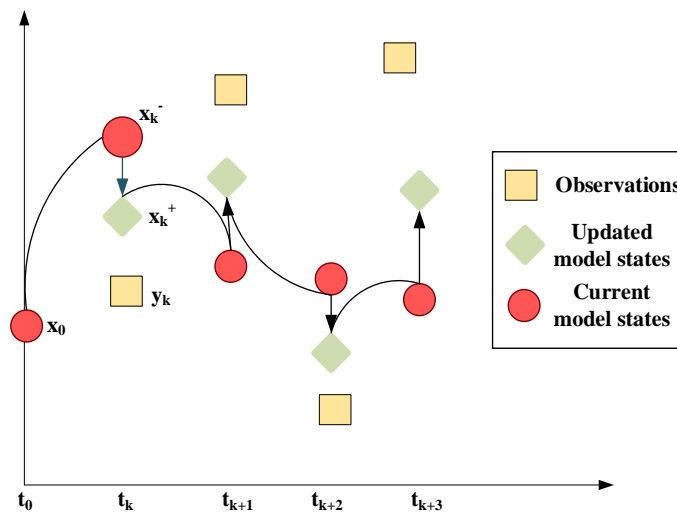
Fig. 2.7 Scheme of sequential DA

Since Sequential DA techniques eliminate the requirement for preserving historical states in DA, they are more popular for high dimensional systems e.g., hydrologic systems. (Hoteit et al. 2002; Bertino et al. 2003; Robert et al. 2006). Two variants of the sequential filtering techniques including the Particle filter (PF) and Ensemble Kalman filters (EnKF) have been used widely in the literature (see, e.g., Moradkhani et al. 2005; Weerts et al. 2006; Zaitchik et al. 2008; Houborg et al. 2012; Moradkhani et al. 2012; Eicker et al. 2014; Renzullo et al. 2014; Tangdamrongsub et al. 2015). A summary of different sequential filtering techniques and their type which are used for hydrological applications is given in Table 2.02.

Table 2.02 Different sequential filtering techniques for hydrological applications

Filter	Abbreviation	Type	Reference
Ensemble Kalman Filter	EnKF	Stochastic Ensemble Kalman Filter	Evensen (1994)
Square Root Analysis	SQRA	Deterministic Ensemble Kalman Filter	Evensen (2004)

Chapter II: Review of Assimilating GRACE Terrestrial Water Storage Data into Hydrological Models

----

Ensemble Transform Kalman Filter	ETKF	Deterministic Ensemble Kalman Filter	Bishop et al. (2001)
Ensemble Square-Root Filter	EnSRF	Deterministic Ensemble Kalman Filter	Whitaker and Hamill (2002)
Ensemble Optional Interpolation	EnOI	Deterministic Ensemble Kalman Filter	Evensen (2003)
Deterministic Ensemble Kalman Filter	DEnKF	Deterministic Ensemble Kalman Filter	Sakov and Oke (2008)
Particle Filter, Multinomial Resampling	PFMR	Particle Filter	Arulampalam et al. (2002)
Particle Filter, Systematic Resampling	PFSR	Particle Filter	Arulampalam et al. (2002)

Sequential methods have shown great promise for assimilation of individual hydrological components, as proven by the previous studies. In any case, assimilation filters' capabilities should be determined from various perspectives. This will help the modeler to properly choose the satellite DA objective. It is expected that DA filters should be able to enhance system state estimation while giving quantitative measures on model uncertainty. In addition, after applying the DA filter, the model should preserve its dynamic stability while the new data are added into the model. In sequential filtering techniques, one of the challenging aspects is observation covariance sampling which is not usually effectively performed (Whitaker and Hamill 2002). For deterministic EnKFs (Hoteit et al. 2015; Sun et al. 2009) and Systematic and Multinomial Resampling particle filtering (PF) (Whitaker and Hamill 2002) there are separate resampling techniques which were developed to solve this problem. This implies that selecting the correct DA filtering method is important and difficult at the same time. Khaki et al., 2018b have dedicated a section to satellite data DA for hydrological modeling and comprehensively describes various methods for differential sequential filtering. Based on Khaki et al. (2018b), prior to and after each assimilation step, it is important to decrease the diagonal values in the error covariance matrices and calculate their mean, min, and

----

max values. Fig. 2.8 shows that the best performances in terms of error reduction in the all-diagonal elements of the error covariance matrices are found for EnSRF, SQRA.
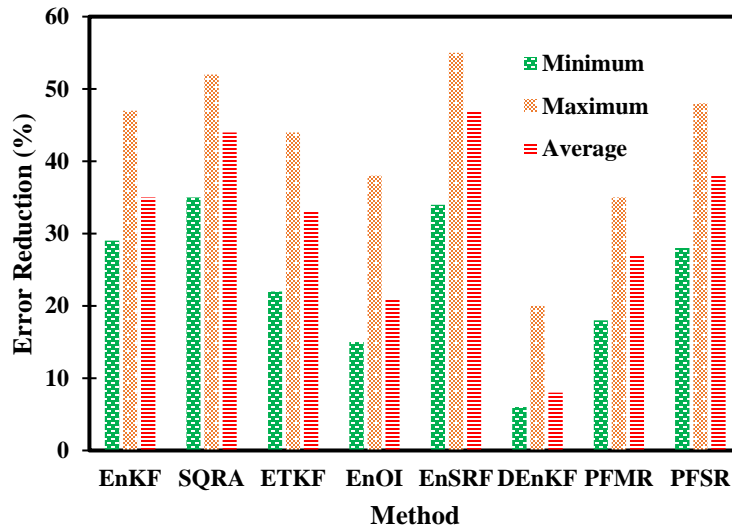
Fig. 2.8 Evaluation of the different sequential filtering techniques performance in terms of error reduction in the all-diagonal elements of the error covariance matrices (Khaki et al., 2018b).

An overview of important studies that address the assimilation of GRACE TWS into hydrological models is given in Table 2.03. In Table 2.03, we extract some important characteristics of these papers including 1) error modeling and 2) chosen assimilation technique to merge GRACE data with hydrological models. The assumption that the observations are not correlated is only true when the observations have higher resolution than the model in reality (the resolution means the independent grid of neighboring points (Stewart et al. 2008; Berger and Forsythe 2004). When GRACE is used, which is typically coarser than other data sets in DA, the assumption that the observations are not correlated will not improve the end results (e.g., Liu and Rabier, 2003; Dando et al., 2007; Stewart et al., 2008).

DA filtering should account for the limitations of GRACE (Schumacher et al., 2016 b). For inverse problems, DA uses the covariance matrix of model states and observations. The error correlations are used to obtain the covariance matrix, and these are typically ill conditioned in GRACE, which hinders the filtering in DA. There is information deficiency, the uncorrelated data is usually synthesized or Gaussian error is used instead. GRACE TWS DA (for basin averaged or grid-based

data) was undertaken previously by assuming that the observations are uncorrelated (white noise) (Zaitchik et al., 2008; Tangdamrongsub et al., 2015; Kumar et al., 2016; Tian et al., 2017). However, in basin-averaged instances, this is correct because averaging increases the non-Gaussian distribution of the noise in the GRACE TWS observations and the result is close to the Gaussian distribution because of the central limit theorem (Stone, 2004).

Chapter II: Review of Assimilating GRACE Terrestrial Water Storage Data into Hydrological Models

----

Table 2.03 Studies on assimilating GRACE TWS into hydrological models

Chapter II: Review of Assimilating GRACE Terrestrial Water Storage Data into Hydrological Models

----

Component	Model	Error	Case study	Filter	References
Groundwater	CLSM	White	Mississippi	EnKS	Zaitchik et al. (2008)
Snow Water Equivalent	CLM	White	North America	EnKF, EnKS	Su et al. (2010)
Snow Water Equivalent	CLSM	White	Mackenzie	EnKS	Forman et al. (2012)
Groundwater, Soil moisture	CLSM	White	Europe	EnKS	Li et al. (2012)
TWS	WGHM	Colored	Mississippi	EnKF	Eicker et al. (2014)
Snow Water Equivalent, River Water Level, Subsurface Storage	W3RA, GLDAS	White	Global	EnKF	van Dijk et al. (2014)
Groundwater, Streamflow	HBV-96	White	Rhine	EnKF	Tangdamrongsub et al. (2015)
Groundwater, Soil moisture	CLSM	White	USA	EnKS	Girotto et al. (2016)
Groundwater, Soil moisture, Snow depth, Streamflow	CLSM	White	USA	EnKS	Kumar et al. (2016)
Snow, Soil moisture, River, Groundwater, Surface Water	WGHM	White, Colored	Mississippi	EnKF, SQRA, SEIK	Schumacher et al. (2016b)
Groundwater	WGHM	Colored	Murray Darling	EnKF	Schumacher et al. (2016a)
Groundwater, Snow, Surface Water	PCR-GLOBWB	White	Northern China	EnKF	Tangdamrongsub et al. (2017)
Groundwater	W3RA	White, Colored	Australia	EnKF, SQRA, ETKF, EnSRF, EnOI, DEnKF, PFSR, PFMR	Khaki, et al. (2017b)
Groundwater	PCR-GLOBWB	Colored	Australia, North China	EnKS	Tangdamrongsub et al. (2018)
Groundwater, Soil moisture	W3RA	Colored	Bangladesh	SQRA	Khaki et al. (2018b)

Groundwater, Soil moisture	W3RA	Colored	Iran	EnSRF	Khaki et al. (2018c)
Groundwater, Soil moisture	W3RA	White, Colored	South America	EnSRF	Khaki et al. (2018d)
Groundwater, Soil moisture	W3RA	Colored	Murray Darling, Mississippi	SQRA, Kalman Takens	Khaki et al. (2019)

2.4.2 Challenges of GRACE DA

Previous studies have shown that RS techniques (using satellite data) have the capability of augmenting hydrological models. However, there are some obstacles when applying observations from RS sources and assimilating them into hydrological models. One of the impediments in this regard is the mismatch in spatial and temporal resolutions between the satellite observations and the model. The model-observation systems are usually nonlinear and the observations have specific error properties. These factors result in problems for applying DA. Because of the complex error properties of GRACE TSW data, merging the dates requires complicated algorithms. Both data and model have uncertainties associated with them, and accurate estimation of the uncertainty properties with improving the DA process. DA process suffers if the uncertainties are either wrongly selected or grossly simplified. As a result, the observation errors should be considered in the model with realistic assumption to ensure that DA will perform satisfactorily using the available metadata and information. Furthermore, it should be noted that satellite DA is a two-edged sword: it can degrade and produce artifacts in certain components of the hydrological model while improving the others. As an example, when performing DA for soil moisture data obtained from satellite readings, the user must be careful that the deep-zone soil moisture is not adversely affected (through wrong corrections or added errors). A central challenge of filtering in DA is upholding the consistency of the hydrological model in terms of closure between the evaporation, precipitation, runoff, and changes in storage. DA may result in the lack of a dynamic balance among the flux terms with the storage variations (Pan and Wood, 2006).

The model structure and the governing equations preserve the changes in water storage consistency with respect to input and output fluxes. Assimilation of GRACE TWS and soil moisture data will result in the lack of model balance because the assimilated states do not have balance closure. As a result, each assimilation cycle may violate the dynamic between water fluxes and water storage changes. This issue needs to be addressed so that the water storage changes can be calculated correctly. Pan and Wood (2006) considered the enforcement of the water balance by using constrained ensemble Kalman filter (CEnKF) (Evensen, 1994). In their study, DA was performed in the southern Great Plains of the US, and an attempt to obtain closure in the water balance equation was made. Pan et al. (2012) and Sahoo et al. (2011) used data merging and CEnKF before

45

using data from different sources, such as ground measurements and satellite data, then performed DA. In this way, the imbalance for the method in a large river basin was mitigated (Zhang et al., 2016). The overarching assumption was that the observations are perfect and enforced closure was attempted. Therefore, the water flux observation uncertainty was not considered in the assimilation process. The resulting strong constraint is not realistic and can lead to overfitting and errors of estimation in different water storage components (Tangdamrongsub et al., 2017). Water storage estimations can be improved by considering the errors in flux observations. To achieve this, the assimilation filter with two steps was performed based on the weakly-constrained ensemble Kalman filter (WCEnKF) (Khaki et al., 2017a).

2.4.3. Future Opportunities

There are many future opportunities for assimilating GRACE TWS data into hydrological models. These are outlined below and in Fig. 2.9.

1) The GRACE Follow-On (GRACE-FO) mission has some improvements as compared to GRACE data e.g., precise measurements of the satellites' pitch and yaw angles and improved the spatial and temporal resolution of the Earth's gravity field solutions. Therefore, the assimilation of GRACE-FO data into hydrological models can improve the performance of hydrological models.

2) Since the accuracy of GRACE TWS data is very important, designing or proposing an efficient and powerful filtering method which should be applied to them in order to improve the data accuracy by removing some of their errors e.g., instruments noise, striping patterns and leakage errors before the assimilation process takes plan is still a challenge. The availability of new user-friendly filters would likely increase the application of GRACE data to study water re-distribution in earth's surface and subsurface in different disciplines e.g., hydrology, earth oceanic and atmospheric science.

3) Separation of the GRACE TWS signals e.g., soil moisture, groundwater in recent studies is still an active research field and has many unresolved issues. Since inversion and statistical decomposition methods which were applied by Rietbroek (2014), Schmeer et al. (2012) and Forootan (2014) have some limitations in separating different GRACE TWS signals, assimilation of GRACE TWS data into hydrological models by considering the physics of the problem and

climate input data provides a unique opportunity to separate different GRACE TWS components. Another important product which is used in DA is satellite or radar soil moisture products e.g., SMOS or AMSR-E, which usually measures top layer soil moisture (e.g., 0–5 cm). Applying different assimilation strategies e.g., simultaneous assimilating GRACE TWS data and soil moisture products, may improve all or some water storage states. The rate of improvement can vary depending on the structure of our chosen hydrological model. We present an example to illustrate the effect of structure of a hydrological model on assimilation results. Since in the structure of the Community Land Model (CLM) which can be coupled with ParFlow (Maxwell et al., 2009), the accuracy of estimation of soil moisture has a great impact on estimating groundwater, soil moisture data along with GRACE data may improve groundwater storage estimates made with hydrological models. It should be noted that we should not expect that all of the estimated water storage states improve significantly, and the improvement may occur for one water storage state. Therefore, designing different scenarios for merging other data with GRACE data, taking into account the climate of each region and the structure of chosen hydrological models, still remains a new and attractive issue for future researches.

4) Several efforts have been made to study design of an innovative assimilation filter to not only improve the model estimation of the water storage states but also manage the dynamical water balances of the hydrological model (Khaki et al., 2018e; Khaki et al., 2017c). Continuing design of assimilation techniques is considered an active research topic. Designing a platform that combines different assimilation techniques with popular hydrological models would be valuable. It is worthy to note that a study has been done before which is called Parallel Framework (PDAF) (Nerger and Hiller, 2013) can be combined with different models e.g., CLM and ParFlow but this platform only provides EnKF and Local Ensemble Transform Kalman Filter (Hunt et al., 2007) for assimilation process.

2.5. Conclusion

Recent studies indicated that merging GRACE data with hydrological models can increase our knowledge regarding water distribution on earth's surface and subsurface. It can also reduce uncertainties of hydrological models originated from the simplification of meteorological

----

processes, insufficient and imperfect climate input data and hydrological model inability to consider anthropogenic and extreme climate change effects.

In this work, challenges and advances of a specific application of GRACE TWS data, which is related to merging them with hydrological models for improvement of a hydrological model's output were reviewed. Important issues were classified to describe the limitations and challenges of GRACE TWS DA into hydrological models. Among the many challenges and limitations reviewed are: 1) application of GRACE TWS data for hydrological purposes. 2) reducing the GRACE TWS data error by using available filtering methods 3) reviewing all applications of different assimilation techniques with a special emphasis on the efficiency of different sequential DA methods. Introducing limitations of available assimilation techniques provides a deeper knowledge of importance of robustness in the DA framework which requires the design and implementation of an appropriate assimilation technique. 4) reviewing some important aspects of well- known hydrological models which are more often chosen in DA e.g., code availability, flexibility in grid structure and resolution. We have also scrutinized a few topics in this field as future opportunities. The coupling DA and GRACE data and hydrological models is a promising and important field for research work.
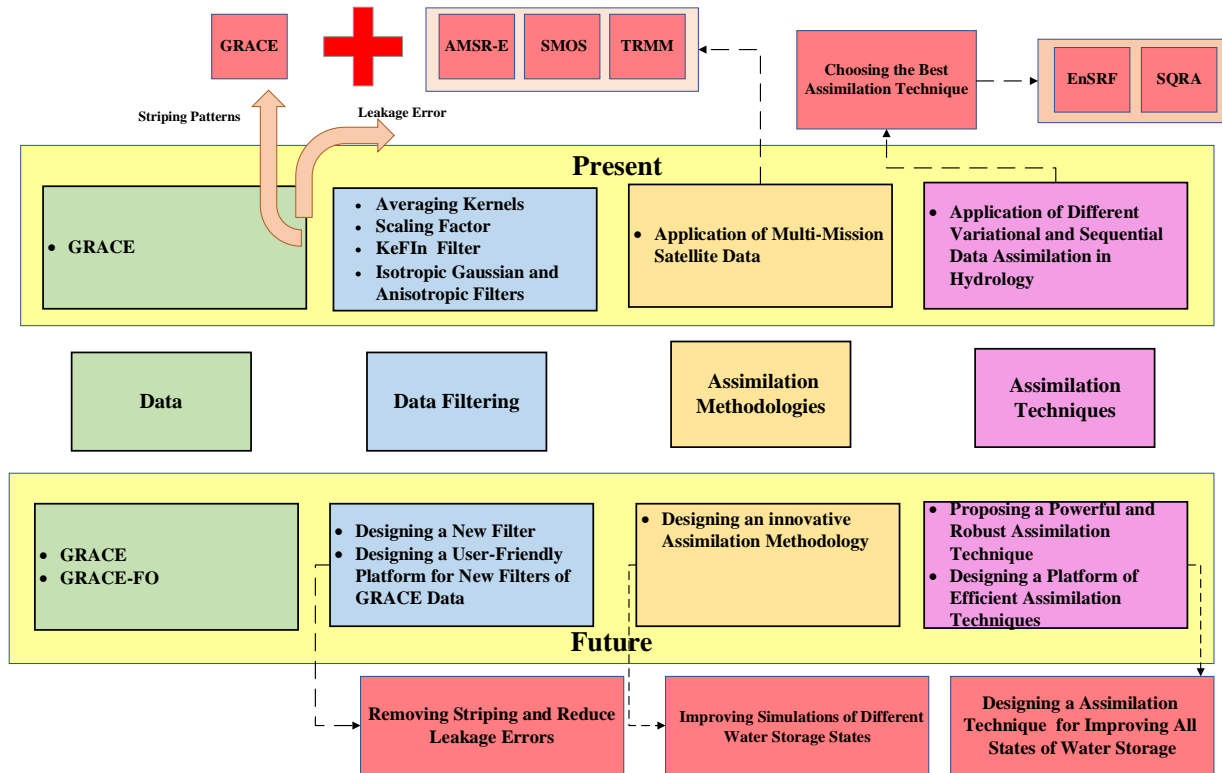
Fig. 2.9 Outline of the future prospects

Chapter III: A probabilistic framework for water budget estimation

----

3.1. Introduction

Although water has been almost free for human use throughout the millennia, it is no longer an abundant commodity as more parts of the world are struggling with water scarcity. Predictions witness that by 2025, 1.7 billion people will live in water-scarce locations while clean water supply will not be available to the two-thirds of the world's population (UN, 2015). Groundwater stores a vast amount of global freshwater resources, accounting for 96% of unfrozen freshwater reserves (Shiklomanov and Rodda, 2003). Lee et al. (2018) estimated that 42% of irrigation water, 36% of drinking water, and 24% of industrial water worldwide are supplied from groundwater. Accordingly, 20% of the aquifers globally have been overexploited in recent decades, which has been exacerbated under drought conditions (Gleeson et al., 2012). Water consumption above its sustainable extraction limit has pushed the environment to the extreme, leading to unforeseen outcomes such as subsidence, intrusion of saline water, and loss of environmental habitats (Gleeson et al., 2012).

Asia is a large groundwater consumer (i.e., 72% of its water needs) due to intensive agricultural water demand and population growth in China, Bangladesh, India, Pakistan, and Iran (FAO, 2016). In Iran, for instance, with most of the country having an arid and semi-arid climate, (i.e., 90%) relies on groundwater withdrawal due to limited surface water resources. The total available water resources per capita has dropped by 65% in Iran since 1960 (Sarraf et al., 2005), which is expected to drop by a further 16% by 2025. Recent investigations on 609 study areas across Iran indicate that almost half of the country suffers high-stress condition while groundwater levels have been falling at remarkably high rates (Hossieni et al., 2019). The above pieces of evidence highlight that groundwater depletion has imposed a serious challenge for managing water resources across the globe, requiring continuous monitoring as frequently and accurately as possible.

Quantifying water budgets in a region is one reliable approach to determine the availability and assess the sustainability of water resources under the current imbalance between supply and demand. However, limited instrumentation and low-quality ground-based measurements impede

Chapter III: A probabilistic framework for water budget estimation

----

a reliable closure of a water budget, especially in large-scale and less-developed regions. Alternatively, remote sensing has played a key role in providing data relevant to the physical processes controlling the water budget in the form of products, individual quantities or aggregated estimates with varying degrees of spatial and temporal resolution at both global and regional scales (McCabe et al., 2008). In particular, the GRACE products have been successfully utilized since 2003 to estimate changes in terrestrial water storage (TWS) that includes ice, snow, surface water, soil moisture, and groundwater storages (Tapley et al., 2004; Chen et al., 2009). For instance, Voss et al. (2013) showed that freshwater sources have diminished by 143.6 km^3 of water in the north-central region of the Middle East (covering vast portions of Tigris-Euphrates basin) between 2003 and 2009. Also, Forootan et al. (2014) reported that water storage has been reduced by approximately 15 mm/year between 2002 and 2011 across Iran.

In this study, we propose a remotely-sensed-based approach to estimate water budget elements in low runoff regions with limited climatologic and hydrometric data. In particular, the objectives of this study are to (1) investigate closure and consistency of the water budget using satellite products; (2) explore the correlation between non-closure and other water budget components to decipher the mutual causes and effects; (3) find the most reliable time scale for water budget closure while leveraging remotely sensed products; and (4) examine the sensitivity of the results to the uncertainty involved in each of the components closing the water budget. To this end, we use the satellite products of precipitation (*P*), evapotranspiration (*ET*), and TWS to estimate the spatial distribution of groundwater depletion in the Central Basin of Iran (CBI) at monthly, seasonal and annual time scales. Where there is a mismatch between the spatial and temporal resolutions of the aforementioned satellite products, we propose and implement a novel application of the First Order Reliability Method (FORM) to examine the failure probability of a Limit State Function (LSF) as a criterion to validate the reliability of the water budget closure. FORM has been proved to be a simple and efficient tool for such purposes, particularly in problems with small probabilities of failure (Lopez et all. 2015).

The rest of this paper is organized as follows. In sections 2, we describe the geographical location of the case study with an emphasis on the long-term climatic condition and the availability of water

Chapter III: A probabilistic framework for water budget estimation

----

resources against water consumption. In section 3, we provide detailed information on the satellite products used to estimate the water budget components. Also, details on the implementation of the FORM frameworks are represented. Section 4 presents the results of the water budget estimation and discusses their validity using the reliability metrics computed from the FORM method. Finally, concluding remarks are summarized in section 5.

3.2. Case Study

Iran is located in the southwest of Asia (25-40°N and 44-64°E; Fig. 3.1) with an area of more than 1.6 million km^2, making it the second largest country in the Middle East. Recognized by a semi-arid and arid climate, the average annual rainfall in Iran is 250 mm (ranging from 50 mm in the dry parts of the central basin to 2275 mm in the northern regions near the Caspian Sea), which is considerably smaller than the global annual average rainfall of 830 mm (FAO, 2009). A relatively small percentage of the country receives enough rainfall to allow unirrigated agriculture. In other regions, groundwater has been largely depleted over the past decades mainly for irrigation purposes. Analysis of groundwater consumption data separately from wells, springs and qanats (results not shown here) indicates that total groundwater consumption volume constituted 30% of total precipitation in 2011 (IWRMC, 2011). Fig 3.2 indicates that a remarkable portion of groundwater withdrawal, i.e., 90%, is used for agriculture as compared to industrial and drinking purposes.

Iran encompasses six first-order (major) basins (Fig. 3.1, namely the 52,000 km^2 Lake Urmia Basin located in the northwest of Iran, the 424,000 km^2 Gulf of Oman and Persian Gulf Basin located in the south and west of Iran, the 825,000 km^2 CBI located in the center of Iran, the 44,000 km^2 Kara-Kum or Sarakhs Basin located in the northeast of Iran, the 103,000 km^2 Lake Hamoon Basin located in the east of Iran, and the 175,000 km^2 Caspian Sea (Khazar) Basin located in the north of Iran. In contrast to the Gulf of Oman and Persian Gulf Basin which covers 25% and 50% of the country's area and renewable water resources, respectively, (UN, 2004), CBI encompasses more than 50% of the area (and population) of the country while containing only 28% of renewable water resources (UN, 2004). The CBI water budget in the 2010-2011 water year indicates that precipitation as the only input is approximately partitioned between evaporation and infiltration

----

by 54% and 23%, respectively (IWRMC, 2011). CBI shares boundaries with the Zagros Mountain range in the West and South, as well as the Alborz Mountains range in the North (Fig. 3.1). These chains of mountains form a rain shadow in the so-called regions, making the CBI very dry. The central and southeast regions of CBI are mainly comprised of gypsum and limestone derived soils with high porosity, causing high infiltration rates and the absence of permanent flows in this basin. Water withdrawn for agricultural purposes is mostly supplied by groundwater due to the very limited surface water resources in this basin.
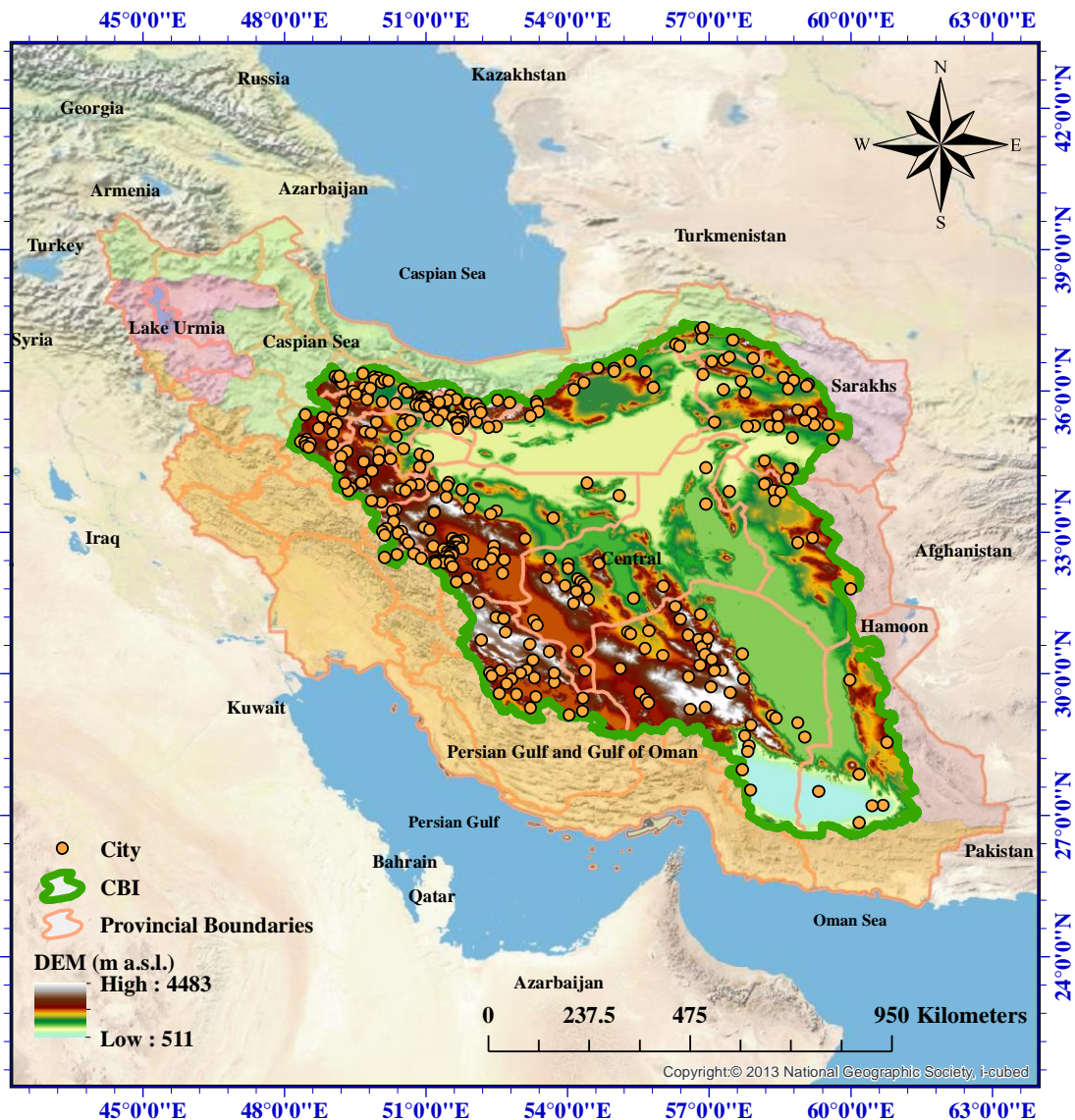
Chapter III: A probabilistic framework for water budget estimation

----

Fig. 3.1 Geographic location of Iran and its six major basins, overlaid by the Digital Elevation Model (DEM) of the CBI as well as the location of cities in the basin. Provincial boundaries are also depicted.
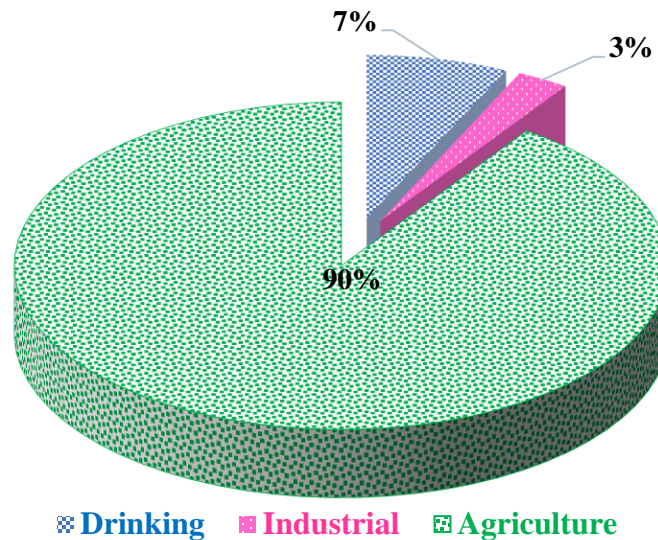
Fig. 3.2 Groundwater consumption for drinking, industrial and agriculture purposes in the CBI in 2011 (data from IWRMC).

3.3. Methods and Data

3.3.1 Water Budget Estimation

In a simplified form, water budget equation can be written as

$$\Delta S = P - ET \tag{3.1}$$

where ΔS is the change in water storage [L], P is precipitation [L], ET is evapotranspiration [L]. This simplified equation holds if water transfer in the horizontal direction through runoff is relatively small (Rodell et al. 2004 and 2011). Under this assumption, the right and left side Eq. (3.1) can be estimated utilizing ground measurements and satellite products depending on the availability of such data for each term in the water budget equation. Due to the lack of ET and ΔS data and disqualified P data concerning the disperse distribution of gauging stations across the CBI, remote sensing data are merely used for the objectives of this study.

Chapter III: A probabilistic framework for water budget estimation

----

3.3.2 Remote Sensing Data

Several satellite data sources are available for obtaining various components of the water budget equation (McCabe et al., 2008). For *P*, these sources include gridded global rain gauge product supplied by the Global Precipitation Climatology Center (GPCC) and the Climate Anomaly Monitoring System (CAMS) produced by National Oceanic and Atmospheric Administration (NOAA). These independent estimates are incorporated in the Tropical Rainfall Measuring Mission (TRMM) Multi-Satellite Precipitation Analysis (TMPA) 3B43 (Huffman et al., 1997 and 2007). Here, we use TMPA 3B43 version 7 to retrieve data for *P* at 0.25°×0.25° spatial resolution and monthly temporal resolution. TMPA products have been validated in many places around the world, such as Greece (Feidas, 2010), Africa (Adeyewa and Nakamura, 2003), Australia (Ebert et al., 2007; Fleming et al., 2011) and Iran (Katiraie-Boroujerdy et al., 2013; Javanmard et al. 2010). For *ET* estimates, we use the Water Productivity Openaccess portal (WaPOR) with 10 days and 250 m temporal and spatial resolution, respectively. WaPOR products aggregate all data relevant to agricultural water in Near East and Africa and have have been validated in some countries such as Iran (Rahimpour et al., 2018).

We obtain Δ*S* from the GRACE data with 1° spatial and monthly temporal resolution, which have been successfully applied in large scale hydrologic modeling (Awange et al., 2009; van Dijk et al., 2011; Rodell and Famiglietti, 2001), e.g., for monitoring groundwater fluctuations (Henry et al. 2011) and to tracking soil moisture dynamics (Niu et al., 2007; Forootan et al. (2017). The Gravity Recovery and Climate Experiment (GRACE) mission which has been active since 2002, has an important role in representing surface and sub-surface physical processes related to water redistribution in the Earth system (e.g., Kusche et al., 2012; Forootan et al., 2014).

The satellite products for TMPA 3B43, WaPOR, and GRACE were used from December 2008 to January 2017 due to the availability of WaPOR evapotranspiration and GRACE data in this period. The gap in the GRACE data in a given month was filled with the average value of the previous and the following months. We obtain *ET* data with 10 days temporal resolution and aggregate them into monthly, seasonal and annual datasets, resulting in 96 months, 32 seasons and 8 years. About *P* and Δ*S*, we aggregate monthly data into seasonal and annual datasets. Fig 3.3. shows the

----

procedure of convereting different temporal and spatial resolutions of water budget components together.
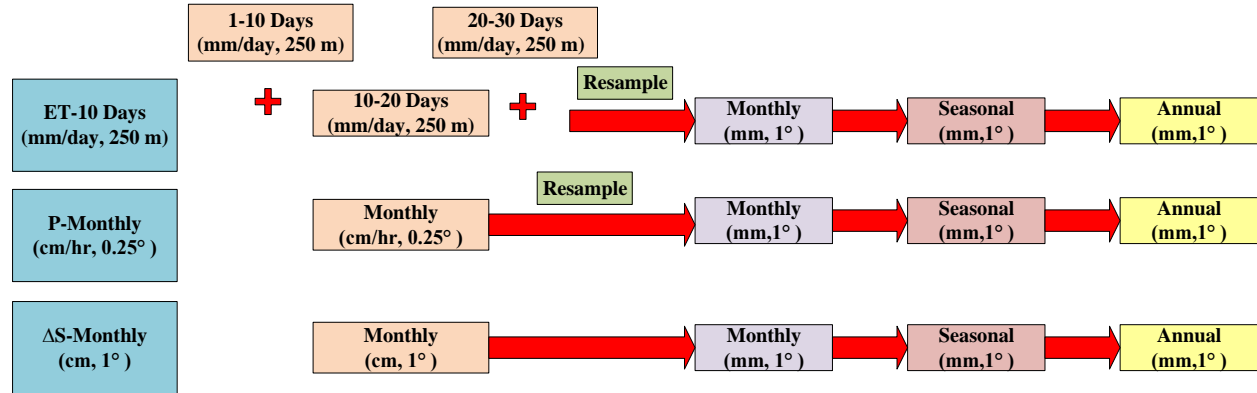
Fig 3.3. The procedure of convereting different temporal and spatial resolutions of water budget components (*ET*, *P* and Δ*S*) into one another

3.3.3 Water Budget Implementation at Different Time Scales

If a grid water storage thickness in a given month is denoted by m, and $\overline{m}$ is the average thickness over the whole study period, i.e., between January 2009 to December 2016 GRACE gives the difference between these two quantities (G) that is expressed as

$$G_j = m_j - \overline{m} \tag{3.2}$$

where the index j refers to a month number. By subtracting G values of two consecutive months, ΔS is obtained as

$$\Delta S_j = m_{j+1} - m_j = G_{j+1} - G_j \tag{3.3}$$

Since G is not given at a definite time from one month to another, P and ET values in month j and $j+1$ are averaged and is expressed as

$$\Delta W_j = \frac{1}{2}(P_j + P_{j+1}) - \frac{1}{2}(ET_j + ET_{j+1}) \tag{3.4}$$

The inconsistency between different remote sensing products (water budget residual) in terms of the mismatch between their spatiotemporal resolutions contributes to the uncertainty in the water budget closure as

Chapter III: A probabilistic framework for water budget estimation

----

$$\Delta_{it} = \Delta W_{it} - \Delta S_{it} \tag{3.5}$$

where i is a pixel number, t is the tth month/season/year, and n is the total number of months/ seasons/years. Also, possible considerable runoff during heavy rain events might impose errors in the water budget expressed as Eq. (3.1). To evaulate the bias in the water budget equation, we estimate the relative residual of the water budget equation, r_{it}, as

$$r_{it} = \sum_{t=1}^{n} \frac{|\Delta_{it}|}{\frac{1}{n}\sum_{t=1}^{n} P_{it}} \tag{3.6}$$

3.3.4 Probabilistic Assessment of the Water Budget Closure

3.3.4.1 First Order Reliability Method (FORM)

In this approach, a Limit State Function (LSF) is defined as the mathematical expression of a system state limit beyond which the criteria determining system reliability is no longer met (Abdelkhalak and Bouchaïb 2013). In analogy to the water budget of a hydrologic system, r_{ij} can be considered as the criterion to examine the reliability of the water budget closure by defining r_{ij} less than 30% as the state limit. Since the renewable water share of precipitation is 30 % in CBI (UN, 2004), r_{ij} is considered to be maximum 30% as the state limit. Based on the assumption that LSF is continuous and first-order differentiable, FORM uses a linear approximation (i.e., first order Taylor expansion) expressed as

$$G(y) \approx L(y) = G(y_{m}) + \nabla G(y_{m})^{T} . (y - y_{m}) \tag{3.7}$$

where $L(y)$ is the linearization of the LSF, $y = (y_1, y_2,..., y_n)$ is the vector of n variables defining the G function, y_m is the expansion point, and $\nabla G(y)$ is the first order gradient vector of $G(y)$. In order to implement FORM, none-normally distributed variables should be transformed into standard normal variables (Madsen et al., 2006) via, e.g., the NATAF transformation (Nataf, 1962).

To minimize the loss of accuracy, LSF is expanded at a point which has the highest contribution to the probability of failure. This is equivalent to finding a point on the transformed LSF with the shortest distance to the origin in the uncorrelated standard normal space (Shinozuka, 1983). This

Chapter III: A probabilistic framework for water budget estimation

----

point is called the design point (or the most probable point) that can be obtained by solving the following constrained optimization problem.

$$y* = \arg\min\left\{\|y\| \,\big|\, G(y) \le 0\right\}$$ (3.8)

Various approaches have been developed during the past decades to solve the constrained optimization problem described in Eq. (3.8). The iHLRF (Zhang and Kiureghian, 1997) is a state-of-the-art method which can be used to obtain the point on the failure surface that is closest to the origin. In this approach, the design point is found by a generic search algorithm via the following iterative equation

$$y_{m+1} = y_m + s_m \cdot d_m$$ (3.9)

where m is the iteration number, s is the step length, and d is the direction of the search. Details on the method of determining d_m and s_m are described in Sudret and Der Kiureghian (2002) and Der Kiureghian (2005). Given y^*, the reliability index, β, is computed as

$$\beta = \|y^*\|$$ (3.10)

and the failure probability of β is given by

$$P_f = \Phi(-\beta)$$ (3.11)

where Φ is the cumulative probability distribution function of β. Fig. 3.4 shows the general procedure of the FORM implementation.
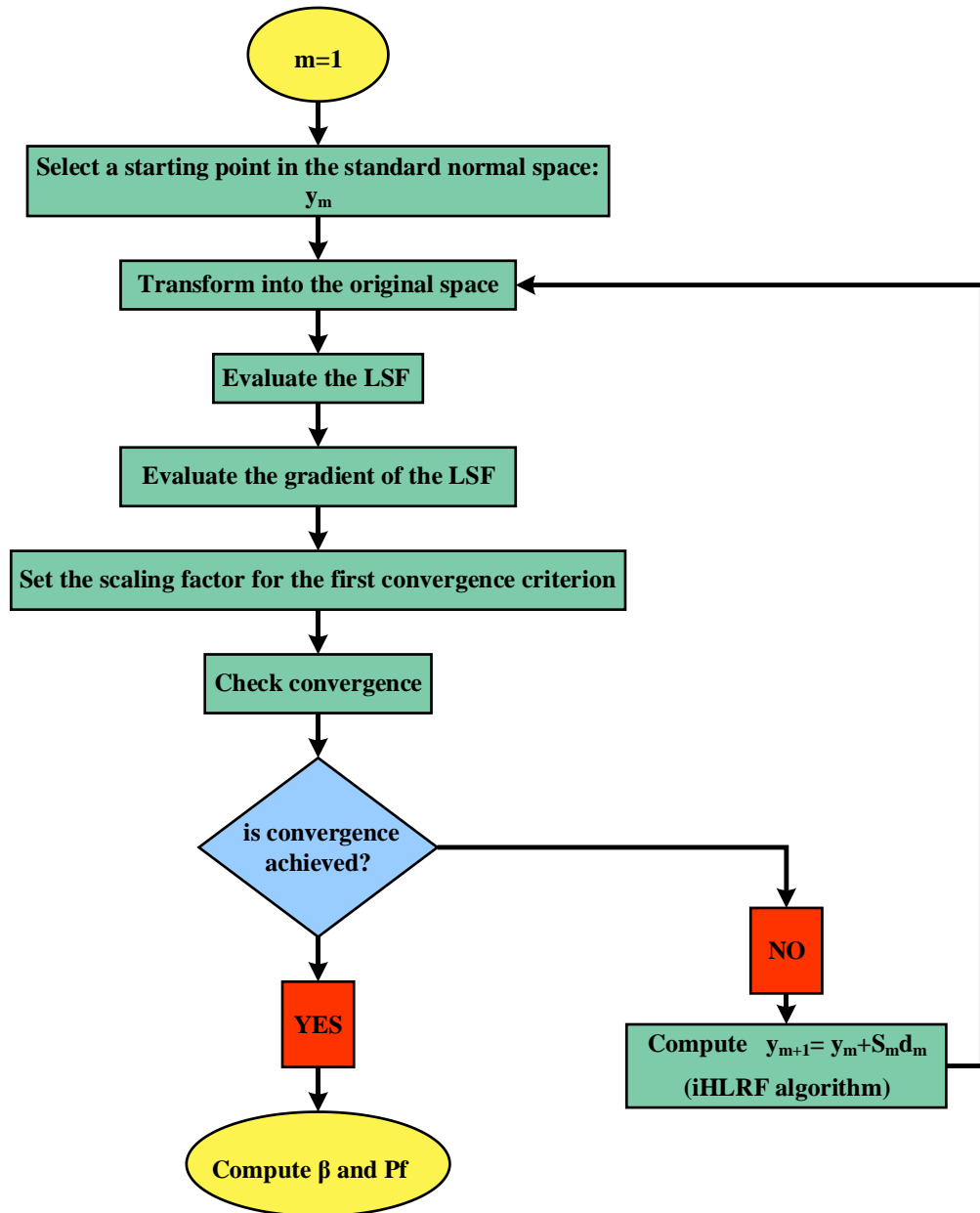
Fig. 3.4 The procedure for the FORM implementation.

3.3.4.2 Sensitivity Measures of the Reliability Analysis

The sensitivity analysis discussed here yields the sensitivity of the reliability analysis to the changes in the input random variables, i.e., how sensitive G in Eq. (3.7) is with respect to the uncertainty involved in the P, ET, and ΔS. This analysis also determines the relative degree of

Chapter III: A probabilistic framework for water budget estimation

----

influence on *G* of the above random variables, which help understand how reliable each remote sensing product is for the estimation of water budget at the basin scale. To this end, importance vectors are employed to determine which variables should be modeled more accurately or are least effective on uncertainty. In problems with a large number of stochastic variables, this information helps to reduce the dimensions of the problem by disregarding the least effective variables. One importance vector is the alpha vector (α) expressed as

$$\alpha = \frac{y^*}{\|y^*\|} \tag{3.12}$$

whose components indicate the relative contribution of each random variable to the total variance of the *G* function in Eq. (3.7) (Der Kiureghian, 2005). The positive and negative sign of each component recognize it as the load and resistance variable, respectively. A larger absolute magnitude of a component in α implies a largest interference in the failure probability of the *G* function.

In case the involving random variables of the *G* function are correlated, another importance measure, γ, is computed as Eq. (3.13) to rank the random variables in the original space (Der Kiureghian 2005).

$$\gamma = \frac{\alpha^T J_{y^*,x^*} \hat{D}}{\left\| \alpha^T J_{y^*,x^*} \hat{D} \right\|} \tag{3.13}$$

where $\mathbf{J}_{\mathbf{y^*,x^*}}$ is the Jacobian matrix and $\hat{\mathbf{D}}$ is a matrix wherein the diagonal elements are equal to the standard deviation of the input random variables (that is, equivalent normal).

3.4. Results and Discussions

3.4.1 Estimation of Water Budget

Fig. 3.5 depicts the spatial mapping of average annual *P*, *ET*, Δ*S*, and Δ from January 2009 to December 2016 in the CBI. *P* is seen to have a larger magnitude in the northern and western part

Chapter III: A probabilistic framework for water budget estimation

----

of the CBI, which appears to be similar to Δ. While *ET* does not show a considerable spatial variation across the CBI, the northern boundary as well as the western regions indicate higher *ET* rates in comparison to the eastern and central parts.

The partitioning of *P* can be determined by the competition between available water and the available energy approximated by the potential evapotranspiration (*PET*) (Budyko, 1958). Fig. 3.6 depicts the index *ET*/*P* and the index *PET*/*P* based on long term (10 years) average of *PET*, *P* and *ET* data which was obtained from available IWRMC data (Source online: http://wrbs.wrm.ir/), TRMM and WaPOR remote sensing data, respectively. Two points are noteworthy based on Fig. 3.6 to provide a reference condition for the CBI. First, *PET*/*P>>1* shows very dry conditions in the CBI which it is indicated on the available energy greatly exceeds the amount required to evaporate the entire annual precipitation. This evidence also illustrates which the assumption of negligible runoff in Eq. (3.1) the CBI is quite logical. Second, Fig. 3.6 shows the major variations of *PET*/*P* index across the CBI. The index *PET* /*P* is higher in central and eastern regions with low elevation (see Fig.3.1 and less precipitation (see Fig. 3.5), since the temperature is too high for generating higher *PET* /*P*. Conversely, *PET*/*P* is lower in western regions with more precipitation.
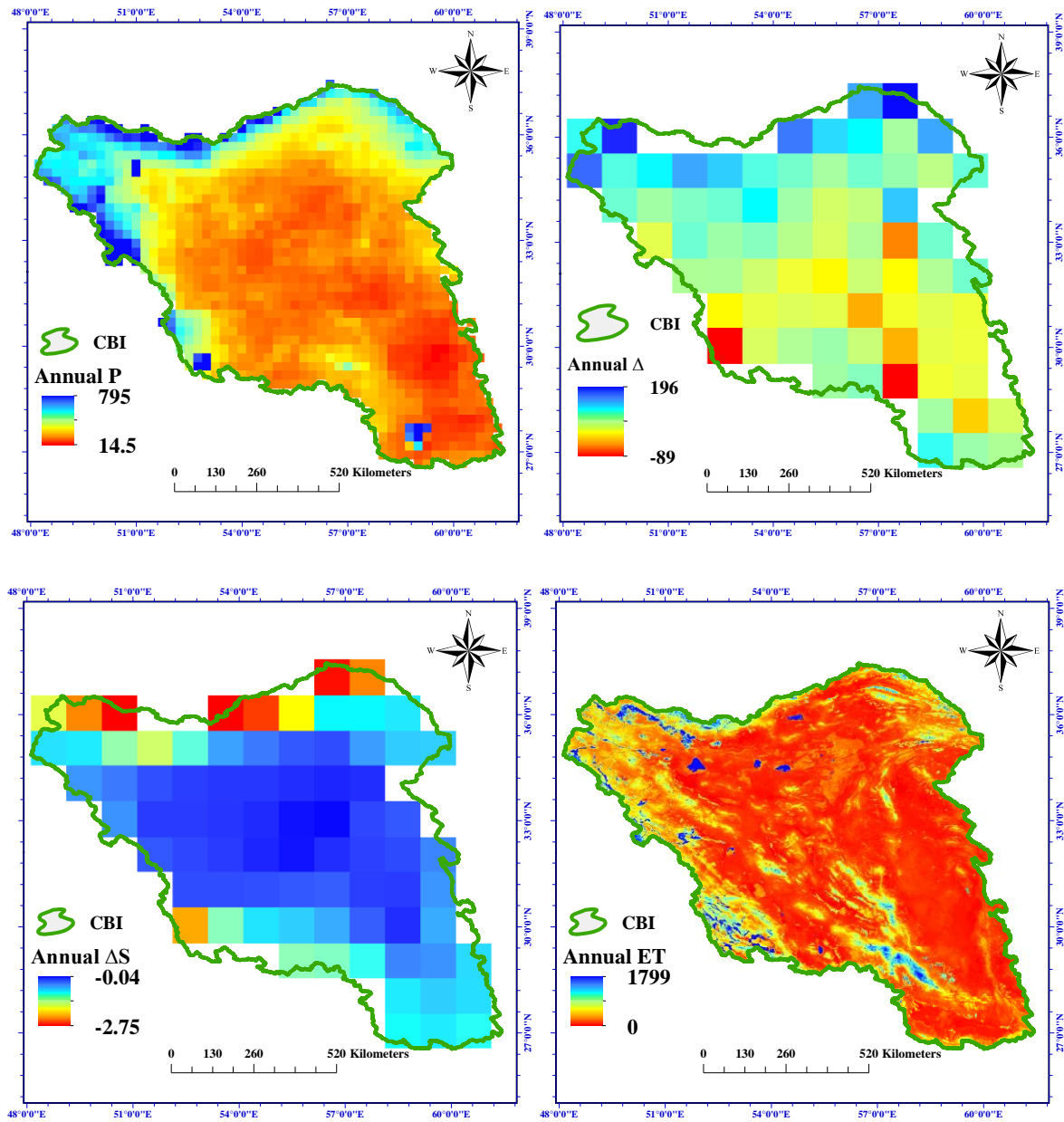
Fig. 3.5 Spatial distribution of annual water budget components and residual in mm over the CBI. No data is shown in white color.
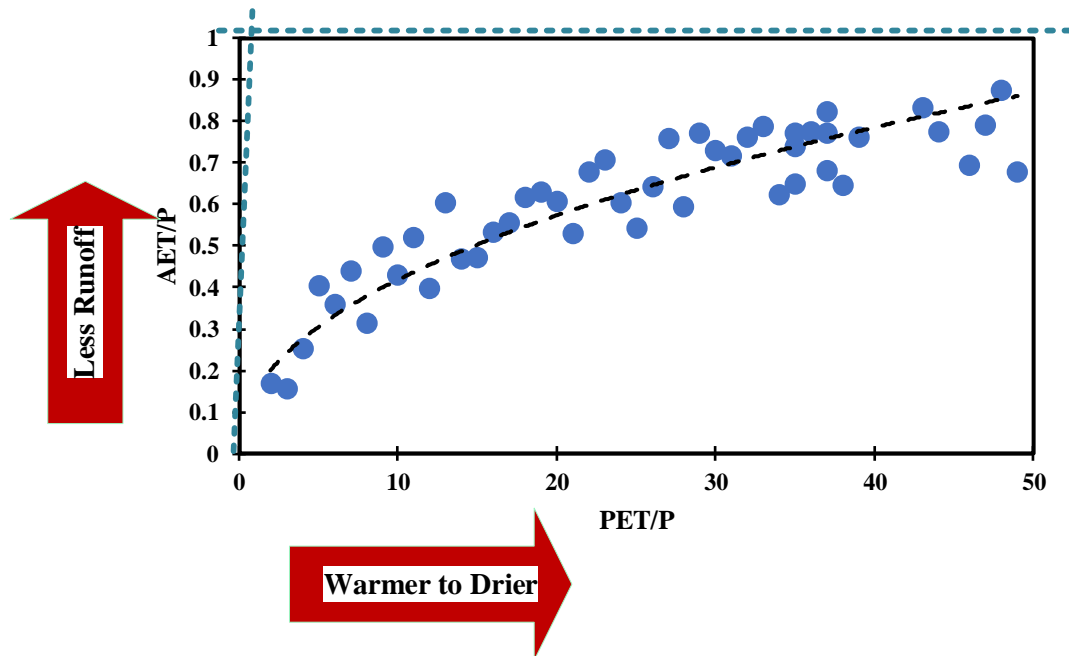
Fig. 3.6 Obtained Budyko curve from long-term (10 years) average of observations. The 1:1 limit expresses the limitation by available energy ($PET/P <1$), and the horizontal limit expresses the limitation by available water ($PET/P >1$).

Fig. 3.7 shows the annual time series of P, ET, ΔS, and Δ from 2009 to 2016. The Mann-Kendall trend analysis at the 0.05 significance level shows no significant trend in any of the above time series. Three points are noteworthy here. First, the retrieved ΔS of -6.5 mm from GRACE in 2011 is in a close agreement with the results of former studies in this basin at the same year, i.e., -6.1 mm (IWRMC, 2011). Second, the estimated Δ at the same year from the water budget Eq. (3.5) shows an acceptable difference from precipitation data, highlighting that the applied remote sensing products for the water budget components are accurate enough to close the water budget appropriately. Third, the strong correlation between P and Δ time series indicates a tight dependency of water budget closure on P. Also, the ratio between ΔS and P does not significantly change over the whole study period, pointing out that even in years with increased P (as compared to other water years), the same percentage of storage had taken place in the CBI which highlights uncontrolled management of water resources.
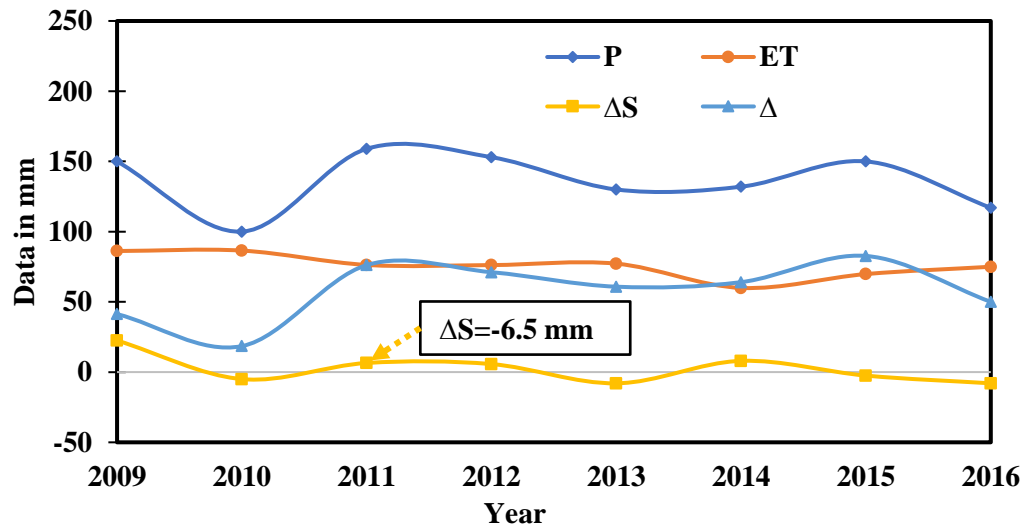
Fig. 3.7 Annual time series of water budget components from 2009 to 2016 over the CBI.

Fig. 3.8 shows Δ in northern and western regions of the CBI is greater than that in the eastern and central regions. We note that Δ values are the byproducts of error integration of the three remote sensing products used in Eq. (3.1) to estimate the water budget. It should be noted that it is not necessarily true that the three datasets are inconsistent and inappropriate for water budget studies for areas with large residuals, because the non-closure may be ascribed to runoff due to a large amount of rainfall in those areas.

Fig. 3.9 shows the spatial distribution of Δ/P in the CBI on the seasonal time scale. It also shows that Δ/P in summer and spring is greater than compared to autumn and winter. In Fig.3.8, red pixels with a negative value have a significant difference in value with their adjacent pixels and indicate that these regions receive water from neighboring cells. These pixels are assumed net water consumption regions which are generally the irrigated areas, lakes and reservoirs. Fig. 3.9 depicts differences in P and ET (ΔW) at the annual time scale. It shows regions with net water production ($\Delta W \succ 0$) and regions with net water consumption ($\Delta W \prec 0$). The pixels that produce water ($\Delta W \succ 0$) are discharge regions responsible for streamflow and groundwater recharge. These regions are located on the north and western regions of CBI. Areas with sparse vegetation and low

----

ET also have higher *P* than *ET* and are water producing areas. 40 % of the CBI comprise such areas.
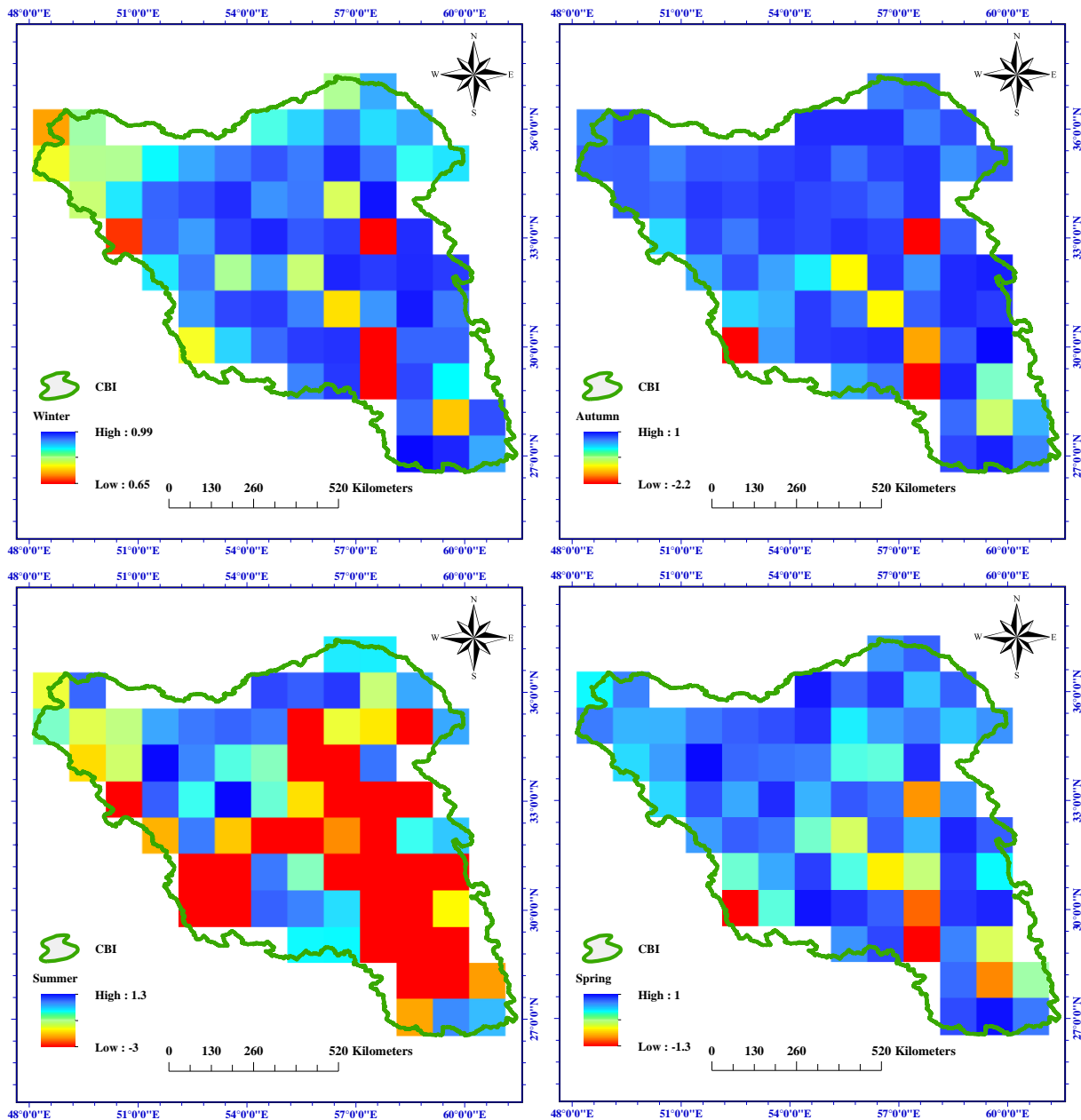
Fig. 3.8 Spatial distribution of the seasonal Δ/*P* in mm over the CBI. No data is shown in white color.
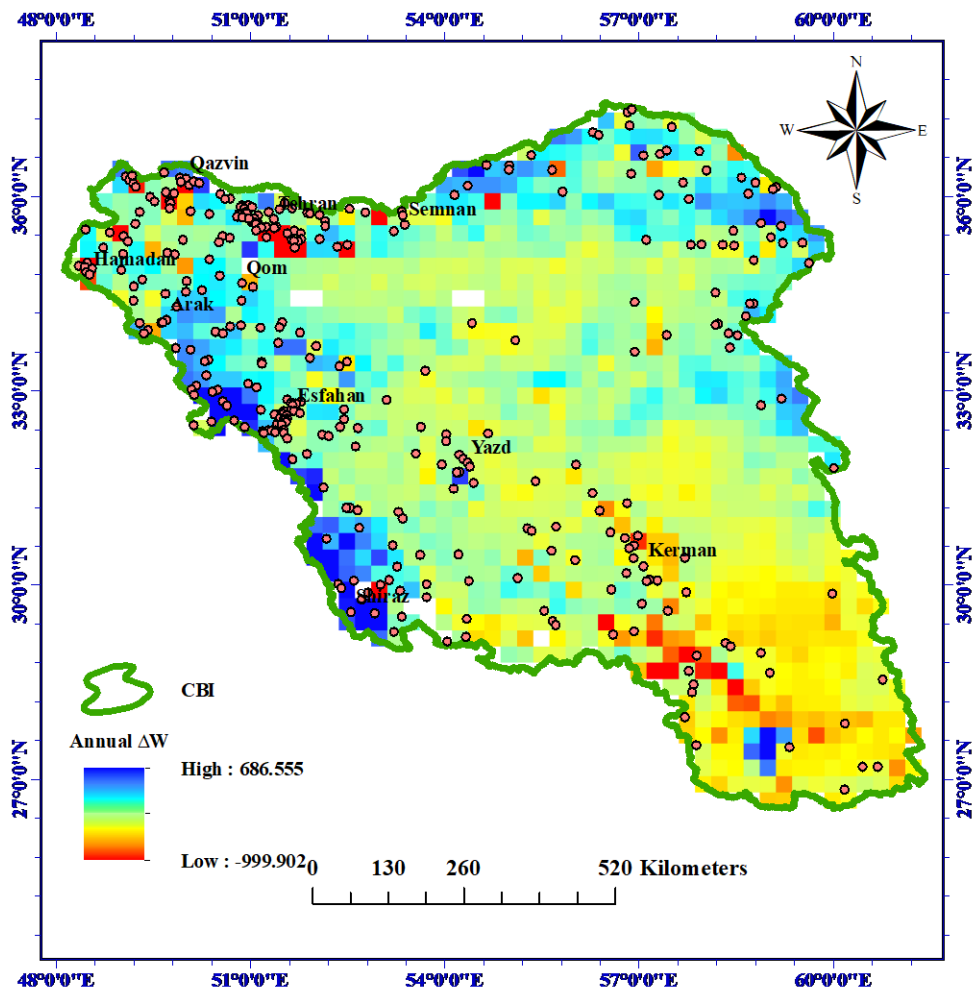
Fig. 3.9 Spatial distribution of the annual ΔW in mm over the CBI. No data is shown in white color.

3.4.2 The relationship between residual and different water budget components

To examine the relationship between residual and each water budget components, we calculated each of these at monthly and seasonal and annual time scales across CBI. Fig. 3.10 depicts the relationship between residual and P, ET and ΔS at the annual time scale.

Table 3.1, represents the correlation coefficient between Δ and other components at monthly and seasonal time sale. Results show the correlation coefficient between Δ and P is higher than other components such as ET and ΔS, which is consistent with previous studies (e.g., Wang et al., 2014;

66

Chapter III: A probabilistic framework for water budget estimation

----

Sheffield et al., 2009). Also, the results reveal that the correlation coefficient of Δ with *P*, *ET* and ΔS increase from monthly to annual time scales.
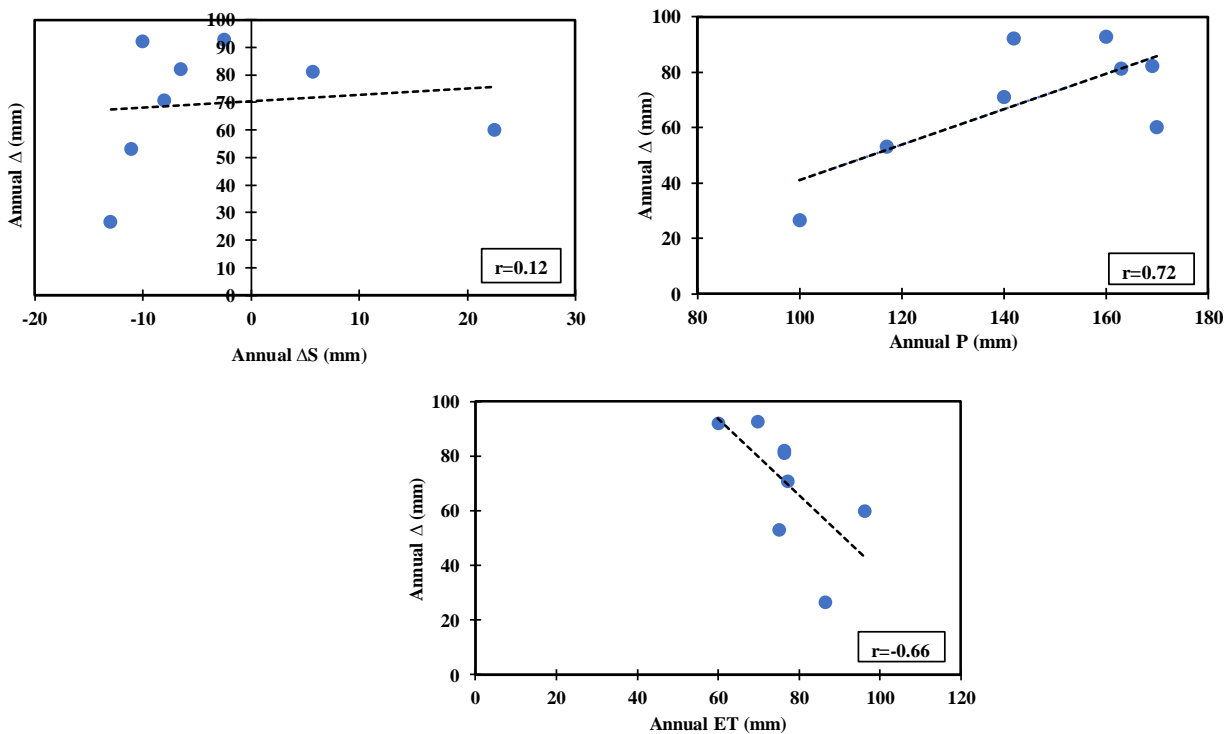
Fig. 3.10 Relationship between annual water budget residual and *ET*, *P* and ΔS over the CBI

Table 3.1. Correlation coefficient between residual and other water budget components at monthly and seasonal time scales over the CBI

	Seasonal			Monthly		
	P	*ET*	ΔS	*P*	*ET*	ΔS
Δ	0.556	-0.472	-0.053	0.371	-0.279	-0.049

To find the best time scale at which the estimated water budget from applied satellite remote sensing provides most closure, we investigated the relationship between ΔW and ΔS at monthly,

67

Chapter III: A probabilistic framework for water budget estimation

----

seasonal and annual time scales across CBI. Table 3.2 shows the correlation coefficient between ΔW and ΔS. Consequently, the estimation of water budget using applied remote sensing data is more consistent and provides better closure in terms of correlation coefficient on seasonal and annual time scales. However, whilst technical results are more reliable on seasonal and annual time scales, some of the water budget terms have high seasonal variations and this makes the annual time scale too long to be useful for water resources management. Therefore, the results show the seasonal scale is better for decision-making on water resources management which is analogues with Pearson (2008).

Table 3.2. Correlation coefficient between ΔW and ΔS at monthly, seasonal and annual time scales over the CBI

	ΔS	ΔW	
	Mean		Correlation coefficient
Monthly	5.7	0.4	0.62
Seasonal	17.9	0.5	0.8
Annual	70.5	1.8	0.55

3.4.3 Evaluating of Uncertainty in Water Budget Estimation

A novel application of the First Order Reliability Method (FORM) is implemented to investigate the LSF failure probability as a criterion to validate the reliability of the water budget closure. In the water budget estimation of a hydrologic system, r_{ij} can be considered as the criterion to examine the reliability of the water budget closure by defining r_{ij} less than the renewable water share of precipitation. To this end, the first-order reliability method finds the reliability index (β) and failure probability (P_f) of water budget closure. Results of the FORM implementation show that β and P_f are 1.02035 and 0.153782, respectively. Since P_f is low, closure and consistency of water budget using applied remote sensing data is acceptable.

68

Chapter III: A probabilistic framework for water budget estimation

----

A sensitivity analysis is also implemented to measure the sensitivity of the reliability to changes in the input random variables and rank the importance order of the random variables of the water budget equation. The results of sensitivity analysis implementation are given in Table 3.3. The absolute magnitude of α importance vector shows that *ET* and then *P* are the most important parameters that are most likely to interfere with the failure of the LSF. In this study, according to *α* importance vector, *ET* is considered as a resistance variable and *P* and Δ*S* are considered as load variables. This means that increasing value of *ET* will increase the reliability index and decrease the LSF failure probability.

Although α is considered as a good importance vector for the random variables in the standard normal space, it may not be an accurate importance measure for the random variables in the original space, when a correlation between different random variables is exist. Therefore, γ is employed to rank the importance of the random variables in the original space (Der Kiureghian, 2005). γ importance vector shows that *ET* is the most important variable which influences greatly on the failure of the LSF (see Table 3.3). As a result, accurate modeling of *ET* increases the accuracy of water budget estimation.

Table 3.3. The results of sensitivity analysis implementation

	α	γ
ET	-0.76908724	5.14671906e-08
Δ*S*	0.08818706	1.77928691e-08
P	0.31212596	2.03410296e-08

Chapter IV: Improvement of soil moisture and groundwater level estimations using a scale-consistent river parameterization

----

Chapter IV: Improvement of soil moisture and groundwater level estimations using a scale-

consistent river parameterization

4.1. Introduction

Hydrological modeling is an important tool for managing both environmental and water resources especially when it incorporates both temporal and spatial variables (Soltani, et al., 2021). Hydrological models are designed and applied for the large global scale (e.g., Döll et al., 2003; Kollet and Maxwell, 2006; Van Dijk et al., 2013), or the smaller regional scales (e.g., Christiansen et al., 2007; Huang et al., 2017). Simulation of hydrological processes including the water cycle in both regional and global scales can be accomplished by these models. Models are still being developed to better simulate are generally better than their predecessors in simulations of the physical processes since they consider the interaction components of the water cycle e.g., the relationship between runoff, evapotranspiration, and precipitation is included in these models (Simmons et al., 2020).

The interaction between subsurface and surface water is also important, particularly for studying rivers. However, these interactions are considered as a numerically challenging task. A common approach has been to use river-routing codes, like Hydrologic Engineering Center (HEC) codes, as well as MODFLOW and its River Package to determine head in the river, and then taking this as the upper boundary condition of the subsurface modeling. This approach does not consider the feedback between surface and subsurface models, and a better representation of the physical processes in these kinds of problems is still a key challenge for modelers (Kuffour et al., 2020). The interaction between surface and groundwater in a dynamic fashion is possible by the integrated approach. Integrated approach is possible either by fully integrated strong coupling where the surface and subsurface equations are solved simultaneously using a non-linear solver (Ababou et al. 2015), or by a two-way iterative coupling where the equations are solved sequentially. Among the parallel integrated two-way coupled hydrologic models, ParFlow has a demonstrated potential

Chapter IV: Improvement of soil moisture and groundwater level estimations using a scale-consistent river parameterization

----

to simulate simultaneously surface and subsurface flow (saturated and unsaturated zone) in 3-D (Maxwell et al., 2009). ParFlow has been extended to coupled surface-subsurface flow to enable the simulation of hillslope runoff and channel routing in a truly integrated fashion (Kollet and Maxwell, 2006). ParFlow simulates variably saturated groundwater flow in 3D using the Richard's equation (Richards, 1931). Overland flow generated by Manning's equation and the kinematic wave formulations of the dynamic wave equation is considered as a boundary condition in the Richard's equation (Kollet and Maxwell, 2006). This boundary condition connects the subsurface flow with land surface flow and removed the exchange flux term from the Richard's equation and calculates the movement of ponded water's free surface at the land surface. The capacity of ParFlow in performing efficient 3-D simulations is relevant as in most existing models (i.e., MIKE SHE) the unsaturated flow is still calculated in 1-D (Graham and Butts, 2005). In addition to this capability, ParFlow is an open access integrated model. The documentation of ParFlow is relatively extensive and it has been tested on the various surface and groundwater problems in large domains (e.g., over $600 \, km^2$) (Ferguson and Maxwell, 2012), small basins (e.g., $30 \, km^2$) (Kollet and Maxwell, 2006; Engdahl et al., 2016), and even subsurface–surface and atmospheric coupling (Williams et al., 2013; Shrestha et al., 2015). Since ParFlow cannot account for surface processes (e.g., evaporation) in integrated studies, ParFlow is often coupled with a land surface model and in particularly to Common Land Model (CLM) (Kollet and Maxwell, 2008).The coupling of a surface and subsurface model improves the model complexity, bringing potentially more realism regarding the physical processes occurring at the interface between the deeper subsurface and the surface (Sulis et al., 2017; Beisman, 2007).

ParFlow is originally a grid based hydrogeological model, and it calculates overland flow usually at much larger grid scales than the width of the rivers (Schalge et al., 2019). On the other hand, other hydrological models usually employ routing schemes for separate channels which are not related to the grid resolution (Schalge et al., 2019). When performing realistic overland flow simulations, the high computational demands of increasing the spatial resolution limits such simulations (Clark et al.,2015; Wood et al., 2011). Therefore, using the sub-grid digital elevation model (DEM) was suggested for the ISBA–TRIP (Decharme et al., 2012) model which are run at relatively low resolution. Neal, et al. (2012) have studied the effect of sub-grid scale channel

Chapter IV: Improvement of soil moisture and groundwater level estimations using a scale-consistent river parameterization

----

routing on flood dynamics. They have shown the improvement of model performance by considering smaller channels. Therefore, applying coarse grids would increase the diffusion and hydrodynamic dispersion, which indirectly reduces the peaks in the surface flows.

As an alternative to explicit sub-grid channel routing, one can consider the scaling of parameters when using grid-scale river routing models (Niedda, 2004). The sub-scale parametrization has been suggested based on the sub-grid scale topographic index by Niedda (2004). The sub-scale parametrization has been also used for flow in rivers and channels with the kinematic wave formulation (Schalge et al., 2019). Thus, an approximation of the sub-scale channel flow by scaling Manning's roughness is used. The scaling coefficient is obtained using a relationship between the river width and the grid cell size. In order to compensate for the rate of ex- and in-filtration rate across the river beds, a grid resolution-aware scaling of saturated hydraulic conductivity is applied for the top layer (Schalge et al., 2019). By supposing a rectangular-shape river channel cross-section, it is possible to scale both the roughness coefficient and the hydraulic conductivity. This method adds no computational cost to the model (Schalge et al., 2019). This method improves the overland-flow parametrization for the distributed hydrological models with constant horizontal grid resolution. When the sub-scale parametrization is not employed, the model output shows smaller river flow velocities when the streams are narrower than the horizontal grid resolution. Furthermore, the surface areas which exchange water with the subsurface in a model with wide rivers are usually larger, which causes the error of unrealistic vertical flows (Schalge et al., 2019). Scaling the roughness coefficients is appropriate when the surface water flow is governing by the open channel hydraulic performance and therefore, it does not address the challenge of the width of the ponded-area and subsequent exchanges.

To our knowledge, the scaling approach has not been tested before to improve soil moisture and groundwater level simulations, though a similar approach with significant simplifications has been recently used to improve surface run-off over some idealized test cases (Schalge et al., 2019). In Schalge et al. (2019), ParFlow without coupling by any land surface the model has been used to investigate impact of scaling river parametrization. In this work, we investigate the impact of the scaling approach over the main components of the model's water budget in a real case study. We

Chapter IV: Improvement of soil moisture and groundwater level estimations using a scale-consistent river parameterization

----

implement the scaling approach in ParFlow (Ashby and Falgout, 1996; Jones and Woodward, 2001; Kollet and Maxwell, 2006; Maxwell, 2013) version 3.5 (Kuffour, 2019) which has been coupled (Maxwell and Miller,2005; Kollet and Maxwell, 2008) with CLM (Dai et al., 2003) version 4.5 (Oleson et al., 2013). The model is used to simulate the subsurface flow with $0.055°$ (~6 km) spatial resolution over the Upper Rhine Basin between France and Germany. ParFlow and CLM have been coupled to better understand the physical processes that occur at the interface between the deeper subsurface and the surface. The basin studied is an important hydro system that exists in Western Europe. Alluvial hydro system such as this can store large quantities of water, although they are vulnerable to excessive abstraction and pollution.

In the present work, the domain is constructed entirely of available data sets including topography, soil texture, and hydrogeology.

The work is organized as follows: Section 2 describes the geographical location of the study area with an emphasis on the long-term climate condition. Section 3 provides a brief overview of the equations used in the model with an emphasis on variably saturated groundwater flow, shallow overland flow and its integration in the fully coupled land surface-subsurface modelling framework, and the scaling approaches for Manning's coefficient and hydraulic conductivity. In addition, the land surface data and atmospheric forcing and evaluation dataset including CCI soil moisture data and in-situ groundwater level data are also presented. Section 4 provides details of the first-order reliability method (FORM) which is a novel probabilistic validation framework for validation purposes. Section 5 presents effect of applying of scaling approaches on model's results including temporal and spatial pattern of soil moisture and groundwater level data which is cross-validated with observations. A discussion of this paper's results with previous studies is also presented in Section 5. Finally, concluding remarks are summarized in Section 6.

4.2. Study Area: Geographical and climate condition

A major part of the Upper Rhine Basin with area of 32.400 Km^2 is located in the east of France and along the France-Germany border from Lauterbourg (north) to Basel (south) as shown in Fig. 4.1. The basin is separated in the west by Vosges Mountains and in the east by the Black Forest. The Rhine alluvial aquifer is mostly made of Quaternary sands and gravels. This aquifer is

Chapter IV: Improvement of soil moisture and groundwater level estimations using a scale-consistent river parameterization

----

represented with high hydraulic conductivity from $k=10^{-4}$ to 10^{-3} m/s (Majdalani and Ackerer, 2011). The aquifer is 200 m thick at the center at the east of Colmar, however, it has a smaller thickness near the alluvial plain borders (Majdalani and Ackerer, 2011). The groundwater main flow is towards the north direction. In the north of the basin, the groundwater aquifer is shallow and the water surface is close to the surface. Water table depth varies between 0-20 m from the surface. In other words, the mid and north parts of the aquifer have a wetlands characteristic because of the shallow groundwater depth.

Several of the river tributaries are fed by groundwater and the river network is very dense (see Fig. 4.1), therefore, there is a great deal of water exchange between surface water and groundwater resources. The River Ill is the main Rhine tributary in a part of the basin, which origins from Sundgau, France (Thierion et al. 2012).

Precipitation is highly variable over the basin, wherein the mountains of Vosges and Black Forest have over 2 meters per year of rainfall wherein in the annual plain average is 550 mm per year. The river changes are hugely affected by the snowfall and it is important to consider this component, both the snowfall and melting processes. The snowfall makes up to three percent of the total precipitation in the plain but it's much higher near the mountain peaks (37%). Therefore, the groundwater recharge is very much affected by the mountain streams. In addition, the Alpine snow melt is a significant source of large quantities of water for Rhine River, especially during the end of spring.

Chapter IV: Improvement of soil moisture and groundwater level estimations using a scale-consistent river parameterization

----
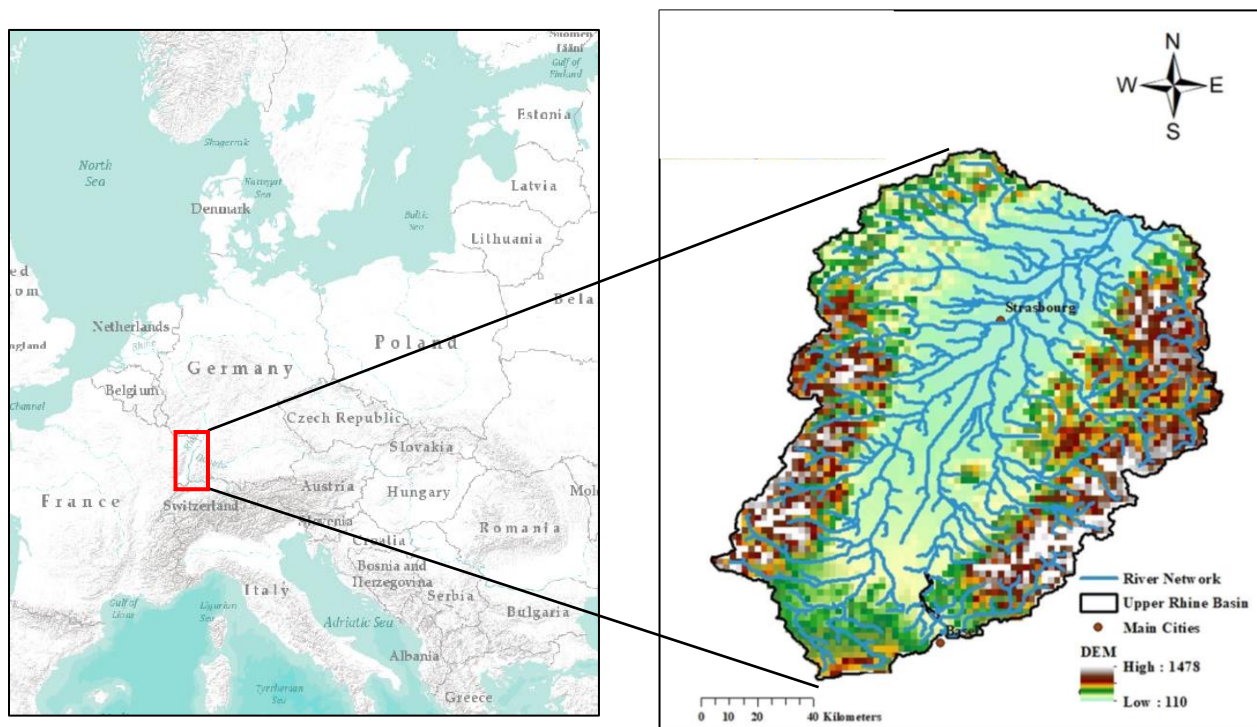
Fig. 4.1. Geographic location of the Upper Rhine Basin, overlaid by the Digital Elevation Model

(DEM) of the basin as well as the river network.

4.3. Methods and Data

4.3.1 Model Description

In this study, the couple surface-subsurface ParFlow (v3.5)-CLM (v4.5) hydrological model is used. The CLM is a land surface model which represents the moisture, energy, and momentum balances at the land surface (Dai et al., 2003). ParFlow is a groundwater model which simulates variably saturated groundwater flow in 3D using the Richard's equation (Richards, 1931).

The coupling of a ParFlow and CLM improves the model complexity, bringing potentially more realism regarding the physical processes occurring at the interface between the deeper subsurface and the surface (Sulis et al., 2017).

ParFlow cannot account for land surface processes (e.g., evapotranspiration and snow water equivalent) and CLM generally do not simulates deeper subsurface flows. Therefore, none of these

Chapter IV: Improvement of soil moisture and groundwater level estimations using a scale-consistent river parameterization

---

models cannot simulate the physical processes occurring at the interface between the deeper subsurface and the surface alone (Ren and Xue, 2004; Beisman, 2007; Shi et al., 2014). Here we provide a brief description of ParFlow (Ashby and Falgout, 1996; Maxwell, 2013). It is a groundwater flow model that considers both saturated and unsaturated flow. The surface water simulator is a 2D model (Kollet and Maxwell 2006) which uses the kinematic wave equation and the groundwater part is a 3D Richards equation solver. The Richards' equation formulation implemented in ParFlow is equivalent to the one in (Kollet and Maxwell 2006)

$$S_s S_W(\psi_p) \frac{\partial \psi_p}{\partial t} + \phi \frac{\partial (S_W(\psi_p))}{\partial t} = \nabla.(q) + q_s \qquad (4.1)$$

Where S_s is the specific storage coefficient [L^{-1}], S_w is the relative saturation [-], ψ_p is sub-surface pressure head of water [L], t is time [T], ϕ is porosity of the medium [-], q is the specific volumetric (Darcy) flux [LT^{-1}] and q_s is the general source/sink term (includes wells and surface fluxes, e.g., evaporation and transpiration) [T^{-1}].

$$q = -K_s(x)K_r(\psi_p)\nabla(\psi_p - z) \qquad (4.2)$$

where K_s is the saturated hydraulic conductivity depends on soil texture [LT^{-1}], K_r is the relative permeability [-], q_s is the general source or sink term [T^{-1}] (includes wells and surface fluxes, e.g., evaporation and transpiration), and z is depth below the surface [L].

The van Genuchten relationships (Van Genuchten, 1980) relationships are utilized to define the relative saturation and permeability functions as follows:

$$S_w(\psi_p) = \frac{s_{sat} - s_{res}}{(1+(\alpha\psi_p)^n)^{(1-1/n)}} + s_{res} \qquad (4.3)$$

$$K_r(\psi_p) = \frac{(1 - \frac{(\alpha\psi_p)^{n-1}}{(1+(\alpha\psi_p)^n)^{(1-1/n)}})^2}{(1+(\alpha\psi_p)^n)^{\frac{(1-1/n)}{2}}} \qquad (4.4)$$

where s_{sat} [–] is the relative saturated water content, s_{res} [–] is the relative residual saturation, α [L^{-1}] and n [–] are soil parameters. Shallow overland flow is now represented in ParFlow by the kinematic wave equation. In two spatial dimensions, the continuity equation can be written as:

Chapter IV: Improvement of soil moisture and groundwater level estimations using a scale-consistent river parameterization

----

$$\frac{\partial \psi_s}{\partial t} = \nabla \vec{v} \psi_s + q_s \qquad (4.5)$$

where v is the depth-averaged velocity vector [LT^{-1}], ψ_s is the surface ponding depth [L], t is time [T] and q_s is a general source/sink (e.g., rainfall) rate [LT^{-1}]. If diffusion terms are neglected the momentum equation can be written as:

$$S_{f,i} = S_{o,i} \qquad (4.6)$$

which is commonly referred to as the kinematic wave approximation. In Eq. 6 $S_{o,i}$ is the bed slope (gravity forcing term) [−], which is equal to the friction slope $S_{f,i}$ [L]; i stands for the x- and y-direction. Manning's equation is used to establish a flow depth-discharge relationship:

$$v_x = \frac{\sqrt{S_{f,x}}}{n} \psi_s^{\frac{2}{3}} \qquad (4.7)$$

$$v_y = \frac{\sqrt{S_{f,y}}}{n} \psi_s^{\frac{2}{3}} \qquad (4.8)$$

where n is the Manning roughness coefficient [$TL^{-1/3}$]. In ParFlow, the overland flow equations are coupled directly to the Richards equation at the top boundary cell under saturated conditions. Conditions of continuity of pressure (i.e., the pressures of the subsurface and surface domains are equal right at the ground surface) and flux at the top cell of the boundary between the subsurface and surface systems are assigned. When coupled with ParFlow, the 1D soil column moisture prediction in CLM is replaced by the ParFlow approach (in 1D or 3D formulation). In the sequential information exchange procedure, ParFlow sends the updated relative saturation (S_W) and pressure (ψ) for the top 10 layers to CLM. In turn, CLM sends the depth-differentiated source and sink terms for soil moisture [top soil moisture flux (q_{rain}), soil evapotranspiration (q_e)] for the top 10 soil layers to ParFlow (see Fig. a). More details on the numerical aspects and other features of the model can be found in Kollet and Maxwell (2006).

We run ParFlow for a long time (100 years) with a steady recharge force to establish the groundwater table until groundwater tables and groundwater storage stopped changing. Following that, we run ParFlow with CLM, performing a 5-year spin-up by simulating the time period from 2012 to 2013 five times in order to acquire equilibrium initial state variables. We have to repeat it

Chapter IV: Improvement of soil moisture and groundwater level estimations using a scale-consistent river parameterization

----

until the differences between years are negligible (Ajamii et., al 20014; Seck et al., 2015) (here we consider differences between years to be less than 0.01 annual precipitation) to ensure that we are not gaining or losing substantial volumes of water to the subsurface over time before we start running test cases.

4.3.2 Land surface data and atmospheric forcing

The land surface input data include topography, land cover, soil characteristics, and physiological parameters of the canopy which are static variables. Global Multiresolution Terrain Elevation Data 2010 (Danielson et al., 2011) was used as Digital elevation model (DEM) which has a resolution of 1km (see Fig.). The Moderate Resolution Imaging Spectroradiomete\r (MODIS) satellite land-use classification (Friedl et al., 2002) was also used, wherein it was converted to Plant Functional Types (PFT). In order to include the soil characteristics, the percentage of soil and clay were obtained using FAO/UNESCO Digital Soil Map of the World (Batjes, 1997) which has numerous soil classes consisting of 19 classes, which was based on Schaap and Leij (1998)'s pedotransfer functions. For hydraulic characteristics of soil such as saturated hydraulic conductivity and Van-Genuchten parameters, the SoilGrids250m as well as the dataset aggregated to 1 km resolution (Hengl et al., 2017) were using by utilizing the European pedotransfer functions (EU-PTFs; Tóth et al., 2015). For the manning's coefficient, the proposed relationship between landcover type and manning's coefficient is used (Asante et al., 2008).

The atmospheric forcing of the coupled ParFlow model with CLM is provided from COSMO-REA6 data, which has a spatial resolution of 0.055° (~6 km) and temporal resolution of daily, and covers the domain defined by CORDEX EUR-11(Gutowski et al., 2016). COSMO-REA6 dataset (Bollmeyer et al., 2015) which is a reanalysis with high resolution from the Hans-Ertel Center for Weather Research is used for the time period of 2012-2014 (HErZ; Simmer et al., 2016).

German Weather Service data were used to obtain barometric pressure, wind speed, precipitation, specific humidity, downward shortwave and longwave radiations and air temperature near the surface. These meteorological data are available to download from the German Weather Service (DWD; ftp://ftp-cdc.dwd.de/pub/REA/). There are some uncertainties in COSMO-REA6 data especially, precipitation data which is used in this study Bollmeyer et al. (2015). They showed that

Chapter IV: Improvement of soil moisture and groundwater level estimations using a scale-consistent river parameterization

---

precipitation data from COSMO-REA6 has a relatively good performance when compared to Global Precipitation Climatology Centre data, however, it under-estimates precipitation in middle and southern Europe and over-estimates in Scandinavia, Russia, and beaches of Norway.

Additionally, Springer et al. (2017) assessed the closure of the water budget in the 6km COSMO-REA6 and compared it to global reanalysis (Interim ECMWF Reanalysis (ERA-Interim), Modern-Era Retrospective Analysis for Research and Applications, Version 2 (MERRA-2)) for major European river basins. In their study, Springer et al. (2017) found that the COSMO-REA6 closes the water budget within the error estimates whereas the global reanalysis underestimates the precipitation minus evapotranspiration deficit in most river basins. A more comprehensive assessment of the precipitation of the HErZ reanalysis can be found in Wahl et al. (2017), albeit based on the 2 km data product, only available for central Europe. The input data sets disused in this section, are summarized in Table 4.1. All model inputs were re-projected to have an equal cell size of 0.055° (~6 km). In this study, the model was directed at the Upper Rhine Basin for a total thickness of 100 m over 300 model layers with different thickness. The model was implemented with a horizontal resolution of 6 km with nx=31, ny=32 for a total model dimension of 186 km *192 km * 100 m and 35712 total compute cells. Since the hydraulic characteristics such as saturated hydraulic conductivity and Van-Genuchten parameters provided by the SoilGrids are available for the first two meters of soil, these hydraulic characteristics for the layers are located lower than 2m are the same as the layer is located at 2m under surface. Table 4. 2b shows a visualization of the model. The porosity and specific storage are constant and equal to 0.35 and 10-5, respectively. ParFlow allows the user to specify the permeability tensor. In this study, permeability is considered heterogeneous and symmetric in all directions (x, y, and z) and it is specified for the whole domain and considered as isotropic. There were two distinct boundary conditions that applied. 1) in the south at Basel, the Rhine River discharge is subjected to temporal variation. 2) in the northern and southern boundaries, a constant piezometric head is applied.

---

a

b

Chapter IV: Improvement of soil moisture and groundwater level estimations using a scale-consistent river parameterization

----

Fig. 4.2 a) Schematic of the coupled ParFlow-CLM model from Kuffour et al. (2020). In the bottom rectangle, ParFlow depicts the root zone, deeper vadose zone, and saturated zone. The top rectangle depicts CLM's atmospheric forcing and land surface processes. It's worth noting the root zone, where the two models exchange information about fluxes and state variables at the conceptual boundaries of the respective compartment models. The downward and upward arrows represent the pathways of information transmission between models. b) Visualization of the model including dimensions of the domain and parametrization of the aquifer. Porosity and specific storage coefficient are constant and the hydraulic characteristics such as saturated hydraulic conductivity and Van-Genuchten parameters are isotopic and non- homogenous and as the same as layer 6 for the layers 7-300.

Chapter IV: Improvement of soil moisture and groundwater level estimations using a scale-consistent river parameterization

----

Table 4.1 The input data for ParFlow-CLM

Input Data	Data Source	Download Link or Reference
Atmospheric forcing (specific humidity, near surface air temperature, barometric pressure, wind speed, precipitation, longwave and shortwave radiation)	COSMO-REA6 dataset	ftp://ftp-cdc.dwd.de/pub/REA/
Plant Functional Type,	MODIS satellite (land-use classification)	https://lpdaac.usgs.gov/products/mcd12q1v006/
Soil Texture Data, Sand and Clay Percentage	FAO/UNESCO Digital Soil Map of the World	(Batjes, 1997)
Hydraulic conductivity	European Soil Data Centre (ESDAC)	https://esdac.jrc.ec.europa.eu/content/3d-soil-hydraulic-database-europe-1-km-and-250-m-resolution
Van- Genuchten Parameters (n, α)	European Soil Data Centre (ESDAC)	https://esdac.jrc.ec.europa.eu/content/3d-soil-hydraulic-database-europe-1-km-and-250-m-resolution
DEM	Global Multiresolution Terrain Elevation Data 2010	https://earthexplorer.usgs.gov/
Manning's coefficient	Relationship between landcover type and manning's coefficient	(Asante et al., 2008)

4.3.3. River Parametrization

Since ParFlow does not address the flow condition (e.g., river network) for the river, ParFlow does not distinguish between hillslope runoff and river flow, and the same horizontal grid resolution applies to the subsurface and surface water domains. Forcing the same coarse horizontal grid resolution for the subsurface and surface water domains, results in an underestimation of the flow velocities while the rate of ex- and in-filtration between the river and the subsurface is overestimated.

Chapter IV: Improvement of soil moisture and groundwater level estimations using a scale-consistent river parameterization

----

Sub grid scaled river channel geometries, such as exchange fluxes with the subsurface, through the use of scaled grid scale parameters is incorporated in modeling to compensate this large rate of ex- and in-filtration between the river and the subsurface. As a result, to use the overland flow boundary condition in ParFlow, we use derived scaled Manning's coefficient (n) and saturated hydraulic conductivity (K_{sat}) by Schalge et al. (2019).

4.3.3.1 Manning's Coefficient Scaling
In order to correct the flow velocity (v) in the grid cell of model which is usually greater than river width (W_1), a scaling of Manning's coefficient is used. In an ideal high-resolution simulation, the width of river channel (W_1) and Manning's coefficient (n_{org}), as well as the flow velocity (v_1) are considered as the same as real river channel. a. In a less resolution model, the width of the river is considered W_2 which is equal to the width of the grid cell and greater than W_1. In this less resolution model, if we consider the same n_{org} the flow velocity (v_2) is lower than flow velocity in river (v_1). Because the water depth is smaller in the wider channel. Therefore, the flow velocity can be corrected using reducing n_{org} to n_{scale}. As a result, in a lower resolution simulation (grid cell is W_2) flow velocity equals to v1(for more details refer to Schalge et al. (2019)). A simple equation is used to scale roughness coefficient as follows:

$$n_{scale} = n_{org} \cdot (\frac{W_1}{W_2})^{2/3} = \lambda . n_{org} \tag{4.9}$$

Where $\lambda = (\frac{W_1}{W_2})^{2/3}$ is the scaling coefficient for Manning's roughness coefficient, which corrects the river flow velocity in a lower resolution simulation which is independent of channel slope S_f and discharge Q.

4.3.3.2 Hydraulic Conductivity Scaling
Because the width of the model river is often larger than the actual river width, a larger surface area will exchange water with the subsurface than the real river. A scaled (lower) hydraulic conductivity can be used to correct this. In order to keep the infiltration/exfiltration fluxes in model equals the true rate in real river fluxes are preserved, by using scaled K_{sat}, resulting in

---

$$\int_{A_2} K_{sat\_scaled} dA_2 = \int_{A_1} K_{sat\_org} dA_1 \qquad (4.10)$$

Where $A_2 = W_2 \times W_2$ is the area of the river in model and $A_1 = W_2 \times W_1$ is the area of the real river. substitution the A_2 and A_1 in the equation above, results in

$$\int_0^{W_2} \int_0^{W_2} K_{sat\_scaled}(x, y) dx dy = \int_0^{W_2} \int_0^{W_1} K_{sat\_org}(x, y) dx dy \qquad (4.11)$$

K_{sat} is homogeneous in each grid cell and by assuming a rectangular river channel cross section, the scaling coefficient is as

$$K_{satscale} = K_{satorg} \cdot \frac{W_1}{W_2} \qquad (4.12)$$

$\chi = \dfrac{W_1}{W_2}$ is the scaling coefficient for the hydraulic conductivity (for more details refer to Schalge et al. (2019)).

4.3.4. Probabilistic Framework of the Validation: First Order Reliability Method (FORM)

In this approach, a Limit State Function (LSF) is defined as the mathematical formulation of a system state limit beyond which the system reliability criteria are no longer satisfied in this method. (Abdelkhalak and Bouchaïb 2013). In analogy to the simulation results of a hydrological model, the standard deviation (SD) can be used as a criterion to examine the reliability of the model by defining LSF less than 10% as the state limit for simulated groundwater level and 25% for simulated soil moisture. This criterion expresses as:

$$\begin{cases} SD(SM) = \dfrac{Model\,Estimation(SM) - Observation(SM)}{Observation(SM)} \leq 0.1 \\ SD(Gr) = \dfrac{Model\,Estimation(Gr) - Observation(Gr)}{Observation(Gr)} \leq 0.25 \end{cases} \qquad (4.13)$$

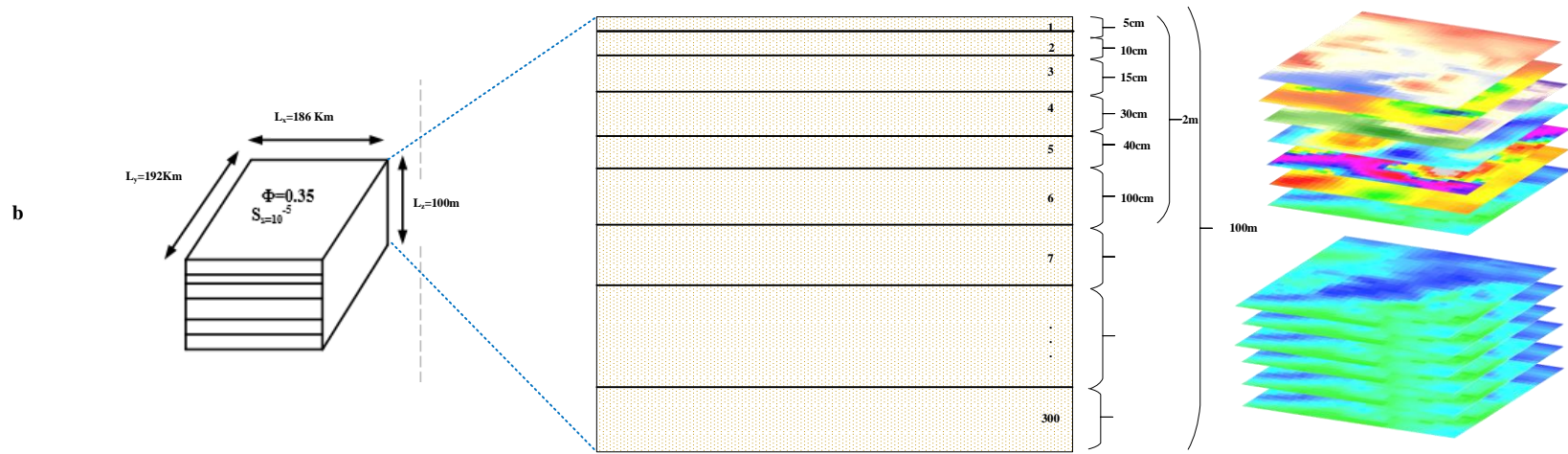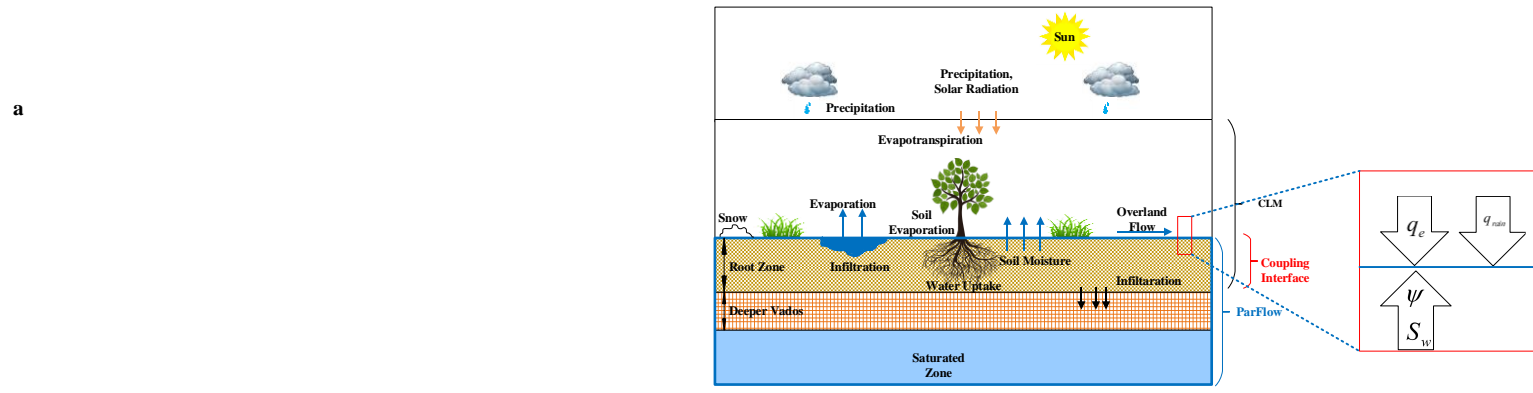**Chapter IV: Improvement of soil moisture and groundwater level estimations using a scale-consistent river parameterization**

Based on the assumption that LSF is continuous and first-order differentiable, FORM uses a linear approximation (i.e., first order Taylor expansion) expressed as

$$G(y) = L(y) = G(y_m) + \nabla G(y_m)^T \cdot (y - y_m) \tag{4.14}$$

where L(y) is the linearization of the LSF, $y = y(y_1, y_2, y_3, \ldots y_n)$ is the vector of n variables defining the G function, y_m is the expansion point, and $\nabla G(y)$ is the first order gradient vector of $G(y)$.

The two critical FORM requirements are explained in detail as follows paragraphs. (For more details refer to Soltani et al., 2020).

1. First, project the variables X (in this case soil moisture or groundwater level) to the independent standard normal space Y. In order to implement FORM, non-normally distributed variables should be transformed into standard normal variables (Madsen et al., 2006) via, e.g., the NATAF transformation (Nataf, 1962).

2. Next, finding a point on the transformed LSF with the shortest distance to the origin in the uncorrelated standard normal space (Shinozuka, 1983). This point is called the design point (or the most probable point) that can be obtained by solving the following constrained optimization problem.

$$y* = \arg\min\{\|y\|\} \tag{4.15}$$

$y *$ is the design point which has the shortest distance to the origin in the uncorrelated standard normal space. Various approaches have been developed during the past decades to solve the constrained optimization problem described in Eq. (10). The iHLRF (Zhang and Kiureghian, 1997) is a state-of-the-art method which can be used to obtain the point on the failure surface that is closest to the origin. In this approach, the design point is found by a generic search algorithm via the following iterative equation:

$$y_{m+1} = y_m + s_m \cdot d_m \tag{4.16}$$

----

where m is the iteration number, s is the step length, and d is the direction of the search. Let y*

be the answer to this optimization problem, and β be the optimal point's distance from the origin.

as a result, the estimated probability of failure is expressed as

$$P_f = \Phi(-\beta) \tag{4.17}$$

where Φ is the cumulative probability distribution function of β. The limitation of FORM is that it

can only give an exact solution if the initial limit state is linear and the basic variables are normally

distributed. The extent of error, on the other hand, is determined by the curvature of the limit state

and the method of projecting X to Y. Fig. 4.3 shows the general procedure of the FORM

implementation.
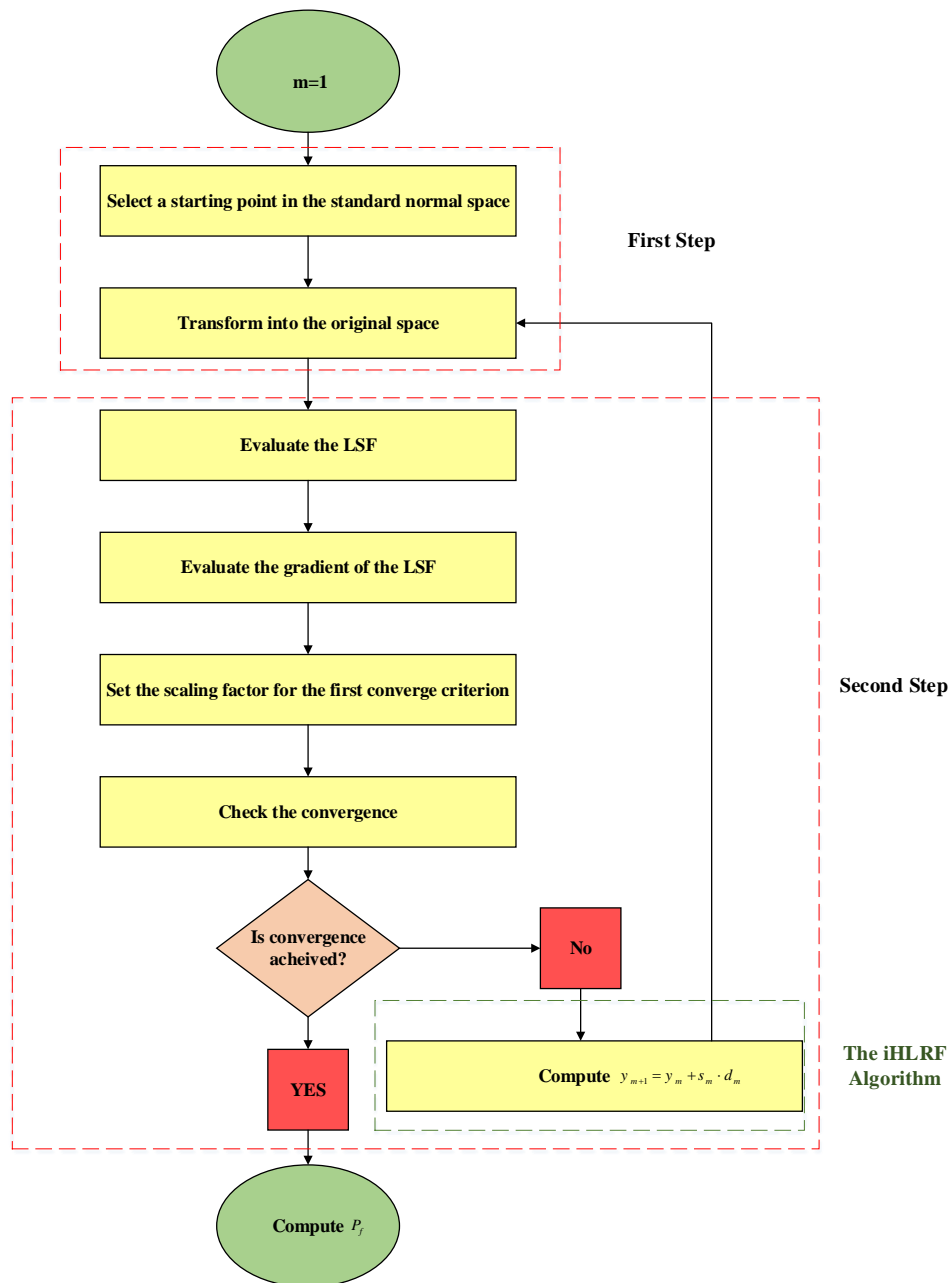
Fig. 4.3 Steps to implement the FORM algorithm. After defining LSF, the variables are transformed to the independent standard normal space in the first step and in the second step, a point on the transformed LSF with the shortest distance to the origin is found. The iHLRF (Zhang and Kiureghian, 1997) is used to obtain this point on the LSF.

Chapter IV: Improvement of soil moisture and groundwater level estimations using a scale-consistent river parameterization

----
4.3.5 Evaluation Dataset

4.3.5.1 Groundwater Level Measurements
Piezometric level data came from 190 observation wells sampled weekly, only a few of them giving daily data. These observation wells are managed mainly by the APRONA (Association pour la PROtection de laNappe d'Alsace) on the French side and by the LUBW-Baden-Württemberg (Landesanstalt für Umwelt, Messungen und Naturschutz in Baden-Württemberg) on the German side. In this case study, the fluctuation of groundwater level is limited to less a few meters. However, this fluctuation is more where the groundwater table is deeper such as the eastern and western borders (Thierion et al. 2012).

4.3.5.2 ESA CCI Microwave Soil Moisture
ESA (European Space Agency)'s CCI program (Climate Change Initiative) provides Soil Moisture (SM) data from 1978 and on a spatial resolution of 0.25°. The CCI-SM data is daily soil moisture for the top milli/centimeters of the soil. The CCI-SM version 05.2 uses microwave wavelengths to obtain soil moisture data using data from several sensors (Dorigo et al., 2017; http://www.esaoilmoisture- cci.org). CCI-SM uses passive microwave measurements (i.e., DMSP SSM/I, TRMM TMI, Aqua AMSR-E, Coriolis WindSat, SMOS and SMAP). On the other hand, active data products are obtained using scatter meters in the C-band which are installed on ERS-1, ERS-2 and ASCAT A-B satellites (Wagner et al., 2013). Cumulative density function matching was used to rescale the absolute soil moisture. For this purpose, the 0.25° resolution land surface soil moisture modeled data were used as a reference (GLDAS-NOAH, Rodell et al., 2004). In addition, both passive and active soil moisture products are merged herein which was better than either one alone (Liu et al., 2011). Resampling and re-gridding to the target resolution of 0.0275° were done on the SM values for matching of the spatial resolution. This was done via the conservative interpolation of first-order one (Jones, 1999). In this technique, the interpolation weights are based on the fractional area-overlap of the source and destination grid cells. The re-gridding in the conservative scheme allows the preservation of flux fields of physical quantities between both the destination and source grids. The CCI-SM data reveals significant data gaps over the Upper Rhine Basin in all seasons. In the time period of 2012-2014, the temporal coverage (i.e., the ratio between the number of days with valid data and the number of total days) ranged from

Chapter IV: Improvement of soil moisture and groundwater level estimations using a scale-consistent river parameterization

---

less than 10% (Southern regions) to over 60% (Northern regions) in Fig. 4.4. Finally, Fig. 4.5

shows the overall scheme of this study that was given in methods and data section.
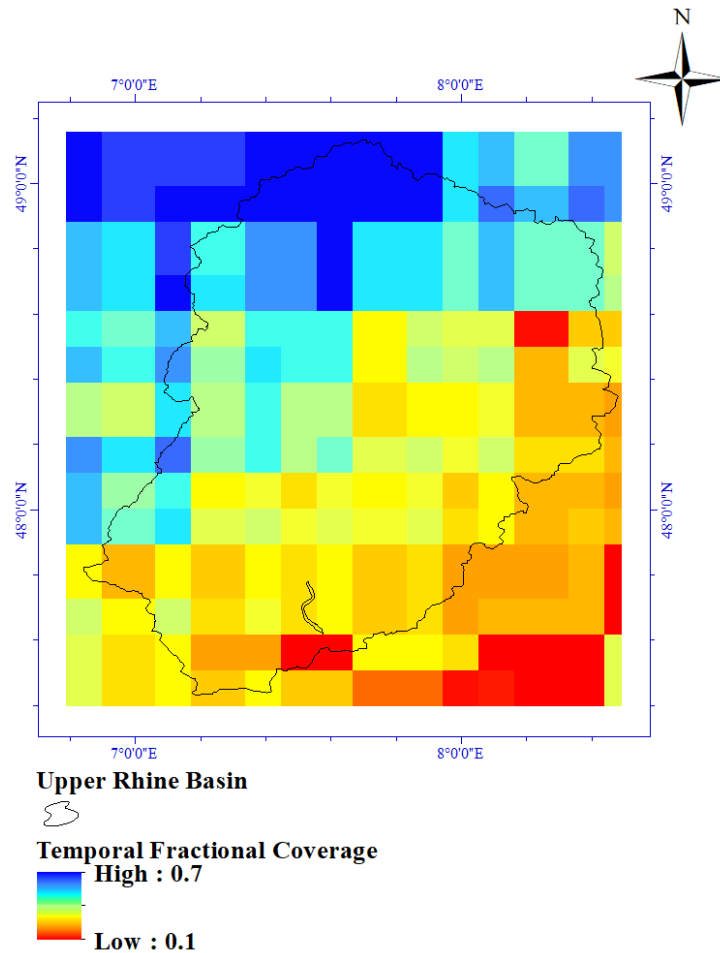
Fig. 4.4 Fraction of days that ESA-CCI SM data was reported over the time period of 2012-2014.

Chapter IV: Improvement of soil moisture and groundwater level estimations using a scale-consistent river parameterization
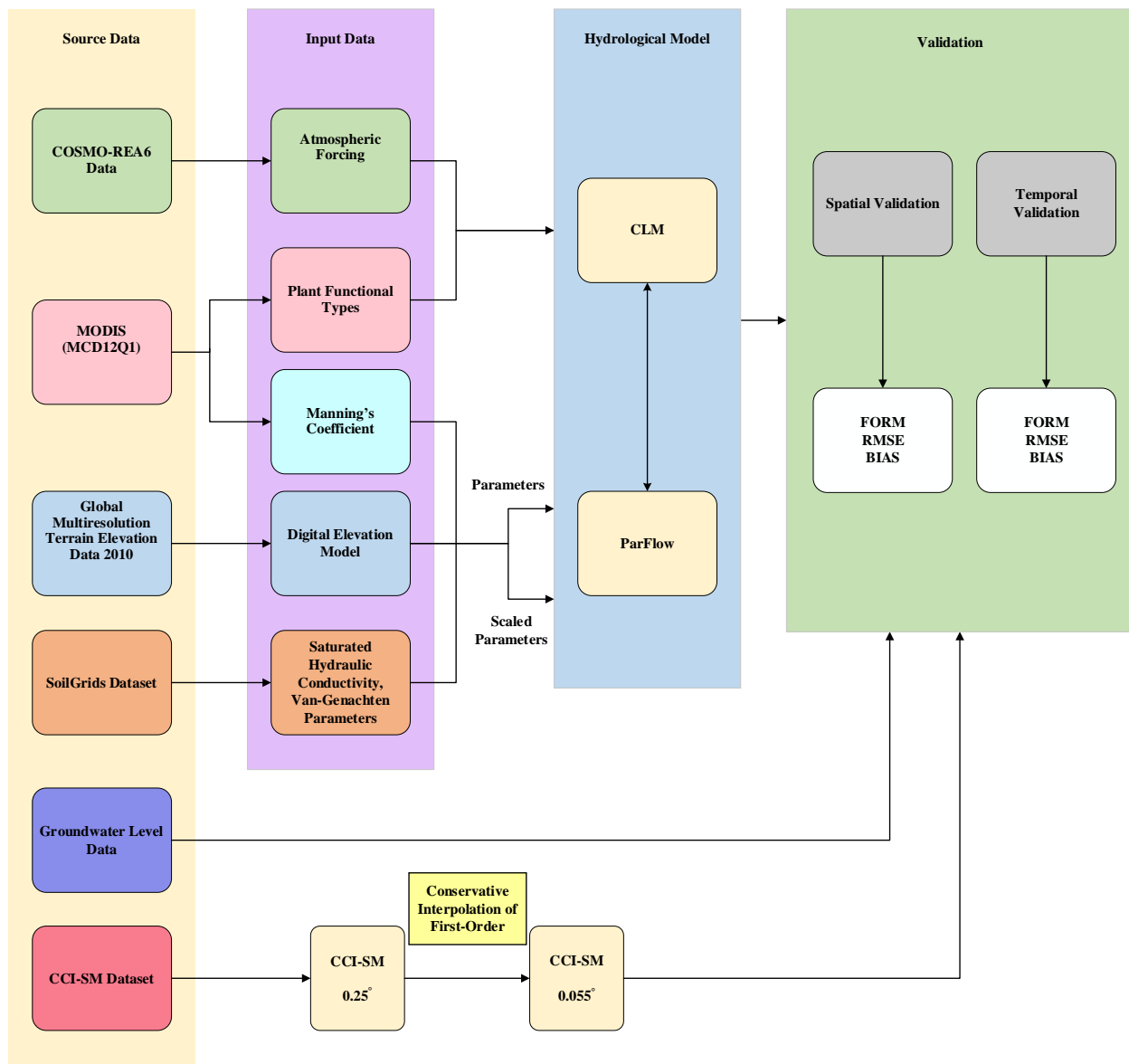
Fig. 4.5 Overall scheme of this study. Overall scheme to identify the used land surface and atmospheric forcing, methodology of research and validation. Abbreviations: RMSE, root-mean-square deviation; FORM, first order reliability method.

4.3.5.3 Finding River Width

By using the Hydro SHEDS river topology dataset (This database is available at http://gaia.geosci.unc.edu/rivers/) as well as geomorphic relationships between parameters such as area, discharge, width and depth of the river, a simple database containing the widths and depths

Chapter IV: Improvement of soil moisture and groundwater level estimations using a scale-consistent river parameterization

----

of the rivers has been created, which can be used when there are no reliable measurements available to input the initial estimation for the hydrological models. The database does not intend to replace detailed estimations of the river width and depth, instead it maps the river characteristics with near-global coverage. However, this database provides estimations with 95% confidence interval which gives a reasonable estimate of the width and depth of the rivers.

The spatial width of the river for the Upper Rhine Basin is shown in Fig. 4.6 a and it ranges from 6.5 m to 325 m. In this simulation, narrow rivers with less than 10 m widths have not been considered, as they are only appearing during and after raining.

Fig. 4.6 b and c show the resulting scaling parameter for saturated hydraulic conductivity and Manning's coefficient following Eq. (4.9) and Eq. (4.12) ranges from 0.01 to 0.16 and 0.001 to 0.065 respectively. Fig. 4.6 d shows the scaling approach to which cells in the basin have been applied. In this figure, the effective cells whose rivers are more than 10 meters wide are blue in color, and these cells have been applied scaled manning's coefficient and saturated hydraulic conductivity. The red color in this figure indicates cells in which the width of the river is less than 10 meters.
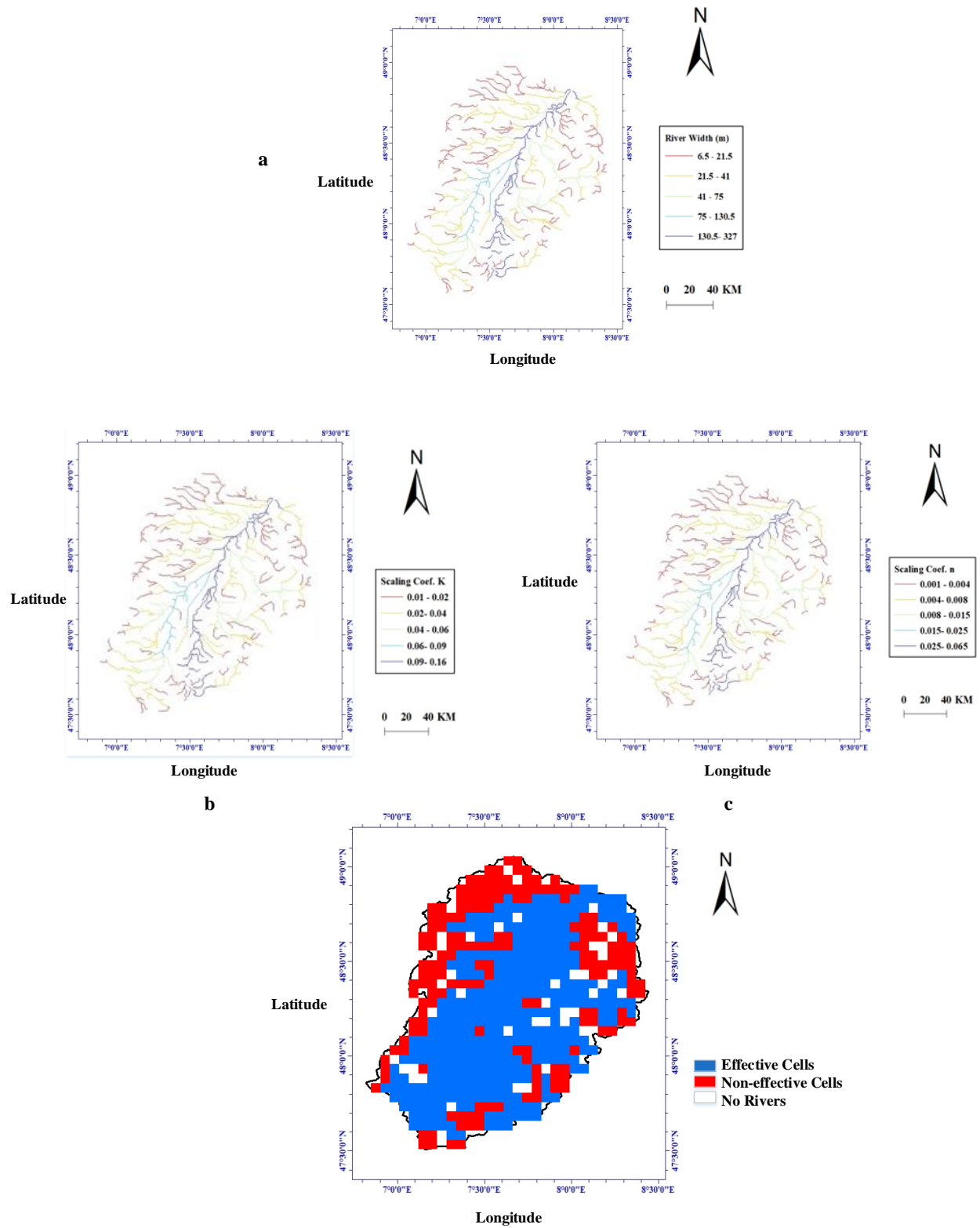
Chapter IV: Improvement of soil moisture and groundwater level estimations using a scale-consistent river parameterization

----

Fig. 4.6 a) River width (W1) in unit of meter, b) scaling coefficient of saturated hydraulic conductivity, c) scaling coefficient of Manning's coefficient and d) effective and non-effective cells in scaling approach over the Upper Rhine Basin

4.4. Results

4.4.1 Evaluation of Soil Moisture

4.4.1.1 Seasonal Mean Comparison
The seasonal volumetric soil water content (SWC) (mm^3/mm^3) from ParFlow-CLM without parameter scaling (ParFlow-CLM) and ParFlow-CLM with n and K_{Sat} scaling (ParFlow-CLM-S) is shown in Fig. 4.7 compared to the seasonal mean CCI-SM data.

In general, the ParFlow-CLM simulation has higher SWC in all seasons (DJF, MAM, JJA, and SON) over most part of the Upper Rhine Basin than the ParFlow-CLM-S simulation.

When comparing the ParFlow-CLM-S simulations to the CCI-SM observations, the spatial distribution of SWC in summer and autumn is better represented in the ParFlow-CLM-S simulations than in the ParFlow-CLM simulations (Fig. 4.7). Naz et al. (2018) assimilated the CCI-SM data into CLM to improve soil moisture and runoff simulations. The assimilation results showed a slightly better agreement with the CCI-SM data in the summer and autumn seasons than the spring and winter seasons. In this regard, data assimilation, n and K_{Sat} scaling improve soil moisture simulations in similar seasonal patterns.

For the time period of 2012-2014, Fig. 4.8 compares the temporally averaged SWC simulated by ParFlow-CLM, ParFlow-CLM-S, to CCI-SM data over the Upper Rhine Basin. In general, the SWC values were overestimated by ParFlow-CLM in all seasons. This overestimation was decreased with scaled n and K_{Sat}, as shown using ParFlow-CLM-S. It is worthy of note that, the narrow spread of quartiles of ParFlow-CLM-S calculated SWC compared to ParFlow-CLM in Fig. 4. indicates that scaling of n and K_{Sat} did not diminish spatial variability. Similarly, when validating models with CCI-SM data, the ParFlow-CLM improvements vary depending on the season. However, improvements were more noticeable for all seasons.

Chapter IV: Improvement of soil moisture and groundwater level estimations using a scale-consistent river parameterization
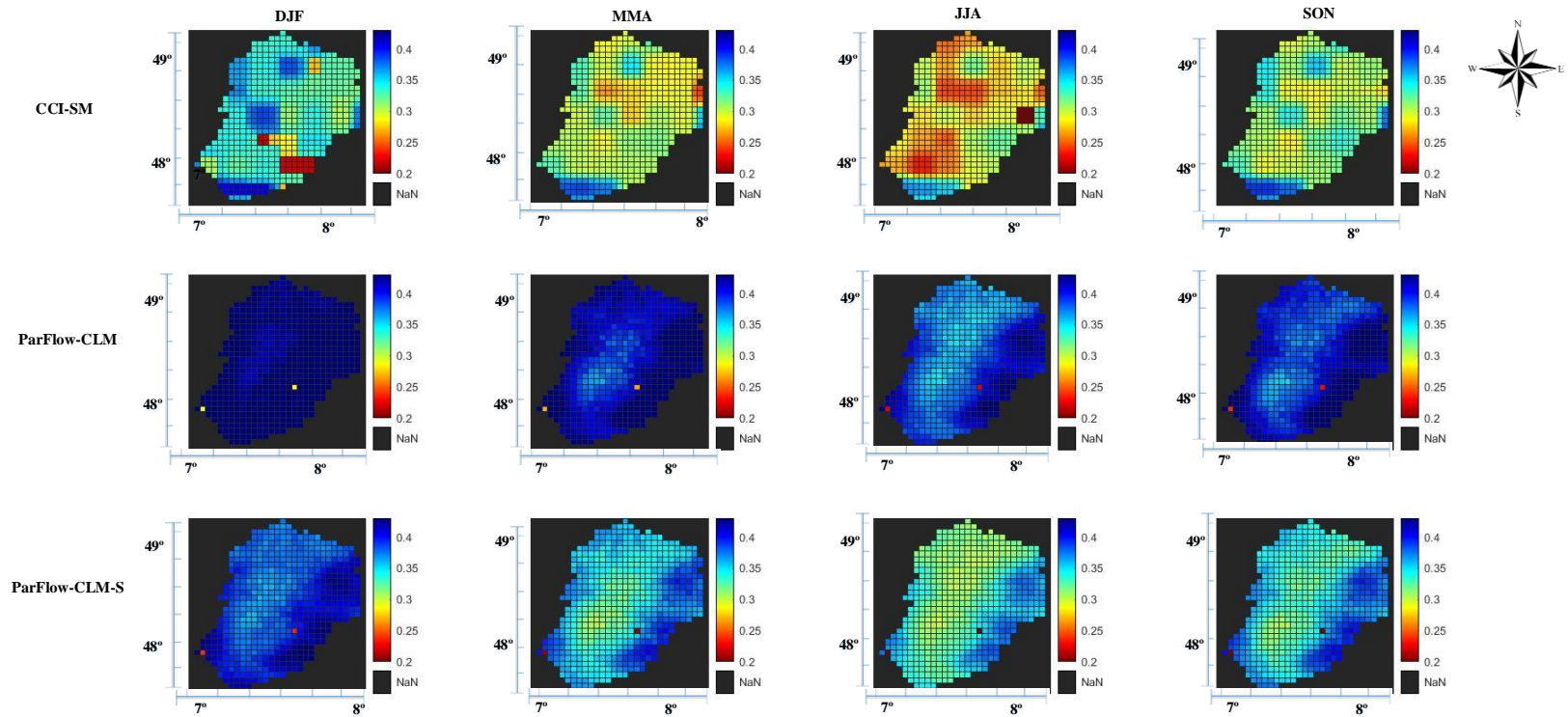

Fig. 4.7 Seasonally averaged SM simulated by ParFlow-CLM and ParFlow-CLM-S for the upper soil layer (0-5 cm) and compared to CCI-SM data for the DJF (December, January, and February), MAM (March, April, May), JJA (June, July, and August), and SON (September, October, and November) seasons from 2012 to 2014.
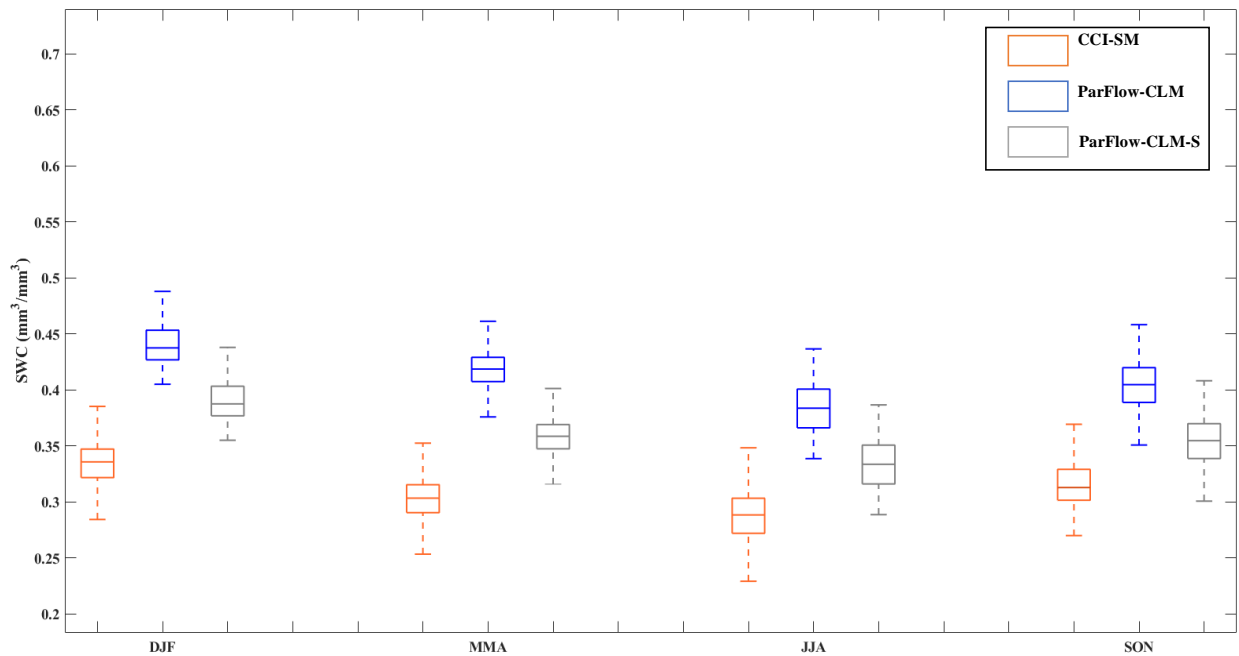
Fig. 4.8 Boxplot of seasonally averaged SWC simulated by ParFlow-CLM, ParFlow-CLM-S, and CCI-SM data from 2012 to 2014. DJF (December, January, and February) represents winter; MAM (March, April, May) represents spring; JJA (June, July, and August) represents summer and SON (September, October, and November) represents autumn. The central, bottom, and top marks on each box represent the median and extreme values, respectively.

Cross-validation with CCI-SM observations was undertaken to assess the skill of ParFlow-CLM-S relative to ParFlow-CLM, and Root Mean Square Error (RMSE) and BIAS for soil moisture were calculated using daily values for the Upper Rhine Basin and all seasons, as shown in Fig. 4.9. Note, that model data was only utilized to calculate these statistics on days when satellite data was available. For all seasons in the Upper Rhine Basin, ParFlow-CLM-S had a consistently lower RMSE than ParFlow-CLM, with the exception of winter, when SWC benefits were relatively minor (Fig. 4.9 c and d).

For all regions, the mean RMSE decreased from 0.03 mm^3/mm^3 (ParFlow-CLM) to 0.005 mm^3/mm^3 (ParFlow-CLM-S). The BIAS shows a substantial overestimation of soil moisture in comparison to satellite CCI-SM observations (Fig. 4.9 a and b), while the BIAS for soil moisture

Chapter IV: Improvement of soil moisture and groundwater level estimations using a scale-consistent river parameterization

----

from ParFlow-CLM-S is considerably decreased (Fig. 4.9 a and b). For all regions, the mean BIAS decreased from 0. 17 mm^3/mm^3 (ParFlow-CLM) to 0. 1 mm^3/mm^3 (ParFlow-CLM-S). In addition, an innovative implementation of the FORM is used to examine the LSF failure probability as a criterion for verifying the model's results closure. By defining r less than 0.25, r can be used as a criterion to assess the reliability of the model's results.

To this end, the first order reliability method finds failure probability (P_f) of the model's results closure. Table 4. 2 Shows results of the FORM implementation for soil moisture simulations of ParFlow-CLM and ParFlow-CLM-S over all seasons. Since P_f in ParFlow-CLM-S is lower than ParFlow-CLM, closure and consistency of model's results using scaling approach is acceptable. FORM results show that the probability of a substantial divergence between ParFlow-CLM-S soil moisture results and CCI-SM observation which is defined more than 0.25 percentage of CCI-SM observation value is 0.05, 0.11,0.15and 0.08 for autumn, winter, spring and summer, respectively. The failure probability of defined LSF in winter is a little more than other seasons.

Chapter IV: Improvement of soil moisture and groundwater level estimations using a scale-consistent river parameterization

---
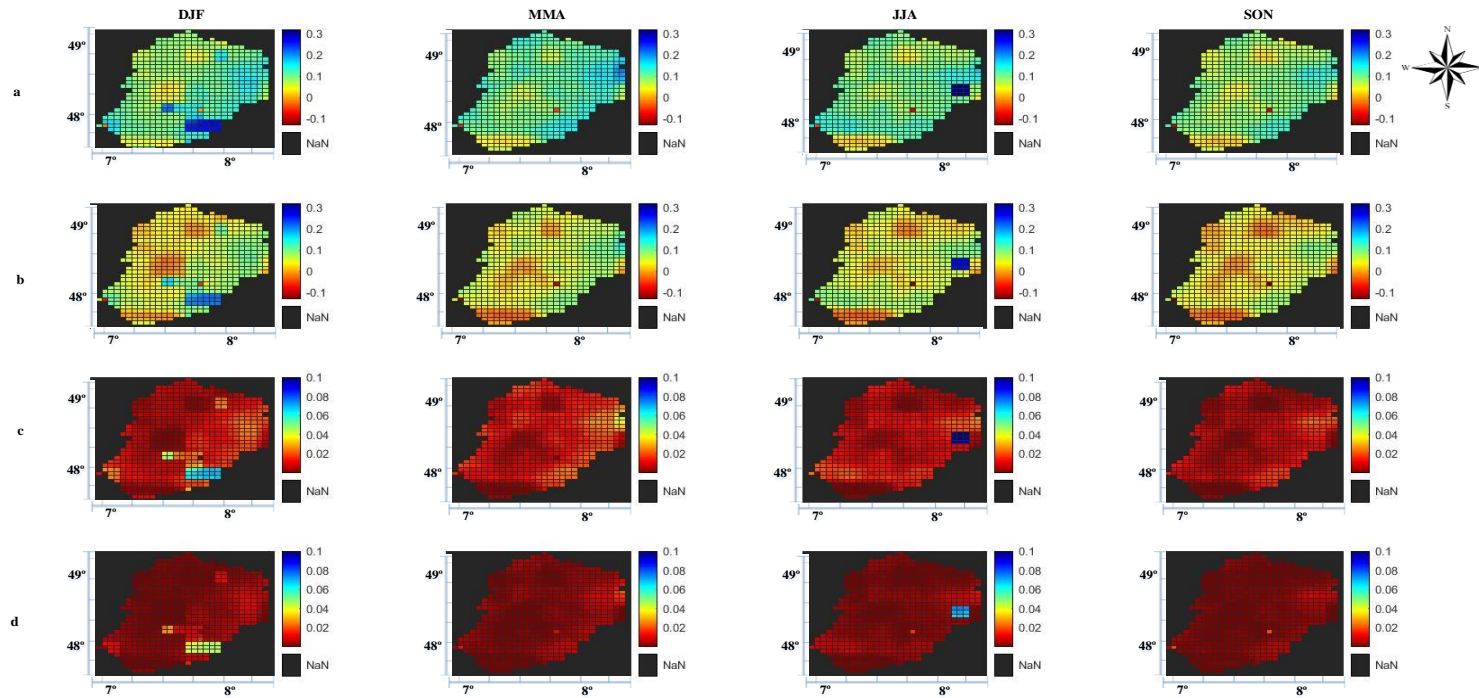
Fig. 4.9 RMSE and BIAS for daily soil water content for the DJF (December, January, and February), MAM (March, April, May), JJA (June, July, and August), and SON (September, October, and November) seasons from 2012 to 2014. (a) BIAS for ParFlow-CLM and (b) BIAS for ParFlow-CLM-S (c) RMSE for ParFlow-CLM and (d) RMSE for ParFlow-CLM-S simulations over the years 2012-2014.

Table 4. 2 The results of FORM implementation for soil moisture simulations of ParFlow-CLM and ParFlow-CLM-S over DJF (December, January, and February), MAM (March, April, May), JJA (June, July, and August), and SON (September, October, and November) seasons.

	P_f	
Seasons	ParFlow-CLM-S	ParFlow-CLM
SON	0.15	0.05
DJF	0.25	0.11
MMA	0.22	0.15
JJA	0.19	0.08

4.4.1.2 Daily Validation

The daily SM averaged from January 2012 to December 2014 over the Upper Rhine Basin (Fig. 4.1), as simulated by ParFlow-CLM and ParFlow-CLM-S, and observed by CCI-SM is presented in Fig. 4.10.

In ParFlow-CLM-S, the scaling approach improved the simulations of SWC. The daily SWC patterns predicted by ParFlow-CLM-S are very similar to the CCI-SM data, with general agreement across the basin.

When compared to the entire period, the CCI-SM observations show increased variability and drier soil moisture values during the summers. In general, the daily soil moisture predicted by the ParFlow-CLM-S agree with the CCI-SM data relatively better in the summer and autumn seasons than in the spring and winter seasons.

Due to dense vegetation, frozen soil, and/or model errors associated to modeling soil moisture in colder climates, ParFlow-CLM-S perform worse in winter season (Oleson et al. 2008). At the beginning of the simulation, especially in the winter 2012, the simulated soil moisture pattern is very different from the moisture obtained from CCI-SM. One of the main reasons for this issue can be related to the limitations of the model in simulating SM in cold seasons, especially when water freezes in the surface layers of the soil. Another case can be related to the steady state conditions of the model used to start.

For the time period of 2012-2014, Table 4.3 compares some important statistical parameters such as mean and variance of the spatially averaged soil moisture simulated by ParFlow-CLM, ParFlow-CLM-S, to CCI-SM data over the Upper Rhine Basin. In general, the soil moisture of the first soil layer simulated by ParFlow-CLM is higher than CCI-SM data in all seasons. This overestimation was decreased by using scaled n and K_{Sat}, as shown using ParFlow-CLM-S. It is worthy of note that soil moisture simulated by ParFlow-CLM-S compared to ParFlow-CLM in Table 4.3 indicates that improvements were more noticeable for all seasons.
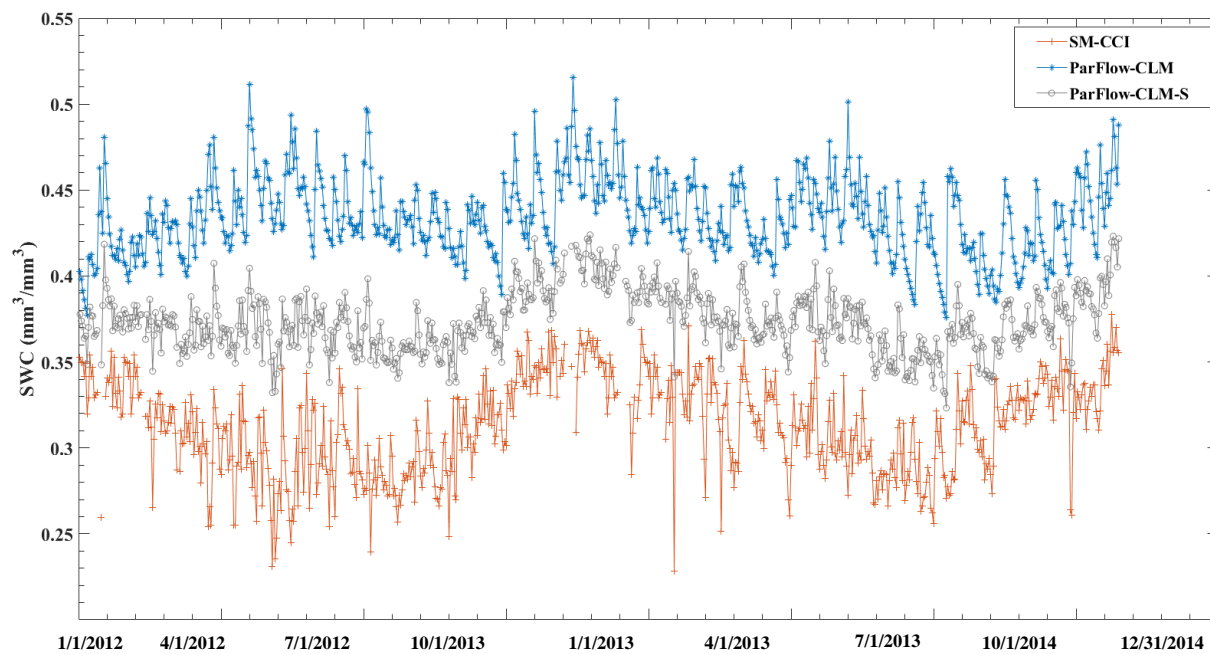
Fig. 4.10 Spatially averaged daily SWC simulated with ParFlow-CLM-S and ParFlow-CLM and compared to CCI-SM data for the Upper Rhine Basin from 2012 to 2014.

Table 4.3 Some statistical parameters for soil moisture simulations of ParFlow-CLM and ParFlow-CLM-S and CCI-SM data over DJF (December, January, and February), MAM (March, April, May), JJA (June, July, and August), and SON (September, October, and November) seasons

Season	CCI-SM		ParFlow-CLM		ParFlow-CLM-S	
	Mean	variance	Mean	variance	Mean	variance
DJF	0.327	0.047	0.44	0.025	0.39	0.019

MMA	0.306	0.0253		0.417	0.022	0.357	0.02
JJA	0.288	0.033		0.354	0.027	0.334	0.023
SON	0.318	0.0247		0.384	0.023	0.354	0.023

4.4.2 Evaluation of Groundwater Level: Annual mean comparison

Fig. 4.11 shows the groundwater level estimates of ParFlow-CLM and ParFlow-CLM-S, compared to groundwater level (from sea level) from well observations. ParFlow-CLM simulates higher magnitudes of groundwater level (on average 146m) over most parts of the basin compared to ParFlow-CLM-S (on average 143 m).

The overestimation in the ParFlow-CLM simulations was more significant in the central regions of the basin (Fig. 4.11). Compared to ParFlow-CLM, regional groundwater level patterns simulated by ParFlow-CLM-S agree better with groundwater level observations. When compared to well data in the central and northern regions of the basin, the ParFlow-CLM-S performs better.

As shown in Fig. 4.11, the scaling approach clearly resulted in an overall improvement in the simulated groundwater level for all regions.

Averaged annual groundwater level improvements are especially noticeable over the central and northern regions, where ParFlow-CLM-S reduced the discrepancy between well data and model's result from 6 m to 3m. Groundwater level from well observations were interpolated using the Kriging method (Krige, 1951). Some part of this difference is related to Kriging uncertainty. Several studies have addressed errors raised from uncertainty in random function estimation steps of the kriging methodology (Loquin and Dubois, 2010; Lloyd and Atkinson, 2001). As a result, uncertainty of the used model by using scaled parameters in groundwater level estimation is less than 3m.

Where the groundwater table is not shallow (more than 5 meters), the improvements over other regions of the basin, such as the southern regions, were relatively small. These findings indicate on the potential of scaling approach to improve shallow groundwater where the surface-subsurface coupling is most impactful.

The failure probability of LSF is investigated as a criterion to assess the reliability of the model's results through using a novel application of the First Order Reliability Method (FORM). By specifying r smaller than 0.1, it can be used as a criterion to assess the reliability of model's results.
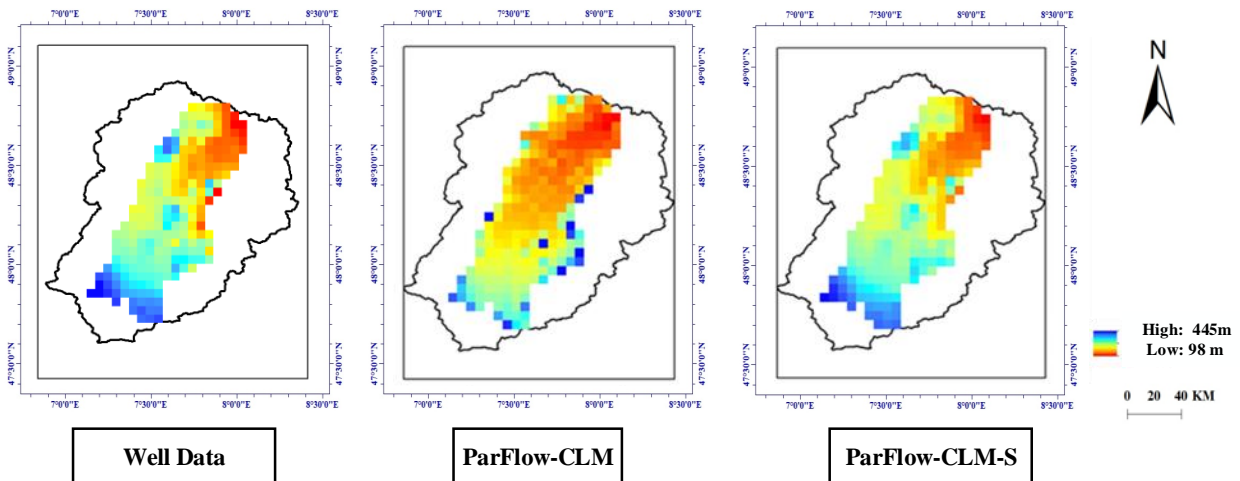
Fig. 4.11 Temporally averaged annual groundwater level from the sea level (m) simulated by ParFlow-CLM and ParFlow-CLM-S for the years 2012 – 2014 over the Upper Rhine Graben. Temporally averaged groundwater level from well data is shown for comparison.

To achieve this, the FORM calculates the failure probability (P_f) of the model's results closure. The results of the FORM implementation show that failure probability of simulated annual groundwater level by ParFlow-CLM and ParFlow-CLM-S is 0.05 and 0.1, respectively. Since P_f in ParFlow-CLM-S is lower than in ParFlow-CLM, the scaling approach is sufficiently accurate for model closure and consistency.

For the time period of 2012-2014, Table 4.4 compares some important statistical parameters such as mean, maximum and minimum of the temporally averaged groundwater level simulated by ParFlow-CLM, ParFlow-CLM-S, to well data over the Upper Rhine Basin.

In general, the groundwater level values (from the see level) decreased by ParFlow-CLM in all seasons. This overestimation (being groundwater level close to the surface) was decreased with scaled n and K_{Sat}, as shown using ParFlow-CLM-S. It is worthy of note that groundwater level

Chapter IV: Improvement of soil moisture and groundwater level estimations using a scale-consistent river parameterization

--

simulated by ParFlow-CLM-S compared to ParFlow-CLM in Table 4.4 indicates that scaling of n

and K_{Sat} did not diminish spatial variability. Improvements were more noticeable for all seasons.

Table 4.4 Some statistical parameters for groundwater level simulations of ParFlow-CLM and ParFlow-CLM-S and well data over DJF (December, January, and February), MAM (March, April, May), JJA (June, July, and August), and SON (September, October, and November) seasons.

Season	Well data			ParFlow-CLM-S			ParFlow-CLM		
	Mean	Max	Min	Mean	Max	Min	Mean	Max	Min
DJF	165.1	708.64	99.98	170.3	713.84	105.18	175.1	718.64	109.98
MMA	163.6	708.01	99.26	168.4	712.81	104.06	171.7	716.11	107.36
JJA	163.09	707.95	99.78	166.99	711.85	103.68	169.89	714.75	106.58
SON	164.46	708.86	99.84	168.96	713.36	104.34	173.46	717.86	108.84

Fig. 4.12 depicts a weekly groundwater level time series that shows ParFlow-CLM greatly overestimates the magnitude of groundwater level. Over all regions, the ParFlow-CLM-S decreases these biases and groundwater level simulations with ParFlow-CLM-S are more consistent with the well observations.

Chapter IV: Improvement of soil moisture and groundwater level estimations using a scale-consistent river parameterization

----
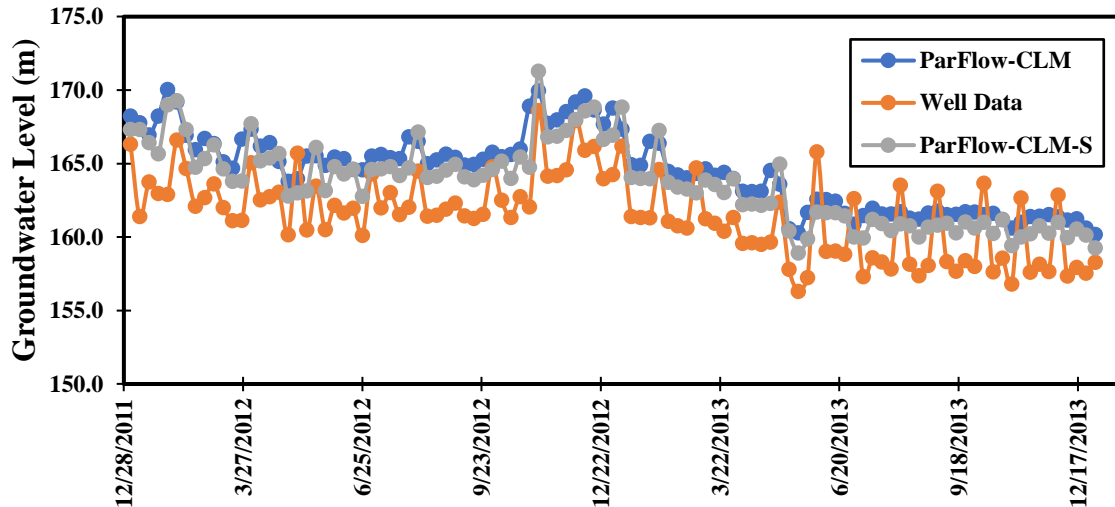
Fig. 4.12 Spatially averaged weekly groundwater levels simulated with ParFlow-CLM-S and ParFlow-CLM and compared to CCI-SM data for the Upper Rhine Basin from 2012 to 2014.

4.5. Discussion

Foster and Maxwell (2019) have proposed a scaling method for effective hydraulic conductivity and Manning's coefficient to compensate the loss of topographic gradients in coarse resolution simulations. In this study, simulations have been done using different hydraulic conductivity over four orders of magnitude in a real case study at 1-km and 100-m resolution. These findings indicate that when simulations are done at a coarse resolution, effective hydraulic conductivity must be biased higher. This study is in a good agreement with our findings and shows that scaling of hydraulic properties such as hydraulic conductivity obviously improves results of ParFlow-CLM model in less resolution simulations.

Other studies have also applied different hydrological models to estimate groundwater level in the Rhine-Meuse Basin. Sutanudjaja et.al (2011) used a MODFLOW transient groundwater model which was forced to recharge and the surface water level which was calculated by the land surface model. Absolute mean bias for some parts of the basin is higher than 50 m, while the maximum absolute mean bias is lower than 3 m in our study. This can be attributed to the use of offline

Chapter IV: Improvement of soil moisture and groundwater level estimations using a scale-consistent river parameterization

----

coupling technique in MODFLLOW that over-simplifies the dynamic feedback between surface water and groundwater loads, and between the moisture state of soil and groundwater level. In the coupled ParFlow-CLM approach we used the interaction between surface and subsurface is more suitable for the case study. It could also be due to differences in model parameters and calibration.

Considering the model calibration, several studies investigated methods to improve the hydrological models' predictions. Sutanudjaja et.al (2014) have investigated the possibility of calibrating the PCRaster Global Water Balance (PCR-GLOBWB) (Van Beek & Bierkens, 2009) which is coupled with MODFLOW (McDonald and Harbaugh, 1988) (PCR-GLOBWB-MOD) model (Sutanudjaja et al. (2011) by using remotely sensed soil moisture data and in situ runoff observations. Calibration is performed by executing of the model for 3045 times with various parameter values that affect the dynamics of the groundwater level in the Rhine-Meuse Basin. Conversely, the suggested methodology based on FORM in our work does not require multiple runs of the ParFlow-CLM model which is computationally expensive. In fact, given the physics of the problem underlying the method used, we run the model only once, using the scaled n and K_{sat} parameters. In order to improve model performance, Tangdamrongsub et. al (2015) have assimilated total water storage (TWS) data obtained from the Gravity Recovery and Climate Experiment (GRACE) data into the OpenStreams wflow-hbv model which is a distributed version of the HBV-96 model (Schellekens, 2014) using an ensemble Kalman filter (EnKF) method over the Rhine River basin. Although their results highlighted the benefit of assimilating GRACE data into hydrological models, they could be improved if limitations such as the lack of sufficient constraints on the soil moisture component did not exist. In the current implementation of ParFlow-CLM-S the enhancement did not rely on the use of additional spatial, but on the better parametrization and scale change which renders it robust as the inaccessibility to a specific dataset does not affect the results. Nevertheless, it would be of interest to test if the combined use of scale change and earth observation data would yield better predictions or reduction of uncertainties.

Selecting the threshold value for effective width affects the number of cells used in the scaling process. If a large threshold value is considered for the effective width, the number of cells for which the scaling process is performed will decrease, and if this value is selected low, the number of these cells will increase. Depending on the climatic conditions of the study area and the density

Chapter IV: Improvement of soil moisture and groundwater level estimations using a scale-consistent river parameterization

----

of the river network, the simulation time period, and the resolution of the model, the effect of the threshold value on the model simulation results changes. For example, if the study area has an arid or semi-arid climate that has been experiencing drought for a long time or a seasonal river is flowing in the study area at a specific time of year, more care should be taken to select the threshold value. Therefore, if a low threshold value is considered, the scaling process is performed for a period when the river is not flowing and thus affects the model simulation results. This is also important for regions that experience severe flooding during a specific time period. In these areas, if the threshold value is considered high, the number of pixels used during the flood and wet season decreases and influences the model simulation results.

There is no a certain criterion for choosing this low limit; However, it is suggested that rivers that do not exist in more than 50% of the simulation time period and flow in a short time due to floods and seasonal variations in rainfall should not be considered in scaling operations. According to Schalge et al (2019) study, model resolution is one of the most critical factors, and the success of scaling process decreases when the river width is less than 1/10 th of the model resolution. However, our findings show that the success of the scaling process is acceptable even if the width of the rivers is less than 1/10 th of the model resolution. It might be related to high density of river network in our case study, which exchange much water between the surface and the subsurface. In this regard, it is suggested that a comprehensive study be done to investigate the effect of model resolution and the river network density on the success of the scaling process in improvement of model results.

In this study, we used an integrated ParFlow-CLM model, which is a physic-based and requires the many input data. Calibration of these models, unlike concept models, Due to the huge computational cost, is not widely used. In addition, only the two parameters of porosity and specific storage are constant and for calibration we can only change the value of these two parameters and run the model for several scenarios. If the number of these scenarios is high, the computational load will increase significantly. However, a calibration with a limited number of scenarios may help to improve the results.

Chapter V: Multivariate satellite remote sensing data assimilation

----

5.1 Introduction

Terrestrial water storage (TWS) is the sum of available GW (groundwater), surface and snow water, as well as soil moisture (SM). TWS is a crucial variable for monitoring water resources in each of the 3 main water sectors (namely agriculture, drinking and industry). TWS estimation is essential for understanding past climate changes as well as future forecast in the hydrology cycle, river flow prediction and available water (Hirschi et al., 2007). TWS estimation can be further analyzed to obtain patterns of floods and heat waves. Each TWS component has a special impact on the climate as a whole. For instance, a major source of atmospheric humidity is supplied by soil moisture (Jung et al., 2010), therefore it is a strong contributor to the climate system (Seneviratne et al., 2010). In order to obtain accurate seasonal forecasts, soil moisture shall be accurately predicted. This was demonstrated successfully as it improved air temperature predictions in Europe and North America (Koster et al., 2010; van den Hurk et al., 2012). In addition, snowpack is an important variable especially for correction of the temperature near the surface mainly in higher latitudes on a monthly temporal scale (Orsolini et al., 2013). Soil moisture is affected by groundwater, which in turn influences evapotranspiration. As a result, this variable is linked to available water in the long term and it is also an important climate change driver (Bierkens and van den Hurk, 2007; Green et al., 2011).

Despite the importance of having reliable estimates of TWS, knowledge about the spatial and temporal variations of TWS and its components is generally lacking. This is particularly true at large scales, or less-developed countries due to the absence of global monitoring systems (Soltani et al., 2020). Ground-based measurements, while very accurate, only provide point-wise estimates (Dorigo et al., 2011; Lettenmaier and Famiglietti, 2006).

This is where hydrological models shine as they are able to fill this gap at high spatiotemporal resolutions (e.g., Koster and Suarez, 1999; Döll et al., 2003; van Dijk, 2010; De Paiva et al., 2013; Getirana et al., 2014). This is specifically true for Iran which lacks a comprehensive climate measurement system. As a result, hydrological models are invaluable tools for sustainable management of water bodies and agriculture (e.g., Bharati et al., 2008; Yu et al., 2015; Kourgialas and Karatzas, 2015). However, lack of reliable data often means that the

Chapter V: Multivariate satellite remote sensing data assimilation

----

modeling process is somewhat a blind process and this problem is compounded by errors in modeling and model parameter uncertainties (van Dijk et al., 2011; Vrugt et al., 2013).

As a result, simulation results can be weakened. Subsequently, models can be made more reliable by data assimilation (Bertino et al., 2003). For this purpose, additional information is supplied by means of new datasets which can constrain the estimators of state to more meaningful values (Bertino et al., 2003; Hoteit et al., 2012).

Assimilation of satellite data has applications in magnetospheric (Garner et al., 1999), ocean (Bennett, 2005; Lahoz et al., 2006) and atmosphere (Elbern and Schmidt, 2001; Schunk et al., 2004; Altaf et al., 2014) studies. It is also predominantly used in hydrological models wherein the accuracy of water components needs to be enhanced (e.g., Reichle, 2002; Alsdorf et al., 2007; de Goncalves et al., 2009; Renzullo et al., 2014; Dillon et al., 2016; Khaki et al., 2018a; Khaki et al., 2018b).

With GRACE TWS data assimilation, the components of the water balance including soil moisture and groundwater storage can be quantified since errors are considered for both observations and the model. In addition, total water storage observation from GRACE can be spatially downscaled with the model, giving better resolution of water storage for the study area (see, e.g., Schumacher and Kusche, 2016). In addition, by using soil moisture data from satellite and assimilation of this dataset, soil moisture component becomes more accurate, thereby improving its updated estimates (e.g., Tian et al., 2017). It has been shown that using total water storage from GRACE and satellite soil moisture product is successful in constraining the hydrologic model outputs to more accurate values (Tangdamrongsub et al., 2020).

Soltani et al. (2021) reviewed several studies that indicate GRACE TWS (e.g., Zaitchik et al., 2008; Houborg et al., 2012; Li et al., 2012; Eicker et al., 2014; Reager et al., 2015; Girotto et al., 2016; Girotto et al., 2017; Khaki et al., 2018a; Khaki et al., 2018b) and satellite soil moisture (e.g., Renzullo et al., 2014; Dumedah et al., 2015; Tian et al., 2017; Kolassa et al., 2017) for data assimilation can successfully constrain the hydrological models simulations.

The main objective of this study is using to use multi-mission satellite data products to improve predictions of sub-surface water storages in the hydrology model over a case study in Iran. As a result, GRACE-derived TWS and soil moisture observations from the SMOS are assimilated in the couple ParFlow-CLM hydrological model (or TerrSys-MP). TerrSys-MP coupled to the

Chapter V: Multivariate satellite remote sensing data assimilation

----

to the PDAF library (Parallel Data Assimilation Framework) (Kurtz et al., 2016; Nerger and Hiller, 2013). This is an efficient numerical tool which is capable of performing assimilation tasks in parallel, thereby making it attractive for applications at large spatial scales and high-resolution over long periods of time (Kurtz et al., 2016). This study uses the Ensemble Kalman Filter (EnKF) filter method (Whitaker and Hamill, 2002) in order to assimilate TWS from GRACE and soil moisture products from SMOS via the ensemble-based sequential technique into the Terrsys-MP.

Data assimilation efficacy is studied herein for missing signals of water storage especially extreme climate change and human effects. By utilizing satellite data assimilations, the model is constrained and the data and model uncertainties become limited. Therefore, the problem of missing signals of water storage can be somewhat alleviated. For this purpose, a case study in the west of Iran is selected, because this basin recently experienced a catastrophic flood which affected several provinces during the spring heavy rains. Unprotected ground by bushes and trees, the surface soil was washed away by the torrential rain, creating mud flow which inundated cities, urban areas and villages. Large scale damage to homes, infrastructures, farmlands and animal production units occurred, while other sectors suffered as well.

It should be pointed out that other similar regions were also studied previously by the authors using different satellite products and hydrological models (e.g., Khaki et al., 2018a; Khaki et al., 2018b; Tangdamrongsub et al., 2020). However, the novelty and the difference between the previous studies and the current study is that for the first time, both soil moisture product from SMOS and TWS data from GRACE are simultaneously assimilated into the ParFlow-CLM hydrology model.

In the remainder of this study, section 2 describes the geographical location of the study area with an emphasis on the long-term climate condition. Datasets and methodology including a brief overview of the equations used in the model and the data assimilation filtering scheme are presented in Section 3. In addition, the input variables and observational data sets used for model comparison are also presented. Results and discussions are provided in Sections 4 and 5, respectively, and the study concluded in Section 6.

Chapter V: Multivariate satellite remote sensing data assimilation

----

5.2 Case Study

The case study is some of the most important sub-basins of the west and southwest of Iran including Karun, Jarahi and Karkheh with a total area of 158,000 km^2, comprising ten percent of Iran's surface area. These sub basins are bounded by [29°N 35° N] and [46° E and 53° E], in the west of Iran (Fig. 5.1). The northern neighbor is the Kordestan province, the north-western neighbor is Ilam province, the southeastern neighbor is Bushehr province, the eastern neighbors are Markazi and Esfahan provinces, the southern neighbor is Persian Gulf, and the western neighbor is Iraq.

The study area has a semi-arid climate zone based on the De Martonne aridity index and the average temperature in the summer and winter are 48° and 4°C, and the annual rainfall is 486.5 mm. Deserts in this zone have an area of 1.3×10^6 ha, which is equal to two percent of the country's area, which are predominantly located in the south and southwest arid and hyper-arid climatic zones (Ardebili and Khademalrasoulb, 2018).

The important rivers that run through this basin are Jarahi, Karkheh, Karun, Zohreh and Dez, supplying 34×10^9 m^3 of water, which is equal to 33% of the total water resources of the entire country. This basin is a center for crops and tree cultivation which are fed off the five big rivers, and grow on the suitable plains of the southwest for agriculture (Ardebili and Khademalrasoulb, 2018).

Fig. 5.1 The geographical location of the case study, located in West of Iran, overlaid by the Digital Elevation Model (DEM) of the basin as well as the river network.

Chapter V: Multivariate satellite remote sensing data assimilation

----

5.3 Methodology and Data

5.3.1 Model Description: TerrSysMP

TerrSysMP (Shrestha et al., 2014) is a new land based hydrologic models which is scale-consistent and modular. It has three models for land surface, atmosphere and the groundwater which are well-known models. TerrSysMP's land surface part is CLM v. 3.5 (Oleson et al., 2004, 2008). The transfer of momentum, energy and the carbon cycle are calculated in CLM by considering 10 layers of soil with varying thicknesses, amounting to 3 meters in total. For calculating soil temperature and moisture dynamics, only the z-direction is considered. In other words, the grid cells do not communicate laterally in this regard. For snow deposition, five layers are used at most over the top of the soil. For plant representation, sixteen plants with various physiological characteristics are considered, each having different land surface flux, vegetative radiative transfer and carbon exchange values. There are prognostic parameters in CLM. These include soil moisture, temperature and water storage in the subsurface part; flow routing model, land fluxes including vegetation and soil evaporation, plant transpiration, and sensible heat flux from both the soil and plants; transfer through radiation via transmittance and adsorption of solar radiation, and emission and adsorption of short wavelength radiations as well as the exchange of carbon.

TerrSysMP uses ParFlow (v3.5) which is the variably saturated finite-difference groundwater model (Ashby and Falgout, 1996; Jones and Woodward, 2001; Kollet and Maxwell, 2006; Maxwell, 2013). ParFlow employs the three-dimensional Richards equation and includes a surface water routing scheme, which is based on the kinematic wave approximation of overland flow coupling subsurface and overland flow in an integrated fashion (Kollet and Maxwell, 2006). The Newton-Krylow scheme (Jones and Woodward, 2001) is used for solving the partial differential equations. In addition, discretization in the z direction is variable and the grid transform follows the terrain (Maxwell, 2013). Thereby, large topographic slopes are permitted for the groundwater flows. More details about this physic-based model can be found in Shrestha et al. (2014).

5.3.1.1 Water Balance

ParFlow can perform water balance calculations for the Richards' equation, overland flow, and CLM capabilities. There are two types of water balance storage: subsurface and surface, as well as two types of flux calculations: overland flow and evapotranspiration. The storage

components are measured in units $[L^3]$, whereas the fluxes can be instantaneous and measured in units $[L^3 T^{-1}]$ or cumulative over an output interval and measured in units $[L^3]$. The water balance has the following form (Maxwell et al., 2016):

$$\frac{\Delta[\text{Vol}_{surface} + \text{Vol}_{subsurface}]}{\Delta t} = Q_{overland} + Q_{evapotranspiration} + Q_{source/\text{sink}} \tag{5.1}$$

where $\text{Vol}_{subsurface}$ is the subsurface storage $[L^3]$, $\text{Vol}_{surface}$ is the surface storage $[L^3]$, $Q_{overland}$ is the overland flux $[L^3 T^{-1}]$, $Q_{evapotranspiration}$ is the evapotranspiration flux passed from CLM $[L^3 T^{-1}]$, and $Q_{sourc/esink}$ are any other source or sink fluxes specified in the simulation $[L^3 T^{-1}]$.

Only the external fluxes passed from CLM are included in $Q_{evapotranspiration}$, which needs to recorded in ParFlow as a variable in ParFlow. It is important to note that these volume and flux quantities, like any other quantity in ParFlow, are computed spatially across the entire domain and returned as array values. The subsurface storage is computed for all active cells in the domain, as follows (the outcomes represent as an array of balances by domain) (Maxwell et al., 2016):

$$\text{Vol}_{subsurface} = \sum_{\Omega} [S(\psi) S_s \, \psi \Delta x \, \Delta y \, \Delta z + S(\psi)(\psi) \phi \Delta x \, \Delta y \, \Delta z] \tag{5.2}$$

The surface storage is determined using the continuity equation over the top surface boundary cells in the domain Γ, as obtained by the mask. This is done on a cell-by-cell basis (resulting in an array of balances across the domain) like follows (Maxwell et al., 2016):

$$\text{Vol}_{surface} = \sum_{\Gamma} \psi \Delta x \, \Delta y \tag{5.3}$$

The following is a brief summary of the continuity equation. The kinematic wave equation is now used in ParFlow to represent shallow overland flow. The continuity equation in two spatial dimensions is written as (Maxwell et al., 2016):

$$\frac{\partial \psi_s}{\partial t} = \nabla.(\vec{v} \psi_s) + q_r(x) \tag{5.4}$$

where $\vec{v}$ represents the depth averaged velocity vector $[LT^{-1}]$, s represents the surface ponding depth [L], and qr(x) represents a general source or ink (e.g., rainfall) rate $[LT^{-1}]$. Any cell at the top boundary with a slope that points out of the domain and is ponded will remove water

----

from the domain for the overland flow outflow. This is determined as a multiple of Manning's equations (which is used to build a flow depth-discharge relationship) and the area in the y-direction (Maxwell et al., 2016):

$$Q_{overland} = VA = -\frac{\sqrt{S_{f,y}}}{n}\psi_s^{5/3}\Delta x \tag{5.5}$$

5.3.2. Data Assimilation Methodologies

5.3.2.1 Data Assimilation Framework

For assimilating satellite product into the ParFlow-CLM, the Parallel Data Assimilation Framework (PDAF) (Nerger and Hiller, 2013) was utilized. It provides data assimilation methods such as local ensemble transform Kalman filter (LETKF) (Hunt et al., 2007) and ensemble Kalman filters (EnKF) (Evensen, 2003; Burgers et al., 1998). EnKF is widely used in the previous studies due to its flexibility and simplicity of use in land surface models (e.g., Draper et al., 2012; Kumar et al., 2008, 2009; Crow and Wood, 2003). Model state ensembles are created for estimating error covariance matrix of the state variable. This allows optimal merging of observations and model prediction.

The updated state variable x_t^+ in EnKF is ensemble of the model prediction of the state variable or x_t for time t, given by:

$$x_t^+ = x_t + k_t\left[l_t - H_t X_t\right] \tag{5.6}$$

Here, the perturbed observation vector is l_t. The Kalman gain vector k_t can be defined via:

$$k_t = P_t H_t^T\left(R_t + H_t P_t H_t^T\right)^{-1} \tag{5.7}$$

Here, R_t is the observation error matrix (a priori assigned as the expected observation error of the soil moisture product from SMOS, H_t^T is the matrix of the observation model at time t (transposed), and P_t is the error covariance matrix for the state variable related to model prediction, which is obtained from:

$$P_t = \frac{\sum_{n=1}^{N}\left(x_n - \overline{x}\right)\left(x_n - \overline{x}\right)^T}{N-1} \tag{5.8}$$

Chapter V: Multivariate satellite remote sensing data assimilation

----

Here, $\bar{x}$ is the ensemble mean soil moisture or head pressure vector that contains values for all of the grid cells. The number of ensemble members is given by N.

Kurtz et al. (2016) recently proposed a framework that integrates PDAF with the land surface–subsurface parts of the Terrestrial Systems Modelling Platform (TerrSysMP) (Shrestha et al., 2014). They demonstrated how TerrSysMP-PDAF makes optimal use of parallel computational resources, which is necessary for simulating predicted states and fluxes over large geographic areas and for prolonged simulations. TerrSysMP-PDAF is used in this work, wherein the PDAF is combined with the ParFlow-CLM for pressure and/or soil moisture data assimilation. Technical explanations of coupling and model performance can be found in Kurtz et al. (2016).

TerrSysMP-PDAF requires (i) filter algorithm parameters, (ii) observation files, and (iii) instructions for building an ensemble of model runs as input (Fig. 5.2). TWS data and error information were derived using GRACE level 2 data, and model input data were generated during pre-processing. Post-processing involves evaluating ParFlow-CLM output against independent data sets. We evaluated the results of simulations by a cross-validation with SMAP data and in-situ groundwater measurements as shown in Fig. 5.2.
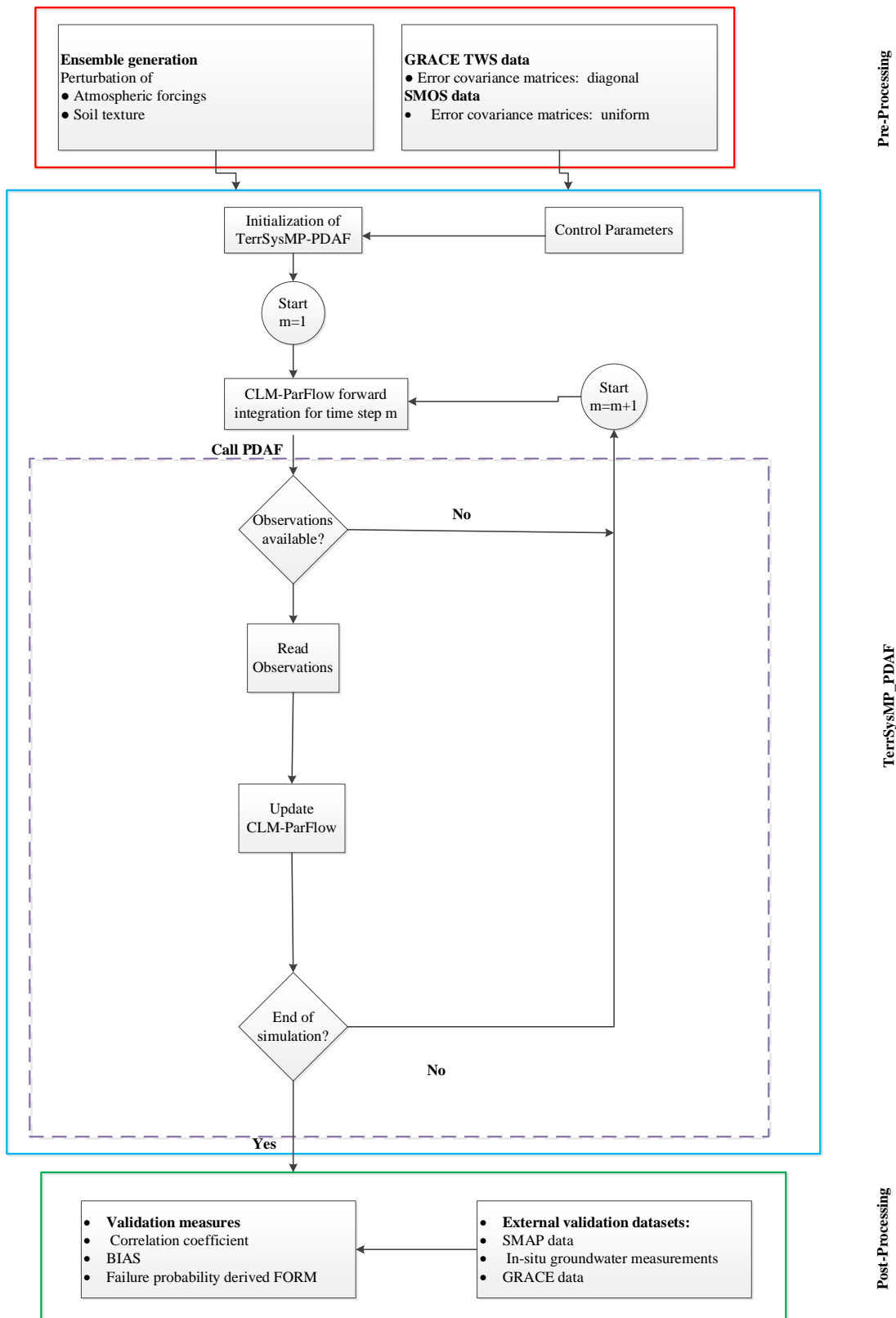
Fig. 5.2 Flowchart showing the general set-up of the data assimilation experiments realized within

Chapter V: Multivariate satellite remote sensing data assimilation

----

this study including (i) the pre-processing of model input and observations, (ii) the data assimilation framework TerrSysMP-PDAF, and (iii) the validation of the performance of the assimilated model.

5.3.1.2 CLM-ParFlow-PDAF experimental design

The assimilation tests were carried out from March 2015 to March 2020. To acquire equilibrium initial state variables, a ten-year spin up was undertaken by simulating the input data of 2015 ten times. We used ParFlow-CLM for a case study of Iran with a spatial resolution of 0. 25° in this work. The model was run with a 3-hour time step and a 5-day time window for soil moisture updates.

Because assimilation observations have various temporal resolutions, such as monthly GRACE TWS and daily soil moisture measurements, soil moisture observation is temporally rescaled into a 5-day resolution for data assimilation and GRACE TWS data is assimilated into the model in monthly time scale. In this study, we assumed a spatially uniform observational error of 0.04 mm^3/mm^3 for SOMS (Colliander et al., 2017; Lievens et al., 2015; Liu et al., 2016) and a diagonal error covariance matrix for GRACE TWS data in the CLM-ParFlow-PDAF setup.

Both atmospheric forcings and soil properties affect the results of a land surface model. Precipitation and soil texture (%sand and %clay) were disturbed in this study to account for uncertainty in atmospheric forcing and soil texture. Precipitation received multiplicative perturbations that were log-normally distributed, geographically homogenous, and temporally uncorrelated. The applied perturbation factors for precipitation had a mean and standard deviation of one and 0.10, respectively. A random noise with a standard deviation of 15% was used to disrupt the sand and clay content. The sand and clay content were confined to have a total of 100% in order to ensure the physical meaning of the soil parameters.

In the simulation/assimilation experiment, the initial ensemble size for precipitation and soil texture was set to 16 to update the soil moisture of the top soil layer (0-5cm) and pressure head. The main experiment consists of four CLM-PDAF simulations: (a) SMOS data assimilation, (b) GRACE TWS data assimilation and (c) combined SMOS and GRACE data assimilation (Fig. 5.11).
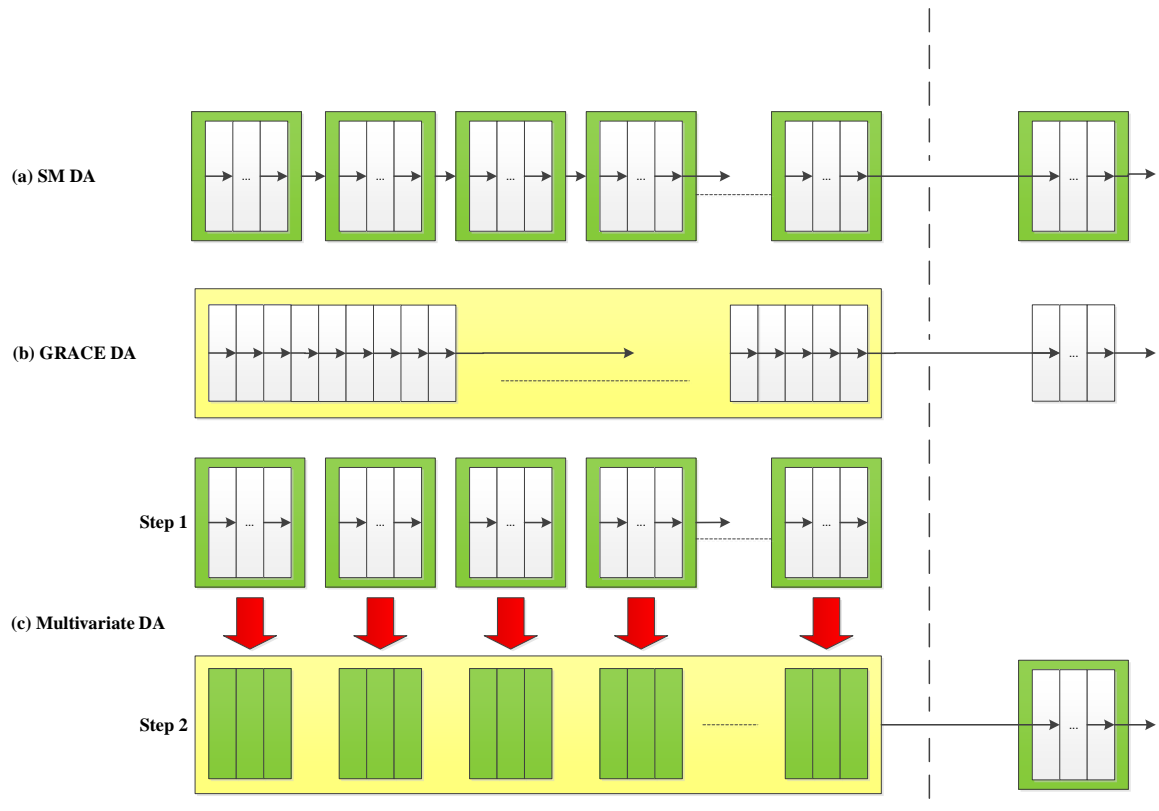
Fig. 5.11 Three different DA scenarios, (a) SM DA, (b) GRACE DA, and (c) multivariate DA. The SM DA updates the state estimate using the time window of approximately five days (green rectangle in (a)) while the GRACE DA uses the time window of approximately one month (yellow rectangle in (b)). In the multivariate DA, the SM DA is first performed, and its updated states are used as the forecast state in the GRACE DA.

5.3.3 Observation Operator

GRACE observations pose particular challenges for the observation operator, which relates the model states to the observations. While GRACE observations are usually available as monthly solution with a spatial resolution of few hundred kilometers, CLM-ParFlow over a case study in Iran runs at 3-hourly time steps at a 0.25° grid. This temporal and spatial resolution mismatch has been addressed by previous studies.

In the following subsections, an overview on different observation operators for GRACE observations is given along with the presentation of the observation operator implemented in this thesis.

Chapter V: Multivariate satellite remote sensing data assimilation

----

5.3.3.1 Temporal Aggregation

3-hourly simulation time steps of CLM-ParFlow have to be matched to monthly averages of TWSA from GRACE. This temporal resolution mismatch is addressed when setting up the state vector, computing the analysis increment, and applying the analysis increment to the model. Technically, the assimilation increment can be calculated at arbitrary points in time within the assimilation interval. In this thesis, the GRACE DA uses the time window of approximately one month. We have applied the whole monthly increment to the last day of the month, followed by the model integration over the next month.

 5.3.3.2 Spatial Aggregation

The model state vector holds temporally averaged compartments of TWS for each of the 0.25° * 0.25° model grid cells. The model state vector is transformed into observation space by the mapping operator, which includes (i) vertical aggregation of all TWS compartments, and (ii) horizontal averaging of the model grid cells to the coarser observation grid (which has a grid size of 1°).

One challenge with respect to the horizontal averaging is that TWS from all model grid cells within a defined distance in longitude and latitude direction to a specific observation was summed up for each 'clump' separately. (In the following, only observations grid cells were considered, which are supported by at least half of the number of possible model grid cells, i.e., in the case of a 1°*1°observation grid $((1°)^2/ (0.25°)^2)/2 =32$ model grid cells (0.25° is the resolution of the CLM-ParFlow grid).

5.3.4 Data

5.3.4.1 Land surface data and atmospheric forcing

The land surface input data include topography, land cover, soil characteristics, and physiological parameters of the canopy which are static variables. Global Multiresolution Terrain Elevation Data 2010 (Danielson et al., 2011) was used as Digital elevation model (DEM) which has a resolution of 1km (see Fig. 5.). The Moderate Resolution Imaging Spectroradiometer (MODIS) satellite land-use classification (Friedl et al., 2002) was also used, wherein it was converted to Plant Functional Types (PFT). In order to include the soil characteristics, the percentage of soil and clay were obtained using FAO/UNESCO Digital Soil Map of the World (Batjes, 1997) which has numerous soil classes consisting of 19 classes,

----

which was based on Schaap and Leij (1998)'s pedotransfer functions. For the manning's coefficient, the proposed relationship between landcover type and manning's coefficient is used (Asante et al., 2008).

The atmospheric forcing of the coupled ParFlow model with CLM including barometric pressure, wind speed, precipitation, specific humidity, downward shortwave and longwave radiations and air temperature near the surface is provided from GLDAS-Noah Land Surface Model L4 V2.1 data (https://disc.gsfc.nasa.gov/datasets/GLDAS_NOAH025_3H_2.1), which has a spatial resolution of 0.25° (~27 km) and temporal resolution of 3-hourly, used for the time period of 2015-2020 (Beaudoing and Rodell., 2020; Rodell et al., 2004). All model inputs were re-projected to have an equal cell size of 0.25°. In this study, the model was directed for a total thickness of 300 m over 100 model layers with different thickness. The model was implemented with a horizontal resolution of 0.25° with n_x=28, n_y=24. The porosity and specific storage are constant and equal to 0.4 and 10^{-5}, respectively.

5.3.4.2 GRACE TWS

The GRACE data release 05 (RL05) was received between March 2015 and June 2017 from the University of Texas at Austin's Center for Space Research (CSR) (Bettadpur, 2012). The monthly spherical harmonic coefficients (SHC) complete up to degree and order 96 is included in the package. The GRACE-derived TWS, as well as its uncertainty over the case study, are calculated as follows: First, the Swenson et al. (2008) degree 1 coefficients (SHC) are restored, and the C20 term is replaced by the value derived from the satellite laser range (Cheng and Tapley, 2004). Second, the mean (March 2015–June 2017) is calculated and subtracted from the monthly product to produce the SHC variations, then restriping (Swenson and Wahr, 2006) and 300-km radius Gaussian smoothing filters are applied to the SHC variations to reduce the high-frequency noise. Third, following the method outlined by Wahr et al. (1998), the TWS variation (TWS) is computed from the filtered SHC variations. The basin averaged TWS is employed in this study because the GRACE-derived TWS exhibits no substantial spatial variations over the study area. Finally, a signal restoration algorithm (e.g., Chen et al., 2014) is used to the computed TWS to restore the damped signal created by the filters used. The strategy iteratively searches for the true TWS using a forward model built entirely from GRACE data. To be consistent with the model estimate, the ParFlow-CLM estimate's temporal mean value of

TWS (March 2015–June 2017) is added to the GRACE-derived TWS to produce the absolute TWS prior to the assimilation procedure (Zaitchik et al., 2008).

5.3.4.3 Error analysis

The GRACE data release 05 (RL05) time series provide monthly means of the spherical coefficients and the associated error information as well. The full covariance matrix of the potential coefficients is available and will be used in the developed assimilation. The variances and covariances comprise the errors in the determination of the satellite's positions, random errors in the measurement of the distance between the two satellites and the non-gravitational forces and random errors of the oscillator. The full error information of the coefficients is used for error propagation of equivalent water heights. Furthermore, the applied background models (atmosphere, ocean, earth tides, etc.) are not free of errors.

Leakage due to filtering has not to be considered in the error propagation because the application of the Ensemble Kalman Filter involves that no filtering during the preprocessing of the GRACE data is required. For the assimilation of GRACE data into the hydrological model CLM-ParFlow the full covariance matrix R_t of the Stokes' coefficients is used up to degree 96. The main diagonal of the matrix contains the variances of the coefficients. The other elements contain the inter-coefficient covariances. The structure of the m×m covariance matrix of the m potential coefficients is displayed below:

$$R_t = \begin{bmatrix} \sigma_{c10}^2 & \sigma_{c10c11} & \cdots & \sigma_{c10c96} \\ & \sigma_{c11}^2 & \cdots & \sigma_{c11c96} \\ & & \sigma_{s95}^2 & \cdots \\ symm & & & \sigma_{c96}^2 \end{bmatrix} \qquad (5.9)$$

5.3.4.4 SMOS

This research relies on daily satellite soil moisture retrievals from the Soil Moisture and Ocean Salinity (SMOS, Kerr et al., 2012) and Soil Moisture Active Passive (SMAP, Entekhabi et al., 2010) missions. The level 3 gridded product (Al Bitar et al., 2017) given by the centre Aval de Traitement des Données SMOS (CATDS, https://www.catds.fr) run by the French Research Institute for Exploitation of the Sea for the Centre National d'Etudes Spatiales (CNES) is used to collect SMOS data (IFREMER). On the Equal-Area Scalable Earth (EASE; Brodzik et al., 2012) grid, data are accessible from January 2010 to present, with a spatial resolution of 25 km.

Chapter V: Multivariate satellite remote sensing data assimilation

----

SMOS data with a daily temporal resolution are spatially rescaled from 25 km×25 km to 0.25◦×0.25◦ resolution using the nearest neighbor interpolation to match CLM-ParFlow.

5.3.4.5 Evaluation Dataset

5.3.4.5.1 SMAP

The National Snow and Ice Data Center Distributed Active Archive Center (NSIDC DAAC, https://nsidc.org/data/smap) supplied a grid product (SPL3SMP). The volumetric soil moisture obtained by the SMAP level 3 (version 4) passive microwave radiometer, available from 2015 to the present, is included in this package. To match the observations with the model grid space, the data for both SMOS and SMAP are resampled to a 25 km regular grid. When more than one SM retrieval is available on a given day, the daily average is employed to assure model time step consistency.

5.3.4.5.2 Groundwater Data

In-situ groundwater level data collected from the Iran Water Resources Management Company (IWRMC) for observation wells scattered across the case study is used (http://www.wrm.ir), to compare our findings with them across the case study. The size of each aquifer is used to convert the IWRMC volumetric groundwater change values to equivalent water height. The results are then evaluated using an area-averaged time series of groundwater changes for each aquifer. The modified in-situ groundwater time series are compared to the aquifer's average assimilation findings individually.

5.3.5 Probabilistic Assessment of Different DA Strategies

5.3.5.1 The First Order Reliability Method (FORM)

The FORM is a frequently used approach for assessing a system's structural reliability (Zhao et al., 2020). In order to approximate the failure function of the examined system, the technique uses a Limit State Function (LSF) constructed via Taylor expansion in Eq. 5.9 (Soltani et al., 2020).

$$G(y) = L(y) = G(y_m) + \nabla G(y_m)^T.(y - y_m) \tag{5.10}$$

where G(y) is the water budget closure failure function of a hydrologic system, L(y) is the LSF linearization, $y = (y_1, y_2, ..., y_n)$ is the vector of n variables in G(y) function, y_m is the expansion point, and ∇G is the first order gradient vector of G(y).

121

Chapter V: Multivariate satellite remote sensing data assimilation

----

In this study, the FORM is used to validate the results of model used for assessing the accuracy of different DA. The failure function G(y) of hydrologic system is defined as follows:

$$G(y) = r_i = \frac{\left| Model\,Estimation_i - Observation_i \right|}{\frac{1}{n}\sum_1^n P_i} \tag{5.11}$$

where *i* is a pixel number, and *n* is the total number of months. Since many current studies found out that the closure of different DA strategies is between 5% and 25% of corresponding average precipitation (Long et al., 2014, Sahoo et al., 2011). We considered that when r_i of hydrologic system is less than 0.2, the model's results from different DA strategies are satisfactory.

The strategy is looking for to a point y* which is called the most probable failure point by calculating the shortest distance between the origin and failure surface with the constraint of $G(y) \leq 0$. This shortest distance is called the reliability index $\beta = \left\| y^* \right\|$ (see Soltani et al., 2020 for point-by-point application forms of this strategy).

The failure probability of a hydrologic system can be approximated using the reliability index β after it has been calculated as follows:

$$P_f = \Phi(-\beta) \tag{5.12}$$

Herein P_f is the hydrologic system's failure probability and $\Phi(-\beta)$ is the standard normal variate's cumulative distribution (Madsen et al., 1986). As a result, the smaller the value, the lower the uncertainties in model's results and the higher the system reliability.

5.4. Results

5.4.1 DA impacts on Spatially-averaged of state variables

5.4.1.1 Soil Moisture Variations

The spatially averaged time series of the SM_{0-5cm} variations estimated from the model top layer open-loop and all DA strategies are presented in Fig. 5.4. The SMAP data is used for validation which shows that the application of data assimilation reduces misfits between the results and SMAP data compared to the open-loop. The validation is carried out in terms of correlation and

----

absolute error, with the estimated values presented in Fig. 5. and Fig. 5.6, respectively. With an averaged correlation value of 0.67, ParFlow-CLM performs very well in the estimate of the SM $_{0-5cm}$ and gives good agreement with SMAP data at all sites (see ensemble open loop in Fig. 5.). The SMOS assimilation also minimizes erroneous peaks of the SM $_{0-5cm}$ estimate, such as in November 2018 (Fig. 5.4) and May 2018 (Fig. 5.4), resulting in greater agreement with the SMAP data. Clearly, the SMOS data should be taken into account in the DA process in order to retain the accuracy (in terms of agreement with the SMAP data) of the SM $_{0-5cm}$ estimate in the case study. The SM DA and multivariate DA increase the correlation value by 0.17 and 0.22, respectively (from 0.67 to 0.84 and 0.89). Since satellite SM observation is employed in the SM DA and multivariate DA, an improved outcome is expected. The GRACE DA, on the other hand, appears to have a negative impact on the SM $_{0-5cm}$ estimate (see, Fig. 5.5 and Fig. 5.6). The GRACE DA reduces the correlation by 0.08 when compared to the ensemble open loop. Poor performance is owing to sensitivity of GRACE data to the signal associated with the top soil component. The results of multivariate DA utilizing SMOS and GRACE data between March 2015 and June 2017 are compared to SMAP data (Fig. 5.4). The daily SM $_{0-5cm}$ estimations of SMOS assimilation clearly show a greater agreement with SMAP data (comparing to the ensemble open loop) (see, Fig. 5.5 and Fig. 5.6).
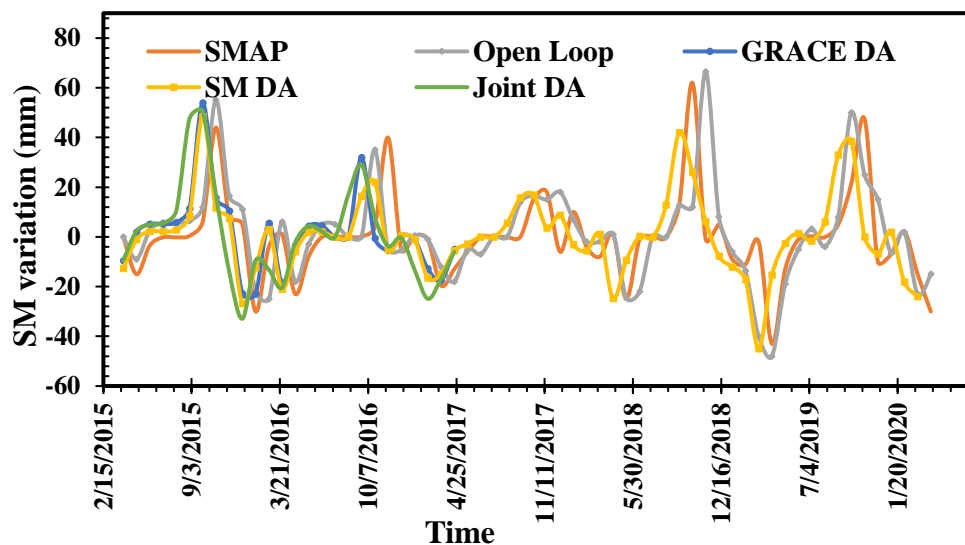
Fig. 5.4 The monthly spatially-averaged of the soil moisture variations simulated for the first soil layer (0-5 cm) from different DA strategies (SM DA, GRACE DA, and multivariate DA). The SMAP observation and the ensemble open loop estimates are also shown for comparison.
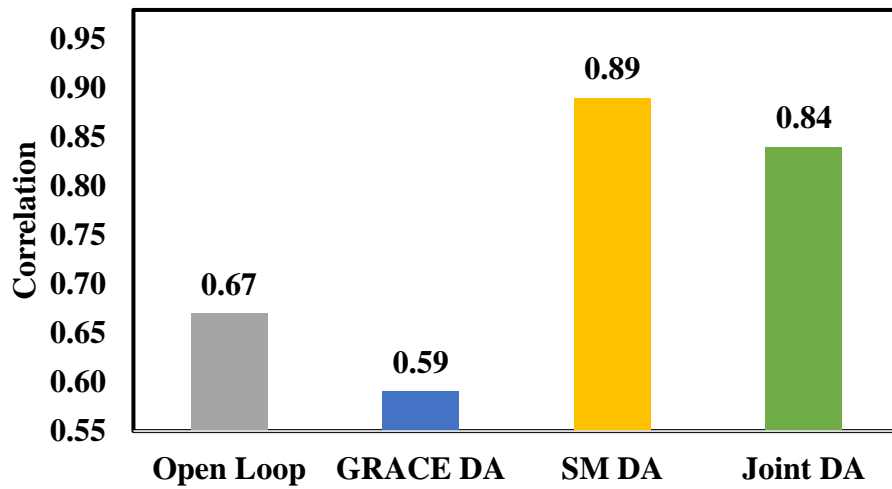
Fig. 5.5 Average correlations between SM $_{0-5\,cm}$ variations derived the SMAP and simulated by ParFlow-CLM before DA (open loop) and after different DA strategies (SM DA, GRACE DA, and joint DA).
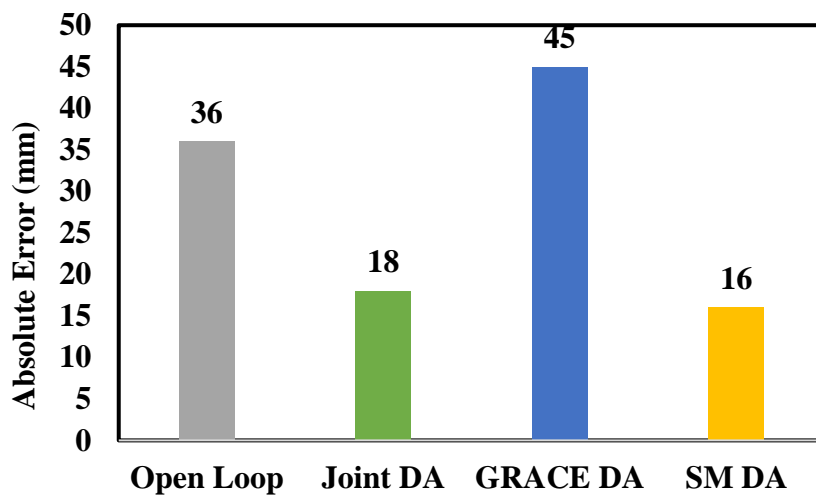
Fig. 5.6 Absolute error bars of the SM $_{0-5\,cm}$ variations simulated by ParFlow-CLM before DA (open loop) and after different DA strategies (SM DA, GRACE DA, and joint DA) in comparison to the SMAP observations.

Chapter V: Multivariate satellite remote sensing data assimilation

----

4.1.2 TWS Variations

The basin-averaged time series of TWS variations from ParFlow-CLM before and after assimilating three different DA strategies is shown in Fig. 5.7. Fig. 5.7 shows larger amplitude of TWS variations for the data assimilation results compared to open-loop results. Also, Fig. 5.8, shows the correlation with respect to GRACE observation. Assimilating SM not only has the least impact on the TWS variations but also results a negative impact. As a result, our findings show a lower level of agreement between the state estimate and the GRACE observation. The SM DA, reduces the averaged correlation value by ~0.07 (Fig. 5.8).

In the GRACE DA, the constraint is applied to the entire water column, leading to an improved agreement between the TWS variation estimate and the GRACE observation. The constraint is applied to the full water column in the GRACE DA, resulting in better agreement between the TWS estimate and the GRACE observation. The averaged correlation value is increased by 0.20 compared to open-loop results (Fig. 5.8). GRACE DA appears to be more useful for improving TWS estimations than SM DA, but it may be of reduced benefit for the estimation of the other components (see, Fig. 5.8 and Fig. 5.9). The idea of incorporating the SM and GRACE observations into the model at the same time is motivated by the underlying strengths.

Fig. 5.7 also shows the multivariate DA results using SMOS and GRACE data between March 2015 and June 2017 are compared with GRACE data. TWS estimations derived joint clearly demonstrate better agreement with GRACE data (comparing to the ensemble open loop and GRACE DA). When compared to open-loop results, the averaged correlation value increases by 0.22 (Fig. 5.8). The SM $_{0-5cm}$ and TWS variations components of the multivariate DA are modified toward the SMAP and GRACE observations, yielding in final state estimates that agree with both observations. TWS variations predicted with multivariate DA agree with GRACE observations by 0. 2 in cross-correlation (Fig. 5.8) while, at the same time, the SM $_{0-5cm}$ estimate has a better correlation with SMAP data by 0.17. (See Fig. 5.8). TWS correlation increased by more than a factor of 1.3 using the GRACE DA and multivariate DA (Fig. 5.8). The SM DA, as expected, cannot provide a reliable TWS estimate, as evidenced by the correlation, which is less than the GRACE DA and multivariate DA (Fig. 5.8).
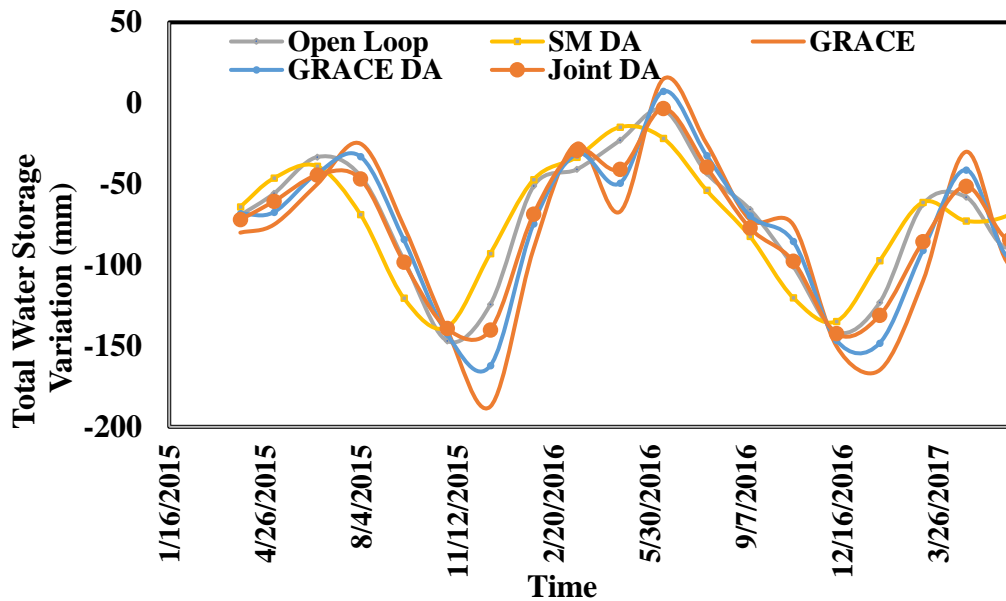
Fig. 5.7 The monthly spatially-averaged of the total water storage variations simulated from different DA strategies (SM DA, GRACE DA, and multivariate DA). The GRACE observation and the ensemble open loop estimates are also shown for comparison.
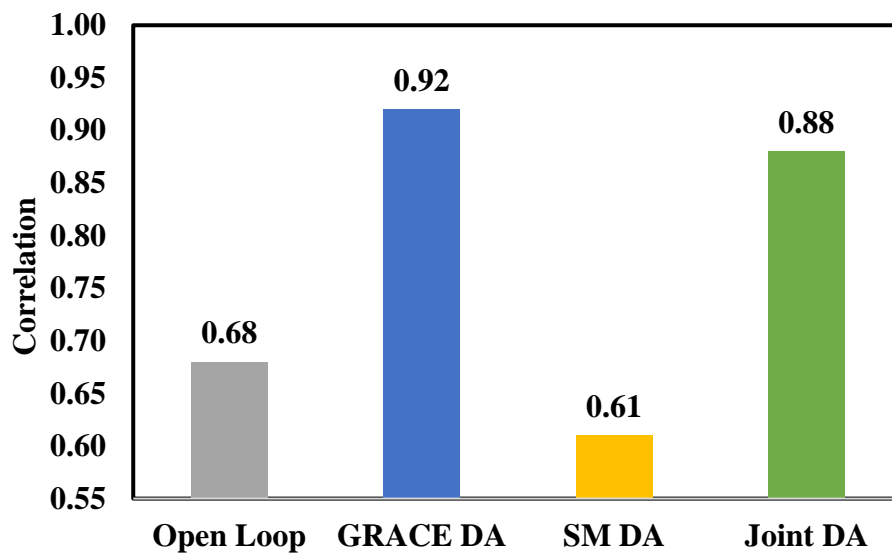
Fig. 5.8 Average correlations between the total water storage variations simulated from different DA strategies (SM DA, GRACE DA, and multivariate DA) and the GRACE data.

4.1.3 Groundwater storage Variations

Fig. 5.9 depicts time series of monthly-averaged of groundwater (GW) variations over the case study for the time period of 2015-2017. In-situ groundwater measurements is used to validate

----

assimilation results of the different DA strategies and the average correlation coefficients and their absolute error regarding to in-situ groundwater measurements are shown in Fig. 5.10 and Fig. 5.11, respectively. The application of the SM DA results in an inaccurate groundwater storage estimate in Fig. 5.9, with a considerable difference between the GW estimate and in-situ groundwater measurements. The lack of groundwater information in the satellite SM observation can be attributed to the poor performance. When compared to the ensemble open loop estimate, the assimilation of GRACE data (in both GRACE DA and multivariate DA) boosts the correlation and decrease absolute error between the GW estimate and in-situ groundwater storage changes by a factor of more than two (see, Fig. 5.10 and Fig. 5.11). As a result, GRACE is more sensitive to the signal from the groundwater than the shallow storage component.

When compared to assimilating GRACE-only, assimilating both GRACE and SMOS observations performs better in the GW variations estimate and delivers a 0.07 greater average correlation (Fig. 5.10). The GRACE DA updates GW variations in the multivariate DA after the SM DA is applied. The use of the SM DA (in the multivariate DA) likely reduces the uncertainty of the state estimate, which increases the contribution of GRACE in the GRACE DA. Groundwater trends are generally negative in all time period. Again, it can be concluded that without using assimilation, these correct negative trends are not captured.
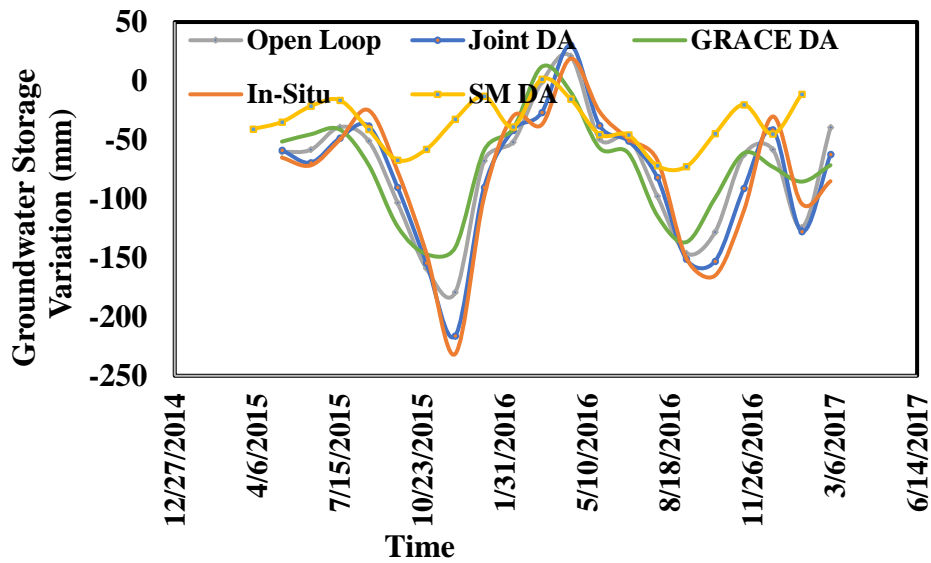
Fig. 5.9 The monthly spatially-averaged of the groundwater variations simulated from different DA strategies (SM DA, GRACE DA, and multivariate DA). The in-situ groundwater measurements and the ensemble open loop estimate are also shown for comparison.
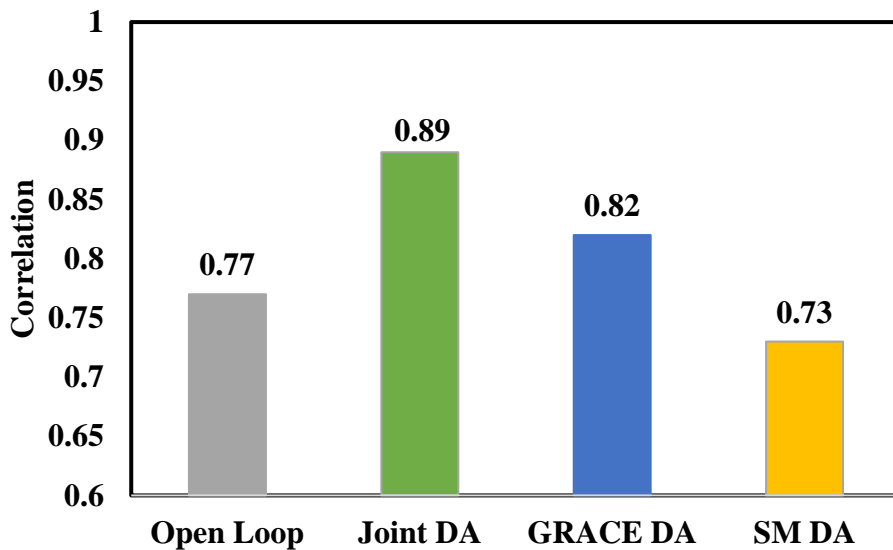
Fig. 5.10 Average correlation coefficients of the groundwater variations simulated from different DA case studies (SM DA, GRACE DA, and multivariate DA) and the in-situ groundwater observation.
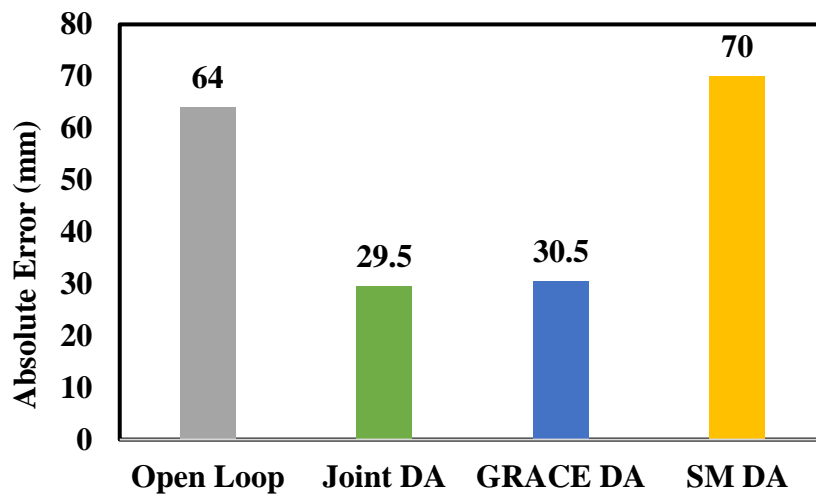
Fig. 5.11 Absolute error bars of the groundwater variations simulated by ParFlow-CLM before DA (open loop) and after different DA strategies (SM DA, GRACE DA, and joint DA) in comparison to in-situ measurements.

5.4.2 DA impacts on Temporally-averaged of state variables

5.4.2.1 Observation impacts on state variables

Fig. 5.12 shows temporally-averaged of the SM $_{0 - 5cm}$ variation from the ParFlow-CLM experiments derived ensemble open loop and different DA strategies (SM DA, GRACE DA, and joint DA) and the SMAP data. Fig. 5.13 evaluates the performance of the DA in terms of BIAS error against the SMAP data to investigate the impact of different DA strategies on the SM $_{0 - 5cm}$ estimates. In comparison to the ensemble open loop, the SM DA and multivariate DA provide smaller BIAS error values (Fig. 5.13). This is to be expected, given that the SMOS data are incorporated into the state estimate via the SM DA and multivariate DA applications. The Kalman gain tries to statistically enhance the fit between the SM $_{0 - 5cm}$ estimates and the SMAP observation, resulting in better agreement.

GRACE DA, on the other hand, increases the BIAS error. The increase is most likely caused by low sensitivity of GRACE observations to top soil moisture. The top soil component is largely influenced by high-frequency meteorological forcing, but GRACE can only monitor monthly basin-averaged TWS changes, which are dominated by deep-water storage component

----

low-frequency variability. It is worthy to note that GRACE data alone cannot offer the high spatiotemporal variability required to simulate water storage in the top soil layer. The BIAS error (ensemble spread) of the SM $_{0-5cm}$ estimate is reduced in all DA strategies (Fig. 5.13). The SM DA and multivariate DA reduce uncertainty when compared to the ensemble open loop, while the GRACE DA reduces uncertainty. Importantly, the SM DA and multivariate DA applications result in less uncertainty than the allocated SMAP uncertainty estimate. Furthermore, the uncertainty of the SM $_{0-5cm}$ estimate is smaller in the south-eastern parts of the basin.

Fig. 5.14 evaluates the performance of the DA in terms of absolute error against the in-situ groundwater measurements data to investigate the impact of different DA strategies on the groundwater variations estimates. As it is shown in Fig. 5.14, the BIAS inaccuracy indicates bigger differences from north to south and the biggest BIAS error is evident in the southwest of the basin and a similar pattern may also be seen in all DA scenarios. The BIAS inaccuracy in Fig. 5.14 clearly demonstrates the effect of DA. In SM DA, the biggest uncertainty is seen compared to other DA scenarios and ensemble open loop estimate, particularly in the central part of the basin. In GRACE DA and Joint DA, the uncertainty decreases and the lowest uncertainty is seen especially for the central part of the basin which extend north and west in Joint DA.
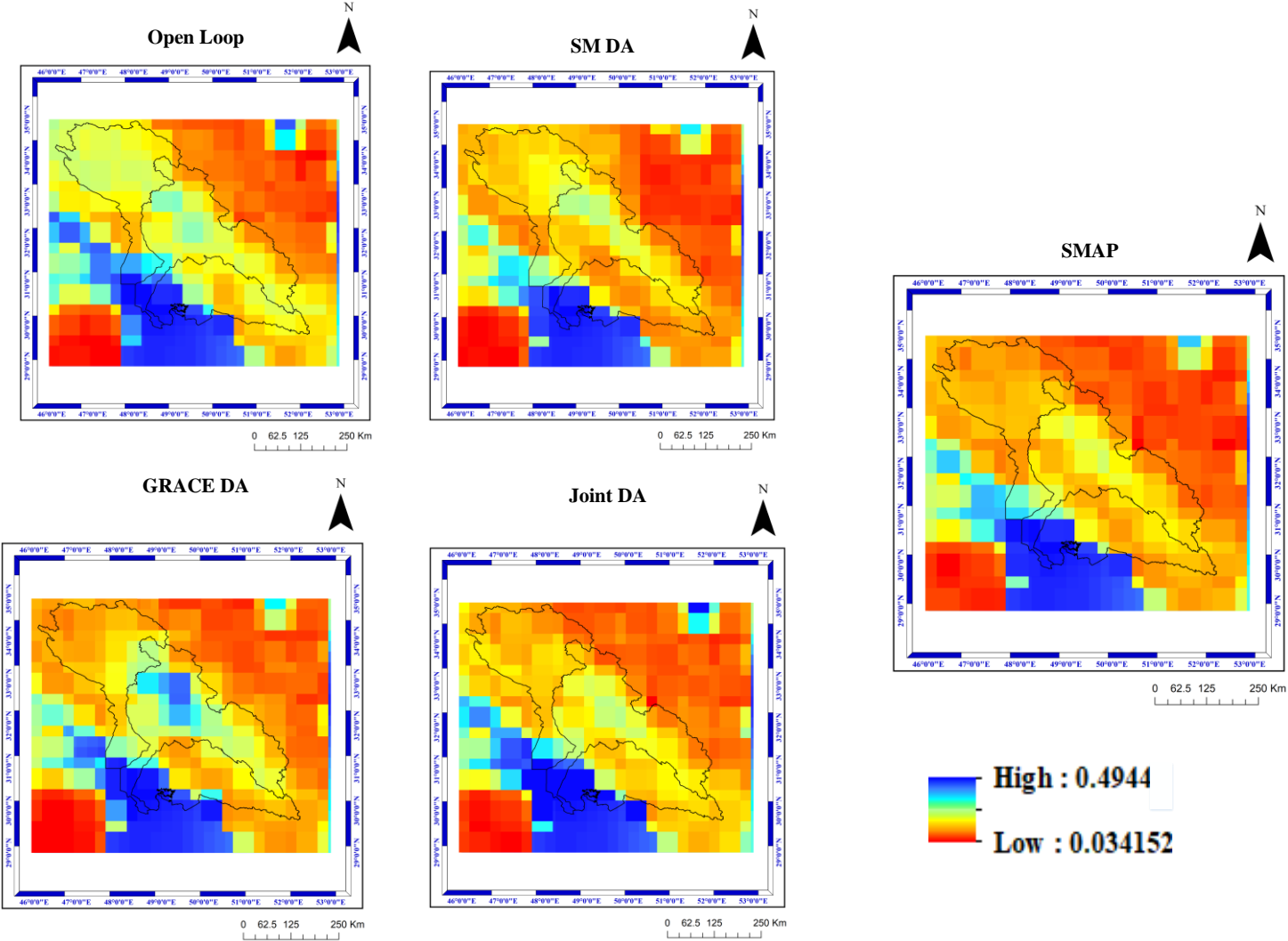
Chapter V: Multivariate satellite remote sensing data assimilation

----

Fig. 5.12 Temporally averaged of soil moisture variations from different DA strategies (SM DA, GRACE DA, and multivariate DA) over the case study. The ensemble open loop estimates and SMAP data are also shown for comparison.
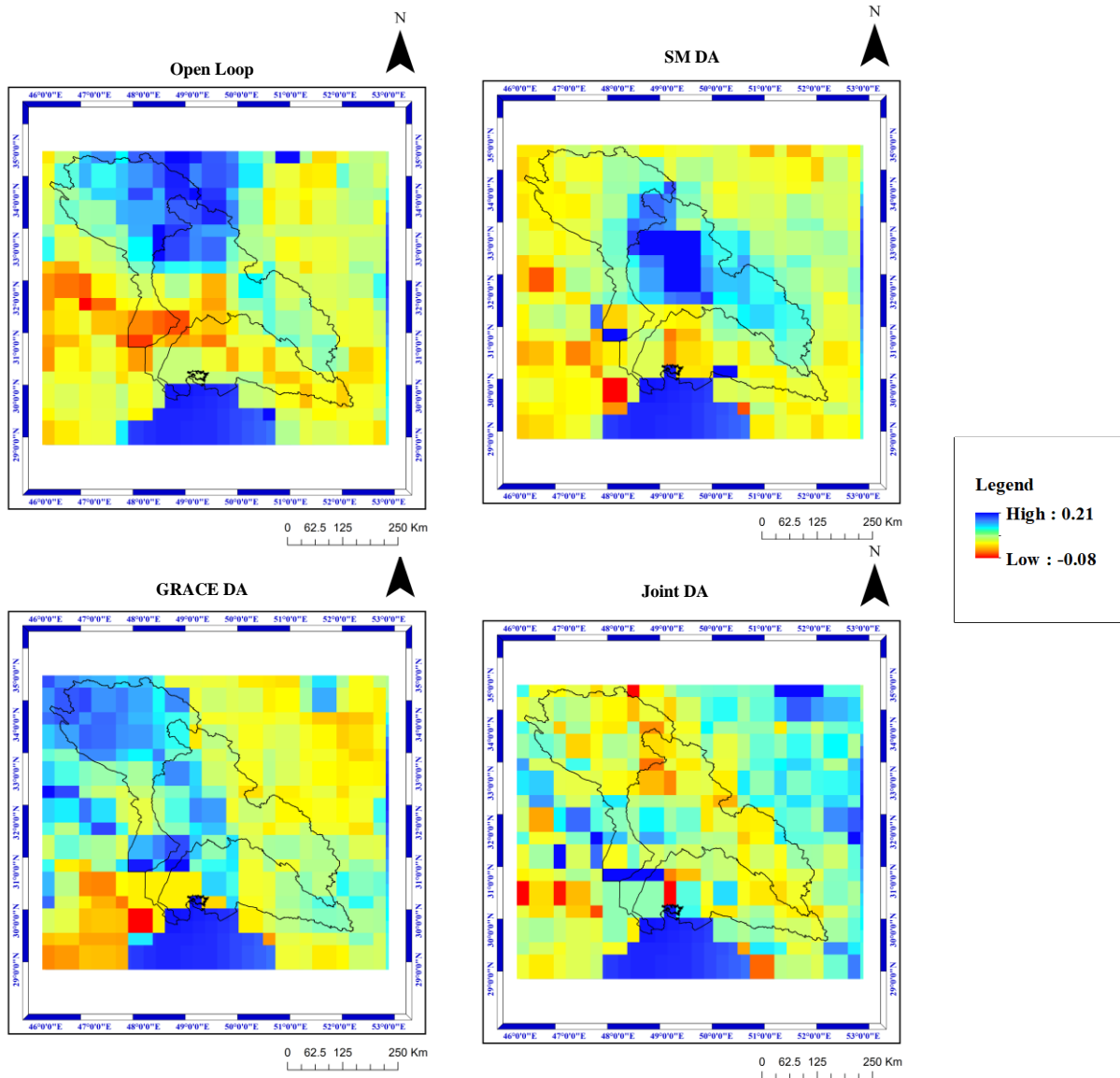
Fig. 5.13 BIAS between temporally averaged of soil moisture variations from different DA strategies (SM DA, GRACE DA, and multivariate DA) and the SMAP data. The ensemble open loop estimate is also shown for comparison.
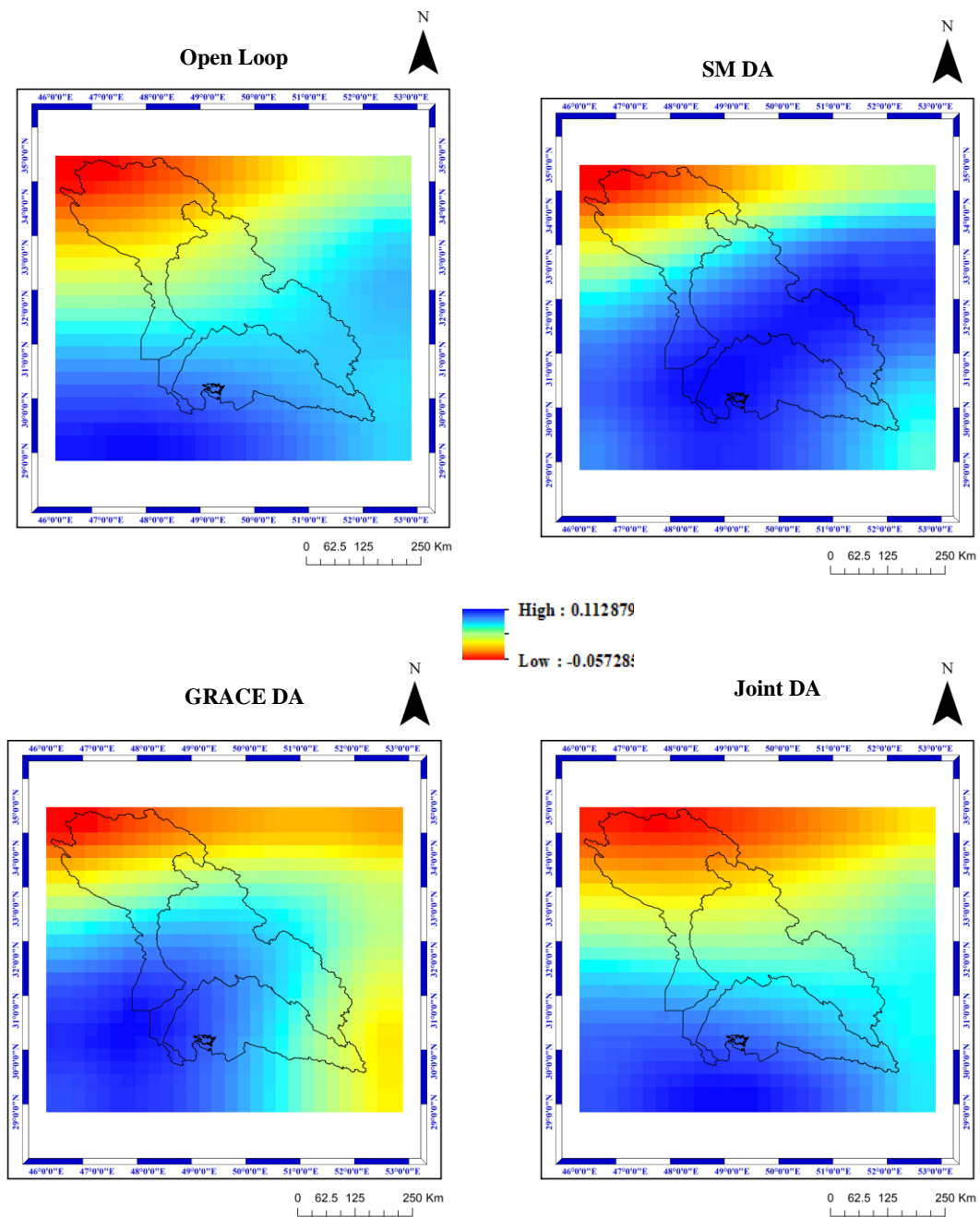
Fig. 5.14 BIAS between temporally averaged of groundwater storage variations from different DA approaches (SM DA, GRACE DA, and multivariate DA) and in-situ groundwater measurements.

Chapter V: Multivariate satellite remote sensing data assimilation

----

5.4.2.2 Evaluating of Uncertainty of Different DA Strategies

5.4.2.2.1The First Order Reliability Method (FORM)

The failure probability of LSF is investigated as a criterion to assess the reliability of the model's results through using a novel application of the First Order Reliability Method (FORM). By specifying r smaller than 0.2 (see, section 3.4.1), it can be used as a criterion to assess the reliability of model's results. To achieve this, the FORM calculates the failure probability (P_f) of the model's results closure. The results of the FORM implementation in Table 5.1 show that failure probability of multivariate data assimilation is lowest value and the best solution was found to be multivariate data assimilation of both GRACE and SMOS data for improving soil moisture and groundwater estimates. P_f of groundwater estimate using SM DA is larger than all DA strategies, and P_f of groundwater estimate using GRACE DA and Joint DA is lower than all DA strategies. P_f of soil moisture estimate using SM DA is lower than all DA strategies, and P_f of soil moisture estimate using GRACE DA is larger than all DA strategies which indicates that the performance of DA mainly depends on the type of observations that are assimilated.

Table 5.1 Evaluating of uncertainty in different DA strategies and ensemble open loop estimate of state variables

DA Strategies	P_f	
	Soil Moisture	Groundwater
Open Loop	7%	5%
SM DA	3%	7%
GRACE DA	9%	3%
Joint DA	4%	2%

5.5. Discussion

Khaki et al. (2018b) included GRACE TWS into the World-Wide Water Resources Assessment (W3RA) model to individually examine different water budget components such as groundwater, soil moisture, and surface water storage over Iran's six major drainage divisions from 2002 to 2012. It has been discovered that using GRACE TWS data assimilation can considerably improve the performance of W3RA in order to better understand water availability in different locations.

Chapter V: Multivariate satellite remote sensing data assimilation

----

Assimilation of GRACE TWS data successfully corrects for open-loop simulation variations which is especially important for groundwater storage which is in agreement with our results. Khaki et al. (2018b) found out that, the groundwater trend is negative in a major part of the western, and southern regions, representing a significant water availability challenge and Iran is becoming significantly dryer.

Khaki and Awange (2019) used the Ensemble Square-Root Filter (EnSRF) to integrate multi-mission satellite datasets such as TWS from the GRACE satellite mission and soil moisture products from the Advanced Microwave Scanning Radiometer-Earth Observing System (AMSR-E) and SMOS into the W3RA model for estimating groundwater and soil moisture over South America. The use of joint data assimilation improves W3RA estimations when compared to groundwater in-situ measurements which is in a good agreement with our results. This effect was clearly seen for TWS estimations and, more critically, groundwater simulations, highlighting the potential for assimilating remotely sensed products to improve the W3RA hydrological model's reliability.

Tangdamrongsub et al. (2020) have assimilated multi-mission remote sensing observations include soil moisture information from SMOS and SMAP missions, and TWS information from GRACE into the Community Atmosphere and Biosphere Land Exchange (CABLE) land surface model over Goulburn River basin in Australia to improve model's results. They validated the performance of data assimilation by using in-situ soil moisture and groundwater level data. They found out that SMOS/SMAP assimilation improves the top soil moisture but degrades the groundwater storage estimates, whereas the GRACE assimilation improves only the groundwater component. They found out that SMOS/SMAP assimilation increases performance of the model in soil moisture estimates of first 5 cm of soil layer but decreases its performance in the groundwater storage estimates, whereas the GRACE assimilation improves only the groundwater component.

Chapter VI: Conclusions and Summary

6.1 Conclusions

A fundamental question regarding the assimilation of GRACE TWSA into hydrological models was "whether it has a benefit for simultaneously data assimilation strategy". To answer the research question, different assimilation strategies including only GRCE TWSA data, SM DA and joint GRACE-SM DA were performed to test the efficiency of data assimilation strategies in subsurface water storage predictions. Since the main objective of assimilating data into a hydrological model is improving model's outputs, this thesis investigated the application of methods for improving hydrological model performances from various perspectives. Special considerations were given to address the limitations in existing methods by proposing new techniques or strategies. The following summarizes the main outcomes of the thesis, which, to the best of the author knowledge, are new scientific contributions.

- The accuracy of GRACE TWS estimation is very important for hydrological data assimilation. To this end, fully error covariance matrix for GRACE TWSA data was proposed. This is particularly important considering that previous studies mostly neglect the impact of GRACE error covariance matrix and existing correlation between grid points that can lead to inaccurate estimates. In other words, by assuming an uncorrelated constant error value, an important part of observations has not been used during data assimilation.

- In addition to GRACE error and an appropriate assimilation technique, a robust data assimilation strategy was required. Various data assimilation strategies were tested to investigate their capabilities in improving model's predictions. These include introducing new assimilation framework, examining various data assimilation strategies for assimilating GRACE TWS and SMOS data, developing techniques to use the full potential of different data source including GRACE and SMOS observations for improving model's predictions.

- This thesis also includes introducing new modeling strategies such as a scale-consistent river parameterization for the coupled ParFlow-CLM hydrological model. This means, by

Chapter VI: Conclusions and Summary

----

knowing the limitations of the model, including structural constraints, it is possible to suggest methods that help to overcome the limitations of modeling in order to improve the performance of the model.

6.1.1 Benefit of GRACE Assimilation for the Representation of Extreme Events

Assimilating GRACE TWS into CLM-ParFlow can be interpreted as downscaling of coarse monthly GRACE observations to daily high-resolution TWS with an added vertical stratification. When assessing extreme events, the high-resolution assimilated model adds information on the evolution of TWS at smaller spatial and temporal scales than available from GRACE.

6.1.2 Benefit of GRACE Assimilation for Reducing Artificial Trends and Phase Shifts of Modeled TWS

Biases in fluxes cause trends in storages. Experiments with artificial biases in precipitation forcings showed that the assimilation of GRACE data corrects the resulting unrealistic trends in storage. In fact, trends from the assimilated model run with biased forcings were similar to trends from the assimilated model run with unbiased forcings. Phase shifts between model and observations were also reduced by data assimilation. Both aspects suggest that the assimilation of GRACE data might be beneficial in data sparse regions, where hydrological models suffer from low-quality and biased input data.

6.2 Summary

The following summarizes the main outcomes of this thesis step by step, which, to the best of the author knowledge, are new scientific contributions.

1. Application of the satellite products for the water budget components estimation in the CBI gives a reasonable estimation of the maximum possible integrated error (Δ) of the three commonly used satellite products (P, ET, ΔS). Since the uncertainty in satellite data sources, as well as the mismatch in the spatiotemporal resolution and time steps of various satellite products, may influence the accuracy of water budget estimation, this assessment needs further verification with other methods. Therefore, the closure and consistency of applied satellite products defining the simplified water budget equation were examined over the CBI using defining the mathematical

Chapter VI: Conclusions and Summary

----

expression of a system state limit beyond which the criteria determining system reliability is no longer met. Our results show that depending on the time scale as well as the hydro-climatology patterns of large regions, using only satellite products has the potential to close the water budget.

This has been better demonstrated in some regions of the CBI (e.g., the central, southern and eastern parts of the CBI) having low latitude, little annual rainfall (50–150 mm) and high ratio of *PET* to *P* (~30), as these conditions hold the assumption of negligible runoff in the water budget calculation.

Although the coarse temporal and spatial resolution (monthly and 1°) makes the data less informative for water resources management in small regions, the evaluation of consistency between the datasets using a novel and strong probabilistic framework, e.g., FORM can give us useful information for the analysis of hydrologic variations and modeling validation using these satellite products at large scales. Since the application of FORM to validate is not limited to specific research fields, it is implemented in all research fields by defining a suitable LSF. This probabilistic method is particularly useful for cases where statistical information tends to be incomplete, such as in some water budget components where only first and second statistical moments and marginal probability distributions are available or can be assumed with confidence. It is also worthy to mention that limited instrumentation and low-quality ground-based measurements of climate input data impede a reliable result of a water budget estimation, especially in large-scale and less-developed regions, remote sensing technology as a cost-effective tool aid in obtaining hydrological parameters. Therefore, the application of remotely sensed datasets and proposing of a reliable method to validate our estimation due to their uncertainty is very valuable in large-scale and less-developed regions.

Since considering remote sensing data, particularly GRACE, along with hydrological models shows a promising potential in assessing the water storage at large scale, the assimilation of GRACE data into hydrological models, e.g., W3RA (Van Dijk, 2010) or ParFlow (Maxwell and Miller, 2005) for storage components estimation (e.g., groundwater or soil moisture) and implementing the reliability method, e.g., FORM and SORM depending on LSF condition (linear or non-linear) for validation purposes is strongly recommended.

Chapter VI: Conclusions and Summary

----

2. We suggest an improvement of soil moisture and groundwater level predictions from a distributed hydrological model by an objective scaling of the Manning's coefficient and saturated hydraulic conductivity. This approach was applied for the Upper Rhine Basin at approximately 6 km resolution for the years 2012 to 2014. Since the interaction between surface and subsurface is significant in this case study, because of the presence of shallow aquifers, an integrated surface-subsurface model, ParFlow, was used. ParFlow is a grid-scale model which calculates overland flow at a constant horizontal grid resolution and employ the kinematic wave approximation for both hillslope and river channel flow. Since the width of rivers is much narrower than the grid size of the model, the exchange between river and subsurface is approximated as higher than realistic rivers, resulting in an erroneously large infiltration/exfiltration rate. The scaling parameters approach is used to compensate this limitation. The impact of the scaling approach on soil moisture and groundwater level was evaluated and cross validated with the CCI-SM data and the groundwater level data from well observations at seasonal scales. Furthermore, the reliability of the used scaling approach is examined by a novel probabilistic framework (FORM). Using this scaling approach, the conclusions of this study are:

- This study showed that scaling of the Manning's coefficient and saturated hydraulic conductivity, improved the soil moisture simulations and groundwater level over most parts of the Upper Rhine Basin relative to model's simulations without parameter scaling. ParFlow-CLM simulations overestimated SM in most parts of the Upper Rhine Basin and in all seasons. Major improvements in ground water level have been made over most of the basin's regions, particularly in the central and northern regions. Our simulation results of ParFlow-CLM and ParFlow-CLM-S in these regions may show that scaling is more successful in shallow groundwater simulation. The average bias in soil moisture for the study domain was decreased from 0.017 mm^3/mm^3 in ParFlow-CLM simulations to 0.01 mm^3/mm^3 in ParFlow-CLM-S simulations.

- The ParFlow-CLM-S soil moisture simulations performed better in the summer and autumn seasons than in the winter and spring seasons on a seasonal time scale. FORM results show that the accuracy of ParFlow-CLM soil moisture simulations by using scaling

Chapter VI: Conclusions and Summary

> approach is more than 0.05, 0.11, 015 and 0.08 for autumn, winter, spring and summer, respectively.

The ParFlow-CLM model simulations of soil moisture and groundwater level over the Upper Rhine Basin benefit from scaling of the Manning's coefficient and saturated hydraulic conductivity, as demonstrated in this work. However, there are a few limitations in this research. The spatial mismatch between our high-resolution land surface model and the coarser resolution CCI-SM was addressed by rescaling the CCI-SM data to the model resolution (6 km) without bias correction. In addition to inconsistencies at the spatial scale, data gaps in satellite soil moisture retrievals, which are limited in regions of pronounced topography, standing water, dense vegetation, snow-covered areas, and frozen soil, can cause inaccuracies in soil moisture estimations (Dorigo et al., 2017).

When the width of a river is known with adequate accuracy, this concept can be simply used in all models that do not explicitly resolve the true river width for river routing. Only a preparation step is necessary in practice, which does not add to the computational load during runtime. No equivalent solutions have been tried to our knowledge because most approaches rely on dedicated channel parameterizations, which are far more difficult to implement. Finally, the results indicate that a modification of model parametrization to take into account impact of scale on hydrodynamic parameters should be done prior to multivariate assimilation approaches.

3. We suggest to use multi-mission satellite data products to improve predictions of sub-surface water storages in the hydrology model over a case study in Iran. As a result, GRACE-derived TWS and soil moisture observations from the SMOS are assimilated in the couple ParFlow-CLM hydrological model (or TerrSys-MP). Based on the validation against SMAP data, the assimilation method was capable of estimating soil moisture when the proper observations were used. Soil moisture assimilation is only beneficial for estimation of the top 5 centimeters of the soil moisture, whereas groundwater storage variation estimate can be improved by assimilating GRACE data.

By assimilation of both data, soil moisture is more accurately estimated, although in order to achieve the highest accuracy, single observation assimilation should be used. This highlights the importance of using SMOS data for data assimilation of soil moisture and increasing its accuracy.

Chapter VI: Conclusions and Summary

For the top five centimeters of the soil, an increase of 0.22 in correlation coefficient with SMAP was achieved in this regard. In addition, the water storage uncertainty in the top layer of the soil can be reduced by assimilating soil moisture, although this does not improve the uncertainty of total water storage. However, it should be mentioned that even though soil moisture data assimilation improves the estimates for the top soil moisture, the accuracy for the whole water column may not necessarily increase. Various papers such as Kumar et al. (2019), Lievens et al. (2017) and Jasinski et al. (2019) have listed numerous benefits for multivariate soil moisture data assimilation. In order to avoid contaminating observation error matrix, one should be aware of systematic errors in the SMOS soil moisture data.

The cross correlation of SMOS error should be analyzed in future studies and its effect on data assimilation should be quantified. Even though GRACE's original resolution is larger than 100 kilometers, it was shown that the groundwater storage estimation accuracy for Iran could be improved in the 25-kilometer resolution via assimilation of GRACE data. Nevertheless, the hydrological model did not benefit from GRACE assimilation for its estimation of surface soil moisture values, which agrees with the findings of Tian et al. (2017) and Li et al. (2012). The uncertainty of total water storage can be reduced by assimilation of GRACE data though its influence on reducing soil moisture uncertainty is marginal. Due to the fact that GRACE values depend on the whole water column especially deep groundwater, it is possible to misattribute deep groundwater into shallow groundwater through assimilation of GRACE data.

For improving soil moisture estimate, the best solution was found to be multivariate data assimilation for both GRACE and SMOS data. Consequently, the high and low frequency values are adjusted by soil moisture and GRACE assimilation, respectively. As a result, correlation values for top 5 centimeters of soil moisture and change in groundwater storage experienced a 0.17 and 0.12 increase in correlation coefficient with SMAP data and in-situ measurements. Nevertheless, it should be mentioned that multivariate data assimilation has a slightly poorer performance than either SM or GRACE data assimilation of their respective target zones (the top 5 centimeters of the soil and ground water surface change, respectively). For optimizing model states in the data assimilation, several cost functions were used for changes in both deep and shallow groundwater

Chapter VI: Conclusions and Summary

----

storage. For this purpose, GRACE and SMAP residuals were minimized. After the calibration process, the optimal solution for multivariate optimization is different from the optimal solution for using either GRACE or SMAP alone as the objective function, but rather it is a compromise between the two data sources, which is in agreement with the work of Tian et al. (2017). As a result, the satellite data and measurements on the ground (subsurface water level data) can be effectively assimilated into the model in order to better represent the physical model. The multivariate data assimilation which was proposed in the current chapter can also be generalized to other data sources such as Sentinel-1 derived soil moisture (Lievens et al., 2017), the equivalent snow water using SnowEx (Kim, 2017) and change in total water storage using GRACE Follow-On (as reported in Flechtner et al., 2014).

6.3 Applications

Data assimilation merges observations and numerical model simulations. In this thesis, data assimilation was used to generate a relatively high-resolution reanalysis of TWS over a case study in Iran. I found that modeled water fluxes and individual storages were also improved to some extent by assimilating GRACE/SMOS data in different assimilation strategies. Thus, the assimilated model provides interesting information on the evolution of different water cycle variables, which might be of use for early warning systems of natural hazards over different spatial domain.

GRACE de-aliasing products aim at removing short-term (< one month) mass redistribution before computing monthly gravity field solutions. As the CLM-ParFlow model runs at hourly time steps, TWSA from the assimilated model provide an interesting option for the use as GRACE de-aliasing product.

Current investigations showed evidence of daily hydrological loading signals in GPS time series (Springer et al., 2019). The GRACE/SMOS assimilating CLM-ParFlow model provides a promising option for removing hydrological-induced vertical deformation from daily GPS time series, thus, demasking geophysical processes such as land subsidence and tectonic or volcanic deformation. Indeed, TWSA from the assimilated CLM-ParFlow model might turn out as a great

Chapter VI: Conclusions and Summary

----

tool for GPS applications, and it could also play a role in improving reference system computations.

6.4 Outlook

Within this thesis, a framework for assimilating GRACE observations into CLM3.5 was optimized regarding the assimilation strategy. However, several aspects can be addressed to further improve the results and to advance applications. The start of the GRACE Follow-On mission in May 2018 ensures that the assimilation of remotely sensed TWSA is going to remain a relevant topic of research.

6.4.1 Study area

The multivariate assimilation framework developed within this thesis is transferable to different resolutions, so that GRACE/SMOS data could be disaggregated to a finer grid over Iran in future experiments. Furthermore, the data assimilation framework is easily transferable to other regions by changing atmospheric forcings and soil maps. The assimilation of GRACE/SMOS data might be particularly helpful in regions of sparse data coverage to obtain more realistic TWS estimates.

6.4.2 Hydrological Model

The land-surface model CLM (version 3.5)-ParFlow was used here as it is part of the TerrSysMP framework.

However, more recent versions of CLM contain improved representations of soil and plant hydrology, snow processes, river modeling and surface water stores. The latest version is CLM5.0, but it is not yet part of TerrSysMP-PDAF. For future investigations, it would be interesting to transfer the data assimilation framework to a more recent CLM version and also to compare the impact of data assimilation on different model versions.

Within this thesis, the CLM and ParFlow componentd of the Terrestrial Systems Modeling Platform (TerrSysMP) were applied. It is tempting to suggest the data assimilation framework should be extended also for coupled applications of CLM-ParFlow and the atmospheric component COSMO. Therefore, using TerrSysMP-PDAF, GRACE/SMOS data could be assimilated into a

Chapter VI: Conclusions and Summary

----

fully coupled system consisting of ParFlow, CLM, and the atmospheric component COSMO together with observations of other key variables of the terrestrial water cycle.

6.4.3 Validation Environment

In this thesis, the performance of data assimilation was validated against in-situ and remotely sensed soil moisture observations. Soil moisture is validated against the remotely sensed soil moisture SMAP dataset which is relatively close to assimilated SMOS. Therefore, for future investigations, it would be interesting to compare simulated soil moisture to one or two more remotely-sensed datasets. It would be a great opportunity, if the performance of data assimilation is validated against in-situ measurement for other regions for which are available.

Bibliography

Abdelkhalak, E.H., Bouchaïb, R., 2013. Incertitudes, optimisation et fiabilité des structures. Lavoisier.

Adeyewa, Z.D., Nakamura, K., 2003. Validation of TRMM radar rainfall data over major climatic regions in Africa. Journal of Applied Meteorology, 42(2): 331-347.

Alazzy, A.A., Lü, H., Chen, R., Ali, A.B., Zhu, Y. and Su, J., 2017. Evaluation of satellite precipitation products and their potential influence on hydrological modeling over the Ganzi River Basin of the Tibetan Plateau. Advances in Meteorology, 2017.

Al Bitar, A. et al., 2017. The global SMOS Level 3 daily soil moisture and brightness temperature maps. Earth System Science Data, 9(1): 293-315.

Alsdorf, D., Rodriguez, E., Lettenmaier, D., 2007. Measuring surface water from space. review of Geophysics 45.

Altaf, M. et al., 2014. A comparison of ensemble Kalman filters for storm surge assimilation. Monthly Weather Review, 142(8): 2899-2914.

Ardebili, S.M.S., Khademalrasoul, A., 2018. An analysis of liquid-biofuel production potential from agricultural residues and animal fat (case study: Khuzestan Province). Journal of cleaner production, 204: 819-831.

Arulampalam, M.S., Maskell, S., Gordon, N. and Clapp, T., 2002. A tutorial on particle filters for online nonlinear/non-Gaussian Bayesian tracking. IEEE Transactions on signal processing, 50(2): 174-188.

Asante, K.O., Artan, G.A., Pervez, S., Bandaragoda, C., Verdin, J.P., 2008. Technical manual for the geospatial stream flow model (GeoSFM). World Wide Web, 605: 594-6151.

Ashby, S. F. and Falgout, R. D.: A Parallel Multigrid Preconditioned Conjugate Gradient Algorithm for Groundwater Flow Simulations, Nucl. Sci. Eng., 124, 145–159, 1996.

Ataie-Ashtiani, B., Rajabi, M.M. and Simmons, C.T., 2020. Improving model-data interaction in hydrogeology: Insights from different disciplines. JHyd, 580: 124275.

Awange, J., Gebremichael, M., Forootan, E., Wakbulcho, G., Anyah, R., Ferreira, V. and Alemayehu, T., 2014. Characterization of Ethiopian mega hydrogeological regimes using GRACE, TRMM and GLDAS datasets. Advances in water resources, 74: 64-78.

Awange, J. et al., 2009. GRACE hydrological monitoring of Australia: Current limitations and future prospects. Journal of Spatial Science, 54(1): 23-36.

Banerjee, C. and Kumar, D.N., 2019. Integration of GRACE Data for Improvement of Hydrological Models, Hydrology in a Changing World. Springer, pp. 1-22.

Bannister, R., 2017. A review of operational methods of variational and ensemble-variational data assimilation. Quarterly Journal of the Royal Meteorological Society, 143(703): 607-633.

Batjes, N., 1997. A world dataset of derived soil properties by FAO–UNESCO soil unit for global modelling. Soil use and management, 13(1): 9-16.

Baur, O., Kuhn, M. and Featherstone, W., 2009. GRACE-derived ice-mass variations over Greenland by accounting for leakage effects. Journal of Geophysical Research: Solid Earth, 114(B6).

Beaudoing, H., Rodell, M., 2020. NASA/GSFC/HSL, GLDAS Noah Land Surface Model L4 3 hourly 0.25× 0.25-degree V2. 1, Greenbelt, Maryland, USA, Goddard Earth Sciences Data and Information Services Center (GES DISC).

Bennett, A.F., 2005. Inverse modeling of the ocean and atmosphere. Cambridge University Press.

Berger, H. and Forsythe, M., 2004. Satellite wind superobbing. Met Office Forecasting Research Technical Report, 451.

Bertino, L., Evensen, G., Wackernagel, H., 2003. Sequential data assimilation techniques in oceanography. International Statistical Review, 71(2): 223-241.

Bettadpur, S., 2012. Gravity recovery and climate experiment utcsr level-2 processing standards document for level-2 product release 0005. Center For Space Research. The University of Texas at, Austin, USA.

Bharati, L. et al., 2008. Integration of economic and hydrologic models: exploring conjunctive irrigation water use strategies in the Volta Basin. Agricultural water management, 95(8): 925-936.

Bierkens, M.F., Van den Hurk, B.J., 2007. Groundwater convergence as a possible mechanism for multi-year persistence in rainfall. Geophysical Research Letters, 34(2).

Bishop, C.H., Etherton, B.J. and Majumdar, S.J., 2001. Adaptive sampling with the ensemble transform Kalman filter. Part I: Theoretical aspects. Monthly weather review, 129(3): 420-436.

Bonan, G.B., Oleson, K.W., Vertenstein, M., Levis, S., Zeng, X., Dai, Y., Dickinson, R.E. and Yang, Z.-L., 2002. The land surface climatology of the Community Land Model coupled to the NCAR Community Climate Model. Journal of climate, 15(22): 3123-3149.

Bousserez, N. and Henze, D.K., 2018. Optimal and scalable methods to approximate the solutions of large-scale Bayesian problems: theory and application to atmospheric inversion and data assimilation. Quarterly Journal of the Royal Meteorological Society, 144(711): 365-390.

Brocca, L., Melone, F., Moramarco, T., Wagner, W., Naeimi, V., Bartalis, Z. and Hasenauer, S., 2010. Improving runoff prediction through the assimilation of the ASCAT soil moisture product. Hydrology and Earth System Sciences, 14(10): 1881-1893.

Brodzik, M.J., Billingsley, B., Haran, T., Raup, B., Savoie, M.H., 2012. EASE-Grid 2.0: Incremental but significant improvements for Earth-gridded data sets. ISPRS International Journal of Geo-Information, 1(1): 32-45.

Budyko, M., 1958. The heat balance of the earth's surface, US Dept. of Commerce. Weather Bureau, Washington, DC, USA.

Burek, P., Van Der Knijff, J. and De Roo, A., 2013. LISFLOOD, distributed water balance and flood simulation model: Revised user manual. European commission, joint research centre, Report EUR, 26162.

Burgers, G., Van Leeuwen, P.J., Evensen, G., 1998. Analysis scheme in the ensemble Kalman filter. Monthly weather review, 126(6): 1719-1724.

Chambers, D.P., 2006. Observing seasonal steric sea level variations with GRACE and satellite altimetry. Journal of Geophysical Research: Oceans, 111(C3).

Chen, J., Famigliett, J.S., Scanlon, B.R. and Rodell, M., 2016. Groundwater storage changes: present status from GRACE observations, Remote Sensing and Water Resources. Springer, pp. 207-227.

Chen, J., Wilson, C.R., Tapley, B.D., Yang, Z.-L., Niu, G.-Y., 2009. 2005 drought event in the Amazon River basin as measured by GRACE and estimated by climate models. Journal of Geophysical Research: Solid Earth, 114(B5).

Chen, J., Li, J., Zhang, Z., Ni, S., 2014. Long-term groundwater variations in Northwest India from satellite gravity measurements. Global and Planetary Change, 116: 130-138.

Cheng, M., Tapley, B.D., 2004. Variations in the Earth's oblateness during the past 28 years. Journal of Geophysical Research: Solid Earth, 109(B9).

Chiew, F., Stewardson, M. and McMahon, T., 1993. Comparison of six rainfall-runoff modelling approaches. Journal of Hydrology, 147(1-4): 1-36.

Christiansen, L., Krogh, P., Bauer-Gottwein, P., Andersen, O., Leiriäo, S., Binning, P.J. and Rosbjerg, D., 2007. Local to regional hydrological model calibration for the Okavango River Basin from In-situ and space borne gravity observations, Proceedings of 2nd Space for Hydrology Workshop, Geneva, Switzerland, 12-14 November 2007.

Colliander, A. et al., 2017. Validation of SMAP surface soil moisture products with core validation sites. Remote Sensing of Environment, 191: 215-231.

Coumou, D. and Rahmstorf, S., 2012. A decade of weather extremes. Nature climate change, 2(7): 491-496.

Courtier, P., Thépaut, J.N. and Hollingsworth, A., 1994. A strategy for operational implementation of 4D-Var, using an incremental approach. Quarterly Journal of the Royal Meteorological Society, 120(519): 1367-1387.

Crow, W.T., Wood, E.F., 2003. The assimilation of remotely sensed soil brightness temperature imagery into a land surface model using ensemble Kalman filtering: A case study based on ESTAR measurements during SGP97. Advances in Water Resources, 26(2): 137-149.

Danesh-Yazdi, M. and Ataie-Ashtiani, B., 2019. Lake Urmia crisis and restoration plan: planning without appropriate data and model is gambling. Journal of Hydrology, 576: 639-651.

Dando, M., Thorpe, A. and Eyre, J., 2007. The optimal density of atmospheric sounder observations in the Met Office NWP system. Quarterly Journal of the Royal

Meteorological Society: A journal of the atmospheric sciences, applied meteorology and physical oceanography, 133(629): 1933-1943

Danielson, J.J., Gesch, D.B., 2011. Global multi-resolution terrain elevation data 2010 (GMTED2010). US Department of the Interior, US Geological Survey Washington, DC, USA.

De Goncalves, L.G.G. et al., 2009. The South American land data assimilation system (SALDAS) 5-yr retrospective atmospheric forcing datasets. Journal of Hydrometeorology, 10(4): 999-1010.

De Paiva, R.C.D. et al., 2013. Large-scale hydrologic and hydrodynamic modeling of the Amazon River basin. Water Resources Research, 49(3): 1226-1243.

Der Kiureghian, A., 2005. First-and second-order reliability methods. Engineering design reliability handbook, 14.

Devia, G.K., Ganasri, B. and Dwarakish, G., 2015. A review on hydrological models. Aquatic Procedia, 4(1): 1001-1007.

Dillon, M.E. et al., 2016. Application of the WRF-LETKF data assimilation system over southern South America: Sensitivity to model physics. Weather and Forecasting, 31(1): 217-236.

Dobslaw, H., Bergmann-Wolf, I., Forootan, E., Dahle, C., Mayer-Gürr, T., Kusche, J. and Flechtner, F., 2016. Modeling of present-day atmosphere and ocean non-tidal de-aliasing errors for future gravity mission simulations. Journal of geodesy, 90(5): 423-436.

Dorigo, W. et al., 2010. The international soil moisture network-a data hosting facility for in situ soil moisture measurements in support of SMOS cal/val, EGU General Assembly Conference Abstracts, pp. 12063.

Draper, C., Reichle, R., De Lannoy, G., Liu, Q., 2012. Assimilation of passive and active microwave soil moisture retrievals. Geophysical Research Letters, 39(4).

Dumedah, G., Walker, J.P., Merlin, O., 2015. Root-zone soil moisture estimation from assimilation of downscaled Soil Moisture and Ocean Salinity data. Advances in Water Resources, 84: 14-22.

Döll, P., Kaspar, F., Lehner, B., 2003. A global hydrological model for deriving water availability indicators: model tuning and validation. Journal of Hydrology, 270(1-2): 105-134.

Ebert, E.E., Janowiak, J.E., Kidd, C., 2007. Comparison of near-real-time precipitation estimates from satellite observations and numerical models. Bulletin of the American Meteorological Society, 88(1): 47-64.

Eicker, A., Forootan, E., Springer, A., Longuevergne, L. and Kusche, J., 2016. Does GRACE see the terrestrial water cycle "intensifying"? Journal of Geophysical Research: Atmospheres, 121(2): 733-745.

Eicker, A., Schumacher, M., Kusche, J., Döll, P., Schmied, H.M., 2014. Calibration/data assimilation approach for integrating GRACE data into the WaterGAP Global Hydrology Model (WGHM) using an ensemble Kalman filter: First results. Surveys in Geophysics, 35(6): 1285-1309.

Elbern, H., Schmidt, H., 2001. Ozone episode analysis by four-dimensional variational chemistry data assimilation. Journal of Geophysical Research: Atmospheres, 106(D4): 3569-3590.

El Gharamti, M., Valstar, J., Janssen, G., Marsman, A. and Hoteit, I., 2016. On the efficiency of the hybrid and the exact second-order sampling formulations of the EnKF: a reality-inspired 3-D test case for estimating biodegradation rates of chlorinated hydrocarbons at the port of Rotterdam.

Entekhabi, D. et al., 2010. The soil moisture active passive (SMAP) mission. Proceedings of the IEEE, 98(5): 704-716.

Evensen, G., 1994. Sequential data assimilation with a nonlinear quasi-geostrophic model using Monte Carlo methods to forecast error statistics. Journal of Geophysical Research: Oceans, 99(C5): 10143-10162.

Evensen, G., 2003. The ensemble Kalman filter: Theoretical formulation and practical implementation. Ocean dynamics, 53(4): 343-367.

Evensen, G., 2004. Sampling strategies and square root analysis schemes for the EnKF. Ocean dynamics, 54(6): 539-560.

Evensen, G., 2009. Data assimilation: the ensemble Kalman filter. Springer Science & Business Media.

Famiglietti, J., Cazenave, A., Eicker, A., Reager, J., Rodell, M. and Velicogna, I., 2015. Satellites provide the big picture. Science, 349(6249): 684-685.

Famiglietti, J.S. and Rodell, M., 2013. Water in the balance. Science, 340(6138): 1300-1301.

Farrell, W., 1972. Deformation of the Earth by surface loads. Reviews of Geophysics, 10(3): 761-797.

FAO, 2009. (Food and Agriculture Organization of the United Nations). FAO water report, 34 .

FAO, 2016. (Food and Agriculture Organization of the United Nations). AQUASTAT Main Database, http://www.fao.org/nr/water/aquastat/water_use.

Feidas, H., 2010. Validation of satellite rainfall products over Greece. Theoretical and Applied climatology, 99(1-2): 193-216.

Flechtner, F., Morton, P., Watkins, M., Webb, F., 2014. Status of the GRACE follow-on mission, Gravity, geoid and height systems. Springer, pp. 117-121.

Fleming, K., Awange, J., Kuhn, M., Featherstone, W., 2011. Evaluating the TRMM 3B43 monthly precipitation product using gridded rain-gauge data over Australia. Australian meteorological and oceanographic Journal, 61.

Friedl, M.A. et al., 2002. Global land cover mapping from MODIS: algorithms and early results. Remote sensing of Environment, 83(1-2): 287-302.

Forman, B.A. and Reichle, R., 2013. The spatial scale of model errors and assimilated retrievals in a terrestrial water storage assimilation system. Water Resources Research, 49(11): 7457-7468.

Forman, B.A., Reichle, R. and Rodell, M., 2012. Assimilation of terrestrial water storage from GRACE in a snow-dominated basin. Water Resources Research, 48(1).

Forootan, E., 2014. Statistical signal decomposition techniques for analyzing time-variable satellite gravimetry data, Universitäts-und Landesbibliothek Bonn.

Forootan, E., Didova, O., Schumacher, M., Kusche, J. and Elsaka, B., 2014a. Comparisons of atmospheric mass variations derived from ECMWF reanalysis and operational fields, over 2003–2011. Journal of Geodesy, 88(5): 503-514.

Forootan, E. et al., 2014b. Separation of large scale water storage patterns over Iran using GRACE, altimetry and hydrological data. Remote Sensing of Environment, 140: 580-595.

Forootan, E. et al., 2017. Large-scale total water storage and water flux changes over the arid and semiarid parts of the Middle East from GRACE and reanalysis products. Surveys in Geophysics, 38(3): 591-615.

Frappart, F. and Ramillien, G., 2018. Monitoring groundwater storage changes using the Gravity Recovery and Climate Experiment (GRACE) satellite mission: A review. Remote Sensing, 10(6): 829.

Frappart, F., Ramillien, G., Biancamaria, S., Mognard, N. and Cazenave, A., 2006. Evolution of high-latitude snow mass derived from the GRACE gravimetry mission (2002-2004)-art. no. L02501. Geophysical Research Letters, 33(2): NIL_32-NIL_36.

Frappart, F., Ramillien, G., Leblanc, M., Tweed, S.O., Bonnet, M.-P. and Maisongrande, P., 2011. An independent component analysis filtering approach for estimating continental hydrology in the GRACE gravity data. Remote Sensing of Environment, 115(1): 187-204.

Frappart, F., Ramillien, G. and Seoane, L., 2016. Monitoring water mass redistributions on land and polar ice sheets using the grace gravimetry from space mission, Land Surface Remote Sensing in Continental Hydrology. Elsevier, pp. 255-279.

Fritsche, M., Döll, P. and Dietrich, R., 2012. Global-scale validation of model-based load deformation of the Earth's crust from continental watermass and atmospheric pressure variations using GPS. Journal of Geodynamics, 59: 133-142.

Garner, T., Wolf, R., Spiro, R., Thomsen, M., 1999. First attempt at assimilating data to constrain a magnetospheric model. Journal of Geophysical Research: Space Physics, 104(A11): 25145-25152.

Getirana, A.C. et al., 2014. Water balance in the Amazon basin from a land surface model ensemble. Journal of Hydrometeorology, 15(6): 2586-2614.

Girotto, M., De Lannoy, G.J., Reichle, R.H., Rodell, M., 2016. Assimilation of gridded terrestrial water storage observations from GRACE into a land surface model. Water Resources Research, 52(5): 4164-4183.

Girotto, M. et al., 2017. Benefits and pitfalls of GRACE data assimilation: A case study of terrestrial water storage depletion in India. Geophysical research letters, 44(9): 4107-4115.

Girotto, M., De Lannoy, G.J., Reichle, R.H., Rodell, M., Draper, C., Bhanja, S.N. and Mukherjee, A., 2017. Benefits and pitfalls of GRACE data assimilation: A case study of terrestrial water storage depletion in India. Geophysical research letters, 44(9): 4107-4115.

Giustarini, L., Matgen, P., Hostache, R., Montanari, M., Plaza Guingla, D.A., Pauwels, V., De Lannoy, G., De Keyser, R., Pfister, L. and Hoffmann, L., 2011. Assimilating SAR-derived water level data into a hydraulic model: a case study. Hydrology and Earth System Sciences, 15(7): 2349-2365.

Gleeson, T., Wada, Y., Bierkens, M.F., van Beek, L.P., 2012. Water balance of global aquifers revealed by groundwater footprint. Nature, 488(7410): 197.

Goff, J., Lamarche, G., Pelletier, B., Chagué-Goff, C., Strotz, L., 2011. Predecessors to the 2009 South Pacific tsunami in the Wallis and Futuna archipelago. Earth-Science Reviews, 107(1-2): 91-106.

Green, T.R. et al., 2011. Beneath the surface of global change: Impacts of climate change on groundwater. Journal of Hydrology, 405(3-4): 532-560.

Grippa, M., Kergoat, L., Frappart, F., Araud, Q., Boone, A., de Rosnay, P., Lemoine, J., Gascoin, S. and Balsamo, G., Ottlé, 15 C., Decharme, B., Saux-Picart, S., and Ramillien, G.,2011. Land water storage variability over West Africa estimated by GRACE and land surface models, Water Resources Research, 47: W05549.

Güntner, A., 2008. Improvement of global hydrological models using GRACE data. Surveys in geophysics, 29(4-5): 375-397.

Han, S.-C., Shum, C., Jekeli, C., Kuo, C.-Y., Wilson, C. and Seo, K.-W., 2005. Non-isotropic filtering of GRACE temporal gravity for geophysical signal enhancement. Geophysical Journal International, 163(1): 18-25.

Hairer, M., Stuart, A. and Voss, J., 2005. A Bayesian approach to data assimilation. Physica D.

Heiskanen, W.A. and Moritz, H., 1967. Physical geodesy. San Francisco, WH Freeman [1967].

Henry, C.M., Allen, D.M., Huang, J., 2011. Groundwater storage variability and annual recharge using well-hydrograph and GRACE satellite data. Hydrogeology Journal, 19(4): 741-755.

Hirschi, M., S. Seneviratne, S. Hagemann, and C. Schär, 2007: Analysis of seasonal terrestrial water storage variations in regional climate simulations over Europe. J. Geophys. Res, 112: D22109.

Houtekamer, P. and Zhang, F., 2016. Review of the ensemble Kalman filter for atmospheric data assimilation. Monthly Weather Review, 144(12): 4489-4532

Hosseini, S.M., Parizi, E., Ataie-Ashtiani, B., Simmons, C.T., 2019. Assessment of sustainable groundwater resources management using integrated environmental index: Case studies across Iran. Science of The Total Environment, 676: 792-810.

Hoteit, I., Luo, X., Pham, D.-T., 2012. Particle Kalman filtering: A nonlinear Bayesian framework for ensemble Kalman filters. Monthly weather review, 140(2): 528-542.

Hoteit, I., Pham, D.-T. and Blum, J., 2002. A simplified reduced order Kalman filtering and application to altimetric data assimilation in Tropical Pacific. Journal of Marine systems, 36(1-2): 101-127.

Hoteit, I., Pham, D.-T., Gharamti, M. and Luo, X., 2015. Mitigating observation perturbation sampling errors in the stochastic EnKF. Monthly Weather Review, 143(7): 2918-2936.

Hoteit, I., Pham, D.-T., Triantafyllou, G. and Korres, G., 2008. A new approximate solution of the optimal nonlinear filter for data assimilation in meteorology and oceanography. Monthly Weather Review, 136(1): 317-334.

Hoteit, I., Triantafyllou, G. and Petihakis, G., 2005. Efficient data assimilation into a complex, 3-D physical-biogeochemical model using partially-local Kalman filters.

Houborg, R., Rodell, M., Li, B., Reichle, R., Zaitchik, B.F., 2012. Drought indicators based on model-assimilated Gravity Recovery and Climate Experiment (GRACE) terrestrial water storage observations. Water Resources Research, 48(7).

Huang, S., Kumar, R., Flörke, M., Yang, T., Hundecha, Y., Kraft, P., Gao, C., Gelfan, A., Liersch, S. and Lobanova, A., 2017. Evaluation of an ensemble of regional hydrological models in 12 large-scale river basins worldwide. Climatic Change, 141(3): 381-397.

Huffman, G.J. et al., 1997. The global precipitation climatology project (GPCP) combined precipitation dataset. Bulletin of the American Meteorological Society, 78(1): 5-20.

Huffman, G.J. et al., 2007. The TRMM multisatellite precipitation analysis (TMPA): Quasi-global, multiyear, combined-sensor precipitation estimates at fine scales. Journal of hydrometeorology, 8(1): 38-55.

Hunt, B.R., Kostelich, E.J., Szunyogh, I., 2007. Efficient data assimilation for spatiotemporal chaos: A local ensemble transform Kalman filter. Physica D: Nonlinear Phenomena, 230(1-2): 112-126.

Huntington, T.G., 2006. Evidence for intensification of the global water cycle: review and synthesis. Journal of Hydrology, 319(1-4): 83-95.

Ilk, K.-H., Flury, J., Rummel, R., Schwintzer, P., Bosch, W., Haas, C., Schröter, J., Stammer, D., Zahel, W. and Miller, H., 2004. Mass Transport and Mass Distribution in the Earth System: Contribution of the New Generation of Satellite Gravity and Altimetry Missions to Geosciences; Proposal for a German Priority Research Program.

Inácio, P., Ditmar, P., Klees, R. and Farahani, H.H., 2015. Analysis of star camera errors in GRACE data and their impact on monthly gravity field models. Journal of Geodesy, 89(6): 551-571.

Irmak, A. and Kamble, B., 2009. Evapotranspiration data assimilation with genetic algorithms and SWAP model for on-demand irrigation. Irrigation science, 28(1): 101-112.

IWRMC, 2011. Iran Water Resource Management Company. The Ministry of power, Iran. http://www.wrm.ir/.

Jasinski, M.F. et al., 2019. NCA-LDAS: overview and analysis of hydrologic trends for the national climate assessment. Journal of hydrometeorology, 20(8): 1595-1617.

Javanmard, S., Yatagai, A., Nodzu, M., BodaghJamali, J., Kawamoto, H., 2010. Comparing high-resolution gridded precipitation data with satellite rainfall estimates of TRMM_3B42 over Iran. Advances in Geosciences, 25: 119-125.

Jazwinski, A., 1970. Stochastic process and filtering theory, academic press. A subsidiary of Harcourt Brace Jovanovich Publishers.

Jekeli, C., 1981. Alternative methods to smooth the Earth's gravity field.

Jiang, D., Wang, J., Huang, Y., Zhou, K., Ding, X. and Fu, J., 2014. The review of GRACE data applications in terrestrial hydrology monitoring. Advances in Meteorology, 2014.

Jia, L. et al., 2009. Regional estimation of daily to annual regional evapotranspiration with MODIS data in the Yellow River Delta wetland. Hydrology and Earth System Sciences, 13(10): 1775-1787.

Joodaki, G., Wahr, J., Swenson, S., 2014. Estimating the human contribution to groundwater depletion in the Middle East, from GRACE data, land surface models, and well observations. Water Resources Research, 50(3): 2679-2692.

Jones, J.E., Woodward, C.S.J.A.i.W.R., 2001. Newton–Krylov-multigrid solvers for large-scale, highly heterogeneous, variably saturated flow problems. 24(7): 763-774.

Jung, M. et al., 2010. Recent decline in the global land evapotranspiration trend due to limited moisture supply. Nature, 467(7318): 951-954.

Kauffeldt, A., Wetterhall, F., Pappenberger, F., Salamon, P. and Thielen, J., 2016. Technical review of large-scale hydrological models for implementation in operational flood forecasting schemes on continental level. Environmental Modelling & Software, 75: 68-76.

Kalnay, E., 2003. Atmospheric modeling, data assimilation and predictability. Cambridge university press.

Katiraie-Boroujerdy, P.-S., Nasrollahi, N., Hsu, K.-l., Sorooshian, S., 2013. Evaluation of satellite-based precipitation estimation over Iran. Journal of arid environments, 97: 205-219.

Kerr, Y.H. et al., 2012. The SMOS soil moisture retrieval algorithm. IEEE transactions on geoscience and remote sensing, 50(5): 1384-1403.

Khaki, M., Ait-El-Fquih, B., Hoteit, I., Forootan, E., Awange, J. and Kuhn, M., 2017c. A two-update ensemble Kalman filter for land hydrological data assimilation with an uncertain constraint. Journal of Hydrology, 555: 447-462.

Khaki, M., Ait-El-Fquih, B., Hoteit, I., Forootan, E., Awange, J. and Kuhn, M., 2018e. Unsupervised ensemble Kalman filtering with an uncertain constraint for land hydrological data assimilation. Journal of Hydrology, 564: 175-190.

Khaki, M., Forootan, E., Kuhn, M., Awange, J., Longuevergne, L. and Wada, Y., 2018a. Efficient basin scale filtering of GRACE satellite products. Remote sensing of environment, 204: 76-93.

Khaki, M., Forootan, E., Kuhn, M., Awange, J., Papa, F. and Shum, C., 2018b. A study of Bangladesh's sub-surface water storages using satellite products and data assimilation scheme. Science of the Total Environment, 625: 963-977.

Khaki, M., Forootan, E., Kuhn, M., Awange, J., van Dijk, A., Schumacher, M. and Sharifi, M., 2018c. Determining water storage depletion within Iran by assimilating GRACE data into the W3RA hydrological model. Advances in Water Resources, 114: 1-18.

Khaki, M., Hoteit, I., Kuhn, M., Awange, J., Forootan, E., Van Dijk, A.I., Schumacher, M. and Pattiaratchi, C., 2017b. Assessing sequential data assimilation techniques for integrating GRACE data into a hydrological model. Advances in Water Resources, 107: 301-316.

Khaki, M., Hoteit, I., Kuhn, M., Forootan, E. and Awange, J., 2019. Assessing data assimilation frameworks for using multi-mission satellite products in a hydrological context. Science of The Total Environment, 647: 1031-1043.

Khaki, M., Schumacher, M., Forootan, E., Kuhn, M., Awange, J. and van Dijk, A., 2017a. Accounting for spatial correlation errors in the assimilation of GRACE into hydrological models through localization. Advances in Water Resources, 108: 99-112.

Khaki, M., Awange, J., 2019. The application of multi-mission satellite data assimilation for studying water storage changes over South America. Science of the Total Environment, 647: 1557-1572.

Khaki, M. et al., 2018a. A study of Bangladesh's sub-surface water storages using satellite products and data assimilation scheme. Science of the Total Environment, 625: 963-977.

Khaki, M. et al., 2018b. Determining water storage depletion within Iran by assimilating GRACE data into the W3RA hydrological model. Advances in Water Resources, 114: 1-18.

Kim, E. et al., 2017. Overview of SnowEx Year 1 Activities, SnowEx Workshop.

Klees, R., Revtova, E., Gunter, B., Ditmar, P., Oudman, E., Winsemius, H. and Savenije, H., 2008. The design of an optimal filter for monthly GRACE gravity models. Geophysical Journal International, 175(2): 417-432.

Koch, K.-R., 2007. Introduction to Bayesian statistics. Springer Science & Business Media.

Kolassa, J. et al., 2017. Data assimilation to extract soil moisture information from SMAP observations. Remote sensing, 9(11): 1179.

Kollet, S.J., Maxwell, R.M.J.A.i.W.R., 2006. Integrated surface–groundwater flow modeling: A free-surface overland flow boundary condition in a parallel groundwater flow model. 29(7): 945-958.

Komma, J., Blöschl, G. and Reszler, C., 2008. Soil moisture updating by Ensemble Kalman Filtering in real-time flood forecasting. Journal of Hydrology, 357(3-4): 228-242.

Koster, R.D. et al., 2010. Contribution of land surface initialization to subseasonal forecast skill: First results from a multi-model experiment. Geophysical Research Letters, 37(2).

Koster, R.D., Suarez, M.J., 1999. A simple framework for examining the interannual variability of land surface moisture fluxes. Journal of Climate, 12(7): 1911-1917.

Kourgialas, N.N., Karatzas, G.P., 2015. A modeling approach for agricultural water management in citrus orchards: cost-effective irrigation scheduling and agrochemical transport simulation. Environmental monitoring and assessment, 187(7): 1-21.

Kumar, S.V. et al., 2008. A land surface data assimilation framework using the land information system: Description and applications. Advances in Water Resources, 31(11): 1419-1432.

Kumar, S., Peters-Lidard, C., Santanello, J., Reichle, R., Draper, C., Koster, R., Nearing, G. and Jasinski, M., 2015. Evaluating the utility of satellite soil moisture retrievals over irrigated areas and the ability of land data assimilation methods to correct for unmodeled processes.

Kumar, S.V., Peters-Lidard, C.D., Mocko, D., Reichle, R., Liu, Y., Arsenault, K.R., Xia, Y., Ek, M., Riggs, G. and Livneh, B., 2014. Assimilation of remotely sensed soil moisture and snow depth retrievals for drought estimation. Journal of Hydrometeorology, 15(6): 2446-2469.

Kumar, S.V., Zaitchik, B.F., Peters-Lidard, C.D., Rodell, M., Reichle, R., Li, B., Jasinski, M., Mocko, D., Getirana, A. and De Lannoy, G., 2016. Assimilation of gridded GRACE terrestrial water storage estimates in the North American Land Data Assimilation System. Journal of Hydrometeorology, 17(7): 1951-1972.

Kumar, S.V., Reichle, R.H., Koster, R.D., Crow, W.T., Peters-Lidard, C.D., 2009. Role of subsurface physics in the assimilation of surface soil moisture observations. Journal of hydrometeorology, 10(6): 1534-1547.

Kumar, S.V. et al., 2019. NCA-LDAS land analysis: Development and performance of a multisensor, multivariate land data assimilation system for the National Climate Assessment. Journal of Hydrometeorology, 20(8): 1571-1593.

Kurtenbach, E., Mayer-Gürr, T. and Eicker, A., 2009. Deriving daily snapshots of the Earth's gravity field from GRACE L1B data using Kalman filtering. Geophysical Research Letters, 36(17).

Kurtz, W. et al., 2016. TerrSysMP–PDAF (version 1.0): a modular high-performance data assimilation framework for an integrated land surface–subsurface model. Geoscientific Model Development, 9(4): 1341-1360.

Kusche, J., 2007. Approximate decorrelation and non-isotropic smoothing of time-variable GRACE-type gravity field models. Journal of Geodesy, 81(11): 733-749.

Kusche, J., Klemann, V., Bosch, W., 2012. Mass distribution and mass transport in the Earth system. Journal of Geodynamics, 59: 1-8.

Lahoz, W. et al., 2006. The Assimilation of Envisat data (ASSET) project. Atmospheric Chemistry and Physics Discussions, 6(6): 12769-12824.

Lahoz, W.A. and Schneider, P., 2014. Data assimilation: making sense of Earth Observation. Frontiers in Environmental Science, 2: 16.

Landerer, F.W. and Swenson, S., 2012. Accuracy of scaled GRACE terrestrial water storage estimates. Water resources research, 48(4).

Lee, E., Jayakumar, R., Shrestha, S., Han, Z., 2018. Assessment of transboundary aquifer resources in Asia: status and progress towards sustainable groundwater management. Journal of Hydrology: Regional Studies, 20: 103-115.

Lee, H., Seo, D.-J. and Koren, V., 2011. Assimilation of streamflow and in situ soil moisture data into operational distributed hydrologic models: Effects of uncertainties in the data and initial model soil moisture states. Advances in water resources, 34(12): 1597-1615.

Lettenmaier, D.P., Famiglietti, J.S., 2006. Water from on high. Nature, 444(7119): 562-563.

Li, B. et al., 2012. Assimilation of GRACE terrestrial water storage into a land surface model: Evaluation and potential value for drought monitoring in western and central Europe. Journal of Hydrology, 446: 103-115.

Liang, X., Lettenmaier, D.P., Wood, E.F. and Burges, S.J., 1994. A simple hydrologically based model of land surface water and energy fluxes for general circulation models. Journal of Geophysical Research: Atmospheres, 99(D7): 14415-14428.

Lievens, H. et al., 2015. SMOS soil moisture assimilation for improved hydrologic simulation in the Murray Darling Basin, Australia. Remote Sensing of Environment, 168: 146-162.

Lievens, H. et al., 2017. Joint Sentinel-1 and SMAP data assimilation to improve soil moisture estimates. Geophysical research letters, 44(12): 6145-6153.

Liou, Y.-A. and Kar, S.K., 2014. Evapotranspiration estimation with remote sensing and various surface energy balance algorithms—A review. Energies, 7(5): 2821-2849.

Liu, P.-W., Judge, J., De Roo, R.D., England, A.W., Bongiovanni, T., 2016. Uncertainty in soil moisture retrievals using the SMAP combined active–passive algorithm for growing sweet corn. IEEE Journal of Selected Topics in Applied Earth Observations and Remote Sensing, 9(7): 3326-3339.

Liu, Y. and Gupta, H.V., 2007. Uncertainty in hydrologic modeling: Toward an integrated data assimilation framework. Water Resources Research, 43(7).

Liu, Z.Q. and Rabier, F., 2003. The potential of high-density observations for numerical weather prediction: A study with simulated observations. Quarterly Journal of the Royal Meteorological Society: A journal of the atmospheric sciences, applied meteorology and physical oceanography, 129(594): 3013-3035.

Llubes, M., Lemoine, J.-M. and Rémy, F., 2007. Antarctica seasonal mass variations detected by GRACE. Earth and Planetary Science Letters, 260(1-2): 127-136.

Long, D., Longuevergne, L., Scanlon, B.R., 2014. Uncertainty in evapotranspiration from land surface modeling, remote sensing, and GRACE satellites. Water Resources Research, 50(2): 1131-1151.

Long, D., Chen, X., Scanlon, B.R., Wada, Y., Hong, Y., Singh, V.P., Chen, Y., Wang, C., Han, Z. and Yang, W., 2016. Have GRACE satellites overestimated groundwater depletion in the Northwest India Aquifer? Scientific reports, 6: 24398.

Longuevergne, L., Scanlon, B.R. and Wilson, C.R., 2010. GRACE Hydrological estimates for small basins: Evaluating processing approaches on the High Plains Aquifer, USA. Water Resources Research, 46(11).

Longuevergne, L., Wilson, C., Scanlon, B.R. and Crétaux, J., 2013. GRACE water storage estimates for the Middle East and other regions with significant reservoir and lake storage.

Lopez, R., Torii, A., Miguel, L., Cursi, J.S., 2015. Overcoming the drawbacks of the FORM using a full characterization method. Structural Safety, 54: 57-63.

Madsen, H.O., Krenk, S., Lind, N.C., 2006. Methods of structural safety. Courier Corporation.

McCabe, M. et al., 2008. Hydrological consistency using multi-sensor remote sensing data for water and energy cycle studies. Remote Sensing of Environment, 112(2): 430-444.

Maxwell, R.M., Miller, N.L., 2005. Development of a coupled land surface and groundwater model. Journal of Hydrometeorology, 6(3): 233-247.

Maxwell, R. M.: A terrain-following grid transform and preconditioner for parallel, large-scale, integrated hydrologic modeling, Adv. Water Resour., 53, 109–117, https://doi.org/10.1016/j.advwatres.2012.10.001, 2013.

Maxwell, R. et al., 2016. ParFlow user's manual (Integrated GroundWater Modeling Center Report GWMI 2016-01). Golden, CO: Integrated GroundWater Modeling Center, Colorado School of Mines.

Maxwell, R.M., Kollet, S.J., Smith, S.G., Woodward, C.S., Falgout, R.D., Ferguson, I.M., Baldwin, C., Bosl, W.J., Hornung, R. and Ashby, S., 2009. ParFlow user's manual. International Ground Water Modeling Center Report GWMI, 1(2009): 129.

Mayer-Gürr, T., 2008. Gravitationsfeldbestimmung aus der Analyse kurzer Bahnbögen am Beispiel der Satellitenmissionen CHAMP und GRACE.

Mayer-Gürr, T., Savcenko, R., Bosch, W., Daras, I., Flechtner, F. and Dahle, C., 2012. Ocean tides from satellite altimetry and GRACE. Journal of geodynamics, 59: 28-38.

McLaughlin, D., 2002. An integrated approach to hydrologic data assimilation: interpolation, smoothing, and filtering. Advances in Water Resources, 25(8-12): 1275-1286.

McMillan, H., Hreinsson, E., Clark, M., Singh, S., Zammit, C. and Uddstrom, M., 2013. Operational hydrological data assimilation with the recursive ensemble Kalman filter. Hydrology and Earth System Sciences, 17(1): 21.

Mehrnegar, N., Jones, O., Singer, M.B., Schumacher, M., Bates, P. and Forootan, E., 2020. Comparing global hydrological models and combining them with GRACE by dynamic model data averaging (DMDA). Advances in Water Resources, 138: 103528.

Montzka, C., Pauwels, V., Franssen, H.-J.H., Han, X. and Vereecken, H., 2012. Multivariate and multiscale data assimilation in terrestrial systems: A review. Sensors, 12(12): 16291-16333.

Moradkhani, H., DeChant, C.M. and Sorooshian, S., 2012. Evolution of ensemble data assimilation for uncertainty quantification using the particle filter-Markov chain Monte Carlo method. Water Resources Research, 48(12).

Moradkhani, H., Hsu, K.L., Gupta, H. and Sorooshian, S., 2005. Uncertainty assessment of hydrologic model states and parameters: Sequential data assimilation using the particle filter. Water resources research, 41(5).

Najmaddin, P.M., Whelan, M.J. and Balzter, H., 2017. Application of satellite-based precipitation estimates to rainfall-runoff modelling in a data-scarce semi-arid catchment. Climate, 5(2): 32.

Nataf, A., 1962. Determination des Distribution don t les marges sont Donnees. Comptes Rendus de l Academie des Sciences, 225: 42-43.

Nations, U., 2015. The millennium development goals report. New York: United Nations.

Nations, U., 2004. Fresh water and sanitation country profile the Islamic Republic of Iran. New York: United Nations.

Neal, J., Schumann, G., Bates, P., Buytaert, W., Matgen, P. and Pappenberger, F., 2009. A data assimilation approach to discharge estimation from space. Hydrological Processes: An International Journal, 23(25): 3641-3649.

Nerger, L., Hiller, W., 2013. Software for ensemble-based data assimilation systems-Implementation strategies and scalability. Computers & Geosciences, 55: 110-118.

Nikolaidis, E., Ghiocel, D.M., Singhal, S., 2004. First-and Second-Order Reliability Methods, Engineering Design Reliability Handbook. CRC Press, pp. 313-336.

Niu, G.Y., Yang, Z.L., Dickinson, R.E., Gulden, L.E., Su, H., 2007. Development of a simple groundwater model for use in climate models and evaluation with Gravity Recovery and Climate Experiment data. Journal of Geophysical Research: Atmospheres, 112(D7).

Oleson, K. et al., 2010. Technical description of version 4.0 of the Community Land Model. NCAR Tech. Note NCAR/TN-4781STR, 257.

Oleson, K. et al., 2008. Improvements to the Community Land Model and their impact on the hydrological cycle. Journal of Geophysical Research: Biogeosciences, 113(G1).

Oleson, K.W. et al., 2004. Technical description of the community land model (CLM). Tech. Note NCAR/TN-461+ STR.

Orsolini, Y. et al., 2013. Impact of snow initialization on sub-seasonal forecasts. Climate dynamics, 41(7): 1969-1982.

Pan, M., Sahoo, A.K., Troy, T.J., Vinukollu, R.K., Sheffield, J. and Wood, E.F., 2012. Multisource estimation of long-term terrestrial water budget for major global river basins. Journal of Climate, 25(9): 3191-3206.

Pan, M. and Wood, E.F., 2006. Data assimilation for estimating the terrestrial water budget using a constrained ensemble Kalman filter. Journal of Hydrometeorology, 7(3): 534-547.

Pearson, C., 2008. Short-and medium-term climate information for water management. World Meteorological Organization (WMO) Bulletin, 57(3): 173.

Pipunic, R., Walker, J. and Western, A., 2008. Assimilation of remotely sensed data for improved latent and sensible heat flux prediction: A comparative synthetic study. Remote Sensing of Environment, 112(4): 1295-1305.

Prakash, S., Mahesh, C., Gairola, R., 2013. Comparison of TRMM Multi-satellite Precipitation Analysis (TMPA)-3B43 version 6 and 7 products with rain gauge data from ocean buoys. Remote sensing letters, 4(7): 677-685.

RAHIMPOUR, M., KARIMI, N., ROUZBAHANI, R., EFTEKHARI, M., 2018. VALIDATION AND CALIBRATION OF FAO'S WAPOR PRODUCT (ACTUAL EVAPOTRANSPIRATION) IN IRAN USING IN-SITU MEASUREMENTS.

Rajabi, M.M., Ataie-Ashtiani, B. and Simmons, C.T., 2018. Model-data interaction in groundwater studies: Review of methods, applications and future directions. Journal of hydrology, 567: 457-477.

Ramillien, G., Cazenave, A. and Brunau, O., 2004. Global time variations of hydrological signals from GRACE satellite gravimetry. Geophysical Journal International, 158(3): 813-826.

Ramillien, G., Famiglietti, J.S. and Wahr, J., 2008. Detection of continental hydrology and glaciology signals from GRACE: a review. Surveys in geophysics, 29(4-5): 361-374.

Ray, R.L., Fares, A., He, Y. and Temimi, M., 2017. Evaluation and inter-comparison of satellite soil moisture products using in situ observations over Texas, US. Water, 9(6): 372.

Reager, J.T. et al., 2015. Assimilation of GRACE terrestrial water storage observations into a land surface model for the assessment of regional flood potential. Remote Sensing, 7(11): 14663-14679.

Reichle, R.H., McLaughlin, D.B., Entekhabi, D., 2002. Hydrologic data assimilation with the ensemble Kalman filter. Monthly Weather Review, 130(1): 103-114.

Reichle, R.H., De Lannoy, G.J., Forman, B.A., Draper, C.S. and Liu, Q., 2014. Connecting satellite observations with water cycle variables through land data assimilation: Examples using the NASA GEOS-5 LDAS. Surveys in Geophysics, 35(3): 577-606.

Renzullo, L.J. et al., 2014. Continental satellite soil moisture data assimilation improves root-zone moisture analysis for water resources assessment. Journal of Hydrology, 519: 2747-2762.

Rietbroek, R., 2014. Retrieval of Sea Level and Surface Loading Variations from Geodetic Observations and Model Simulations, Universitäts-und Landesbibliothek Bonn.

Robert, C., Blayo, E. and Verron, J., 2006. Comparison of reduced-order, sequential and variational data assimilation methods in the tropical Pacific Ocean. Ocean Dynamics, 56(5-6): 624-633.

Rodell, M., Chen, J., Kato, H., Famiglietti, J.S., Nigro, J. and Wilson, C.R., 2007. Estimating groundwater storage changes in the Mississippi River basin (USA) using GRACE. Hydrogeology Journal, 15(1): 159-166.

Rodell, M. and Famiglietti, J., 1999. Detectability of variations in continental water storage from satellite observations of the time dependent gravity field. Water Resources Research, 35(9): 2705-2723.

Rodell, M. et al., 2004a. Basin scale estimates of evapotranspiration using GRACE and other observations. Geophysical Research Letters, 31(20).

Rodell, M. et al., 2004b. The global land data assimilation system. Bulletin of the American Meteorological society, 85(3): 381-394.

Rodell, M., Famiglietti, J.S., 2001. An analysis of terrestrial water storage variations in Illinois with implications for the Gravity Recovery and Climate Experiment (GRACE). Water Resources Research, 37(5): 1327-1339.

Rodell, M., McWilliams, E.B., Famiglietti, J.S., Beaudoing, H.K., Nigro, J., 2011. Estimating evapotranspiration using an observation based terrestrial water budget. Hydrological Processes, 25(26): 4082-4092.

Sahoo, A.K. et al., 2011. Reconciling the global terrestrial water budget using satellite remote sensing. Remote Sensing of Environment, 115(8): 1850-1865.

Sakov, P. and Oke, P.R., 2008. A deterministic formulation of the ensemble Kalman filter: an alternative to ensemble square root filters. Tellus A: Dynamic Meteorology and Oceanography, 60(2): 361-371.

Scanlon, B.R., Zhang, Z., Save, H., Sun, A.Y., Schmied, H.M., Van Beek, L.P., Wiese, D.N., Wada, Y., Long, D. and Reedy, R.C., 2018. Global models underestimate large decadal declining and rising water storage trends relative to GRACE satellite data. Proceedings of the National Academy of Sciences, 115(6): E1080-E1089.

Sarraf, M., Owaygen, M., Ruta, G., Croitoru, L., 2005. Islamic Republic of Iran: Cost assessment of environmental degradation. Sector Note(32043-IRN).

Schaap, M.G., Leij, F.J., 1998. Database-related accuracy and uncertainty of pedotransfer functions. Soil Science, 163(10): 765-779.

Schmidt, R., Schwintzer, P., Flechtner, F., Reigber, C., Güntner, A., Döll, P., Ramillien, G., Cazenave, A., Petrovic, S. and Jochmann, H., 2006. GRACE observations of changes in continental water storage. Global and Planetary Change, 50(1-2): 112-126.

Schumacher, M., 2012. Assimilation of GRACE data into a global hydrological model using an ensemble Kalman filter, Citeseer.

Schumacher, M., Forootan, E., van Dijk, A., Schmied, H.M., Crosbie, R., Kusche, J. and Döll, P., 2018. Improving drought simulations within the Murray-Darling Basin by combined calibration/assimilation of GRACE data into the WaterGAP Global Hydrology Model. Remote Sensing of Environment, 204: 212-228.

Schumacher, M., Forootan, E., Van Dijk, A.I., Müller Schmied, H., Crosbie, R.S., Kusche, J. and Döll, P., 2016a. GRACE Assimilation into Hydrological Model Improves Representation

of Drought-induced Groundwater Trend over Murray-Darling Basin, Australia, EGU General Assembly Conference Abstracts.

Schumacher, M., Kusche, J., Döll, P., 2016b. A systematic impact assessment of GRACE error correlation on data assimilation in hydrological models. Journal of Geodesy, 90(6): 537-559.

Schunk, R.W., Scherliess, L., Sojka, J.J., Thompson, D.C., 2004. USU global ionospheric data assimilation models, Atmospheric and Environmental Remote Sensing Data Processing and Utilization: an End-to-End System Perspective. International Society for Optics and Photonics, pp. 327-336.

Schuurmans, J., Troch, P.A., Veldhuizen, A., Bastiaanssen, W. and Bierkens, M., 2003. Assimilation of remotely sensed latent heat flux in a distributed hydrological model. Advances in Water Resources, 26(2): 151-159.

Seitz, F., Hedman, K., Walter, C., Meyer, F. and Schmidt, M., 2010. Towards the assessment of regional mass variations in continental surface water storages from a combination of heterogeneous space and in-situ observations, Proceedings of the ESA Living Planet Symposium, ESA Publication SP-686.

Seneviratne, S.I. et al., 2010. Investigating soil moisture–climate interactions in a changing climate: A review. Earth-Science Reviews, 99(3-4): 125-161.

Seo, K.-W. and Wilson, C.R., 2005. Simulated estimation of hydrological loads from GRACE. Journal of Geodesy, 78(7-8): 442-456.

Sheffield, J., Ferguson, C.R., Troy, T.J., Wood, E.F., McCabe, M.F., 2009. Closing the terrestrial water budget from satellite remote sensing. Geophysical Research Letters, 36(7).

Shiklomanov, I., Rodda, J.C., 2003. World water resources at the beginning of the 21st century. International hydrology series. Cambridge University Press, Cambridge.

Shinozuka, M., 1983. Basic analysis of structural safety. Journal of Structural Engineering, 109(3): 721-740.

Shrestha, P., Sulis, M., Masbou, M., Kollet, S., Simmer, C., 2014. A scale-consistent terrestrial systems modeling platform based on COSMO, CLM, and ParFlow. Monthly weather review, 142(9): 3466-3483.

Simmons, C.T., Brunner, P., Therrien, R. and Sudicky, E.A., 2019. Commemorating the 50th anniversary of the Freeze and Harlan (1969) Blueprint for a physically-based, digitally-simulated hydrologic response model. Journal of Hydrology: 124309.

Soltani, S.S., Ataie-Ashtiani, B., Danesh-Yazdi, M., Simmons, C.T., 2020. A probabilistic framework for water budget estimation in low runoff regions: A case study of the central Basin of Iran. Journal of Hydrology, 586: 124898.

Soltani, S.S., Ataie-Ashtiani, B., Simmons, C.T., 2021. Review of assimilating GRACE terrestrial water storage data into hydrological models: Advances, challenges and opportunities. Earth-Science Reviews, 213: 1 Sood, A. and Smakhtin, V., 2015. Global hydrological models: a review. Hydrological Sciences Journal, 60(4): 549-565.

Soltani, S. S., Fahs, M., Al Bitar, A., and Ataie-Ashtiani, B.: Fully coupled subsurface-land surface hydrological models: A scaling approach to improve subsurface storage predictions, EGU General Assembly 2022a, Vienna, Austria, 23–27 May 2022, EGU22-2828, https://doi.org/10.5194/egusphere-egu22-2828, 2022.

Soltani, S.S., Fahs, M., Al Bitar, A. and Ataie-Ashtiani, B., 2022b. Improvement of soil moisture and groundwater level estimations using a scale-consistent river parameterization for the

coupled ParFlow-CLM hydrological model: A case study of the Upper Rhine Basin. Journal of Hydrology, 610, p.127991.

Springer, A., Karegar, M. A., Kusche, J., Keune, J., Kurtz, W., and Kollet, S., 2019. Evidence of daily hydrological loading in GPS time series over Europe. Journal of geodesy, 93, 2145-2153.

Stewart, L.M., Dance, S. and Nichols, N., 2008. Correlated observation errors in data assimilation. International journal for numerical methods in fluids, 56(8): 1521-1527.

Stocker, T.F., Qin, D., Plattner, G.-K., Tignor, M.M., Allen, S.K., Boschung, J., Nauels, A., Xia, Y., Bex, V. and Midgley, P.M., 2014. Climate change 2013: the physical science basis. Contribution of working group I to the fifth assessment report of IPCC the intergovernmental panel on climate change. Cambridge University Press.

Stone, J.V., 2004. Independent component analysis: a tutorial introduction. MIT press. 03487.

Su, H., Yang, Z.L., Dickinson, R.E., Wilson, C.R. and Niu, G.Y., 2010. Multisensor snow data assimilation at the continental scale: The value of Gravity Recovery and Climate Experiment terrestrial water storage information. Journal of Geophysical Research: Atmospheres, 115(D10).

Subramanian, A.C., Hoteit, I., Cornuelle, B., Miller, A.J. and Song, H., 2012. Linear versus nonlinear filtering with scale-selective corrections for balanced dynamics in a simple atmospheric model. Journal of the atmospheric sciences, 69(11): 3405-3419.

Sudret, B., Der Kiureghian, A., 2002. Comparison of finite element reliability methods. Probabilistic Engineering Mechanics, 17(4): 337-348.

Sun, A.Y., Morris, A. and Mohanty, S., 2009. Comparison of deterministic ensemble Kalman filters for assimilating hydrogeological data. Advances in Water Resources, 32(2): 280-292.

Swenson, S., Chambers, D., Wahr, J., 2008. Estimating geocenter variations from a combination of GRACE and ocean model output. Journal of Geophysical Research: Solid Earth, 113(B8).

Swenson, S., Wahr, J., 2006. Post-processing removal of correlated errors in GRACE data. Geophysical research letters, 33(8).

Syed, T., Famiglietti, J., Chen, J., Rodell, M., Seneviratne, S.I., Viterbo, P. and Wilson, C.R., 2005. Total basin discharge for the Amazon and Mississippi River basins from GRACE and a land-atmosphere water balance. Geophysical Research Letters, 32(24).

Talagrand, O. and Courtier, P., 1987. Variational assimilation of meteorological observations with the adjoint vorticity equation. I: Theory. Quarterly Journal of the Royal Meteorological Society, 113(478): 1311-1328.

Tangdamrongsub, N., Han, S.-C., Tian, S., Müller Schmied, H., Sutanudjaja, E.H., Ran, J. and Feng, W., 2018. Evaluation of groundwater storage variations estimated from GRACE data assimilation and state-of-the-art land surface models in Australia and the North China Plain. Remote Sensing, 10(3): 483.

Tangdamrongsub, N. et al., 2017. Improving estimates of water resources in a semi-arid region by assimilating GRACE data into the PCR-GLOBWB hydrological model. Hydrology and Earth System Sciences, 21(4): 2053-2074.

Tangdamrongsub, N., Steele-Dunne, S.C., Gunter, B.C., Ditmar, P.G., Weerts, A.H., 2015. Data assimilation of GRACE terrestrial water storage estimates into a regional hydrological model of the Rhine River basin. Hydrology and Earth System Sciences, 19(4): 2079-2100.

Tangdamrongsub, N. et al., 2020. Multivariate data assimilation of GRACE, SMOS, SMAP measurements for improved regional soil moisture and groundwater storage estimates. Advances in Water Resources, 135: 103477.

Tapley, B.D., Bettadpur, S., Watkins, M., Reigber, C., 2004. The gravity recovery and climate experiment: Mission overview and early results. Geophysical Research Letters, 31(9).

Tian, S. et al., 2017. Improved water balance component estimates through joint assimilation of GRACE water storage and SMOS soil moisture retrievals. Water Resources Research, 53(3): 1820-1840.

Van Beek, L. and Bierkens, M., 2009. The global hydrological model PCR-GLOBWB: Conceptualization, parameterization and verification, report, Dep. of Phys. Geogr., Utrecht Univ., Utrecht, Netherlands.

Van den Hurk, B. et al., 2012. Soil moisture effects on seasonal temperature and precipitation forecast scores in Europe. Climate dynamics, 38(1): 349-362.

Van Dijk, A., Renzullo, L.J., Rodell, M., 2011. Use of Gravity Recovery and Climate Experiment terrestrial water storage retrievals to evaluate model estimates by the Australian water resources assessment system. Water Resources Research, 47(11).

Van Dijk, A., 2010. AWRA Technical Report 3. Landscape Model (Version 0.5) Technical Description, Canberra available at: http://www. clw. csiro. au/publications/waterforahealthycountry/2010/wfhc-aus-water-resourcesassessment-system. pdf, (last accessed 01.10. 14.).

Van Dijk, A., Renzullo, L., Wada, Y. and Tregoning, P., 2014. A global water cycle reanalysis (2003–2012) merging satellite gravimetry and altimetry observations with a hydrological multi-model ensemble.

Van Dijk, A.I., Peña-Arancibia, J.L., Wood, E.F., Sheffield, J. and Beck, H.E., 2013. Global analysis of seasonal streamflow predictability using an ensemble prediction system and observations from 6192 small catchments worldwide. Water Resources Research, 49(5): 2729-2746.

Van Dijk, A., Warren, G., 2010. The Australian water resources assessment system. Version 0.5, 3(5).

Van Leeuwen, P.J. and Evensen, G., 1996. Data assimilation and inverse methods in terms of a probabilistic formulation. Monthly Weather Review, 124(12): 2898-2913.

Vrugt, J.A., Gupta, H.V., Nualláin, B. and Bouten, W., 2006. Real-time data assimilation for operational ensemble streamflow forecasting. Journal of Hydrometeorology, 7(3): 548-565.

Vrugt, J.A., ter Braak, C.J., Diks, C.G., Schoups, G., 2013. Hydrologic data assimilation using particle Markov chain Monte Carlo simulation: Theory, concepts and applications. Advances in Water Resources, 51: 457-478.

Voss, K.A. et al., 2013. Groundwater depletion in the Middle East from GRACE with implications for transboundary water management in the Tigris-Euphrates-Western Iran region. Water resources research, 49(2): 904-914.

Wahr, J., Molenaar, M., Bryan, F., 1998. Time variability of the Earth's gravity field: Hydrological and oceanic effects and their possible detection using GRACE. Journal of Geophysical Research: Solid Earth, 103(B12): 30205-30229.

Wahr, J., Swenson, S., Zlotnicki, V. and Velicogna, I., 2004. Time-variable gravity from GRACE: First results. Geophysical Research Letters, 31(11).

Wang, H., Guan, H., Gutiérrez-Jurado, H.A., Simmons, C.T., 2014. Examination of water budget using satellite products over Australia. Journal of Hydrology, 511: 546-554.

Whitaker, J.S., Hamill, T.M., 2002. Ensemble data assimilation without perturbed observations. Monthly weather review, 130(7): 1913-1924.

Watkins, M.M., Wiese, D.N., Yuan, D.N., Boening, C. and Landerer, F.W., 2015. Improved methods for observing Earth's time variable mass distribution with GRACE using spherical cap mascons. Journal of Geophysical Research: Solid Earth, 120(4): 2648-2671.

Weerts, A.H. and El Serafy, G.Y., 2006. Particle filtering and ensemble Kalman filtering for state updat Wiese, D., 2015. Grace mascon ocean and hydrology equivalent water heights JPL rl05m. 1.

Wilson, C.R. and Rodell, M., 2006. Attenuation effect on seasonal basin-scale water storage change from GRACE time-variable gravity.

Winsemius, H., Savenije, H., Van De Giesen, N., Van Den Hurk, B., Zapreeva, E. and Klees, R., 2006. Assessment of Gravity Recovery and Climate Experiment (GRACE) temporal signature over the upper Zambezi. Water Resources Research, 42(12).

ing with hydrological conceptual rainfall-runoff models. Water resources research, 42(9).

Wooldridge, S.A. and Kalma, J.D., 2001. Regional-scale hydrological modelling using multiple-parameter landscape zones and a quasi-distributed water balance model.

Wouters, B., Bonin, J.A., Chambers, D.P., Riva, R.E., Sasgen, I. and Wahr, J., 2014. GRACE, time-varying gravity, Earth system dynamics and climate change. Reports on Progress in Physics, 77(11): 116801.

Yamamoto, K., Fukuda, Y., Nakaegawa, T. and Nishijima, J., 2007. Landwater variation in four major river basins of the Indochina peninsula as revealed by GRACE. Earth, planets and space, 59(4): 193-200.

Yeh, P., Ä., S. Swenson, J. Famiglietti, and M. Rodell. 2006. Remote sensing of groundwater storage changes in Illinois using the Gravity Recovery and Climate Experiment (GRACE). Water Resources Research, 42: W12203.

Yu, Y. et al., 2015. Large-scale hydrological modeling and decision-making for agricultural water consumption and allocation in the main stem Tarim River, China. Water, 7(6): 2821-2839.

Zaitchik, B.F., Rodell, M., Reichle, R.H., 2008. Assimilation of GRACE terrestrial water storage data into a land surface model: Results for the Mississippi River basin. Journal of Hydrometeorology, 9(3): 535-548.

Zhao, W., Chen, Y., Liu, J., 2020. An effective first order reliability method based on Barzilai–Borwein step. Applied Mathematical Modelling, 77: 1545-1563.

Zhang, Y., Pan, M. and Wood, E.F., 2016. On creating global gridded terrestrial water budget estimates from satellite remote sensing, Remote Sensing and Water Resources. Springer, pp. 59-78.

List of Abbreviations

The following table describes the significance of various abbreviations and acronyms used throughout the thesis.

Abbreviation	Meaning
CBI	**C**entral **B**asin of **I**ran
CLM	**C**ommunity **L**and **M**odel
DA	**D**ata **A**ssimilation
DEnKF	**D**eterministic **En**semble **K**alman **F**ilter
DEnKF	**D**eterministic **En**semble **K**alman **F**ilter
EnKF	**En**semble **K**alman Filter
EnOI	**En**semble **O**ptional Interpolation
EnOI	**En**semble **O**ptional Interpolation
EnSRF	**En**semble **S**quare-**R**oot Filter
EnSRF	**En**semble **S**quare-**R**oot Filter
ESA CCI	**E**uropean **S**pace **A**gency **C**limate **C**hange **I**nitiative
ET	**E**vapo**t**ranspiration
ETKF	**En**semble **T**ransform **K**alman **F**ilter
ETKF	**En**semble **T**ransform **K**alman Filter
FORM	**F**irst **O**rder **R**eliability **M**ethod
GRACE	**G**ravity **R**ecovery **a**nd **C**limate **E**xperiment
GRACE-FO	**G**ravity **R**ecovery and **C**limate **E**xperiment-**F**ollow **O**n
GW	**G**round **W**ater

181

IWRMC	**I**ran **W**ater **R**esources **M**anagement **C**ompany
KeFIn	**Ke**rnel **F**ourier **In**tegration
LSF	**L**imit **S**tate **F**unction
P	**P**recipitation
ParFlow	**PAR**allel **FLOW**
PCR-GLOBWB	**PCR**aster **Glob**al **W**ater **B**alance
PDAF	**P**arallel **D**ata **A**ssimilation **F**ramework
PDF	**P**robability **D**istribution **F**unction
PF	**P**article **F**ilter
PFMR	**P**article **F**ilter, **M**ultinomial **R**esampling
PFMR	**P**article **F**ilter, **M**ultinomial **R**esampling
PFSR	**P**article **F**ilter, **S**ystematic **R**esampling
PFSR	**P**article **F**ilter, **S**ystematic **R**esampling
SM	**S**oil **M**oisture
SMAP	**S**oil **M**oisture **A**ctive **P**assive
SMOS	**S**oil **M**oisture and **O**cean **S**alinity
SQRA	**Sq**uare **R**oot **A**nalysis
TRMM	**T**ropical **R**ainfall **M**easuring **M**ission
TWSA	**T**errestrial **W**ater **S**torage **A**nomaly
W3RA	**W**orld-Wide **W**ater **R**esources **A**ssessment
WGHM	**W**aterGAP **G**lobal **H**ydrology **M**odel

List of Publications

Published

1. Soltani, S.S., Ataie-Ashtiani, B., Danesh-Yazdi, M. and Simmons, C.T., 2020. A probabilistic framework for water budget estimation in low runoff regions: a case study of the central Basin of Iran. Journal of Hydrology, p.124898, 10.1016/j.jhydrol.2020.124898.

2. Soltani, S.S., Ataie-Ashtiani, B. and Simmons, C.T., 2021. Review of Assimilating GRACE Terrestrial Water Storage Data into Hydrological Models: Advances, Challenges and Opportunities. Journal of Earth Science Reviews, 10.1016/j.earscirev.2020.103487.

3. Soltani, S. S., Fahs, M., Al Bitar, A., and Ataie-Ashtiani, B.: Fully coupled subsurface-land surface hydrological models: A scaling approach to improve subsurface storage predictions, EGU General Assembly 2022, Vienna, Austria, 23–27 May 2022, EGU22-2828, https://doi.org/10.5194/egusphere-egu22-2828, 2022.

4. Soltani, S.S., Fahs, M., Al Bitar, A., Ataie-Ashtiani, B., 2022. Improvement of soil moisture and groundwater level estimations using a scale-consistent river parameterization for the coupled ParFlow-CLM hydrological model: A case study of the Upper Rhine Basin. Journal of Hydrology, 610: 127991.

5. Soltani, S.S., Fahs, M., Bitar, A.A. and Ataie-Ashtiani, B., 2022. Multivariate satellite data assimilation for improving coupled ParFlow-CLM hydrological model: a case study of Iran. International conference Groundwater, key to the sustainable development goals, Paris.

Under Review

6. Soltani, S.S., Ataie-Ashtiani, B., Fahs, M. and Bitar, A.A., 2022. Multi-mission data assimilation of GRACE and SMAP into a hydrological model for studying subsurface storage changes over a case study in Iran, under review (Hydrology and Earth System Sciences Journal).

7. Ahmadi, N., Soltani, S.S., Ataie-Ashtiani, B., 2022 and Simmons, C.T., Estimation of groundwater storage changes using GRACE and GLDAS: a case study of the Central Basin of Iran, under review (Journal of Hydrogeology).

SOLTANI Samirasadat

Assimilating remote sensing information into a distributed hydrological model for improving water budget predictions

Résumé

Cette thèse a étudié l'application de méthodes pour améliorer les performances des modèles hydrologiques terrestres sous différents angles. Des considérations particulières ont été accordées pour répondre aux limites des méthodes existantes en proposant de nouvelles techniques. Celles-ci incluent l'introduction d'un nouveau cadre d'assimilation, l'examen de diverses stratégies d'assimilation de données pour assimiler les données GRACE TWS et SMOS, le développement de techniques pour utiliser le plein potentiel de différentes sources de données, y compris les observations GRACE et SMOS pour contraindre les états du système, et la proposition d'une nouvelle stratégie d'assimilation pour la mise à jour du sous-sol. états de stockage de l'eau, c'est-à-dire l'équation fondamentale du bilan hydrique, sur leurs estimations. Cela comprend également l'introduction de nouvelles stratégies de modélisation telles qu'une paramétrisation de rivière cohérente à l'échelle pour le modèle hydrologique couplé ParFlow-CLM. Cela signifie qu'en connaissant les limites du modèle, y compris les contraintes structurelles, il est possible de proposer des méthodes qui aident à surmonter les limites de la modélisation afin d'améliorer les performances du modèle.

Mots clés : Modélisation hydrologique, Assimilation de données multi-missions, Filtre de Kalman d'ensemble, GRACE, SMOS

Abstract

This thesis investigated the application of methods for improving land hydrological model performances from various perspectives. Special considerations were given to address the limitations in existing methods by proposing new techniques. These include introducing new assimilation framework, examining various data assimilation strategies for assimilating GRACE TWS and SMOS data, developing techniques to use the full potential of different data source including GRACE and SMOS observations for constraining system states, and proposing a new assimilation strategy for updating subsurface water storage states, i.e., the fundamental water balance equation, on their estimates. These also includes introducing new modeling strategies such as a scale-consistent river parameterization for the coupled ParFlow-CLM hydrological model. This means, by knowing the limitations of the model, including structural constraints, it is possible to suggest methods that help to overcome the limitations of modeling in order to improve the performance of the model.

Keywords : Hydrological Modeling, Multi-Mission Data Assimilation, Ensemble Kalman Filter, GRACE, SMOS